SAHC

Study of the seismic vulnerability of Catalonian Romanesque churches: the churches of the monasteries of Santa Maria de Poblet and Sant Miquel de Cruïlles

Ellen Tatiana Key

Spain | 2019

ADVANCED MASTERS IN STRUCTURAL ANALYSIS OF MONUMENTS AND HISTORICAL CONSTRUCTIONS

Master's Thesis

Ellen Tatiana Key

Study of the seismic vulnerability of Catalonian Romanesque churches: the churches of the monasteries of Santa Maria de Poblet and Sant Miquel de Cruïlles

UNIVERSITAT POLITÈCNICA DE CATALUNYA

University of Minho

Spain | 2019

ADVANCED MASTERS IN STRUCTURAL ANALYSIS
OF MONUMENTS AND HISTORICAL CONSTRUCTIONS

Master's Thesis

Ellen Tatiana Key

Study of the seismic vulnerability of Catalonian Romanesque churches: the churches of the monasteries of Santa Maria de Poblet and Sant Miquel de Cruïlles

Spain | 2019

DECLARATION

Name: Ellen Tatiana Key

Email: ellenkey@ucla.edu

Title of the MSc Dissertation: Study of the seismic vulnerability of Catalonian Romanesque churches: the churches of the monasteries of Santa Maria de Poblet and Sant Miquel de Cruïlles

Supervisor(s): Professors Pere Roca and Luca Pelà

Year: 2018 - 2019

I hereby declare that all information in this document has been obtained and presented in accordance with academic rules and ethical conduct. I also declare that, as required by these rules and conduct, I have fully cited and referenced all material and results that are not original to this work.

I hereby declare that the MSc Consortium responsible for the Advanced Masters in Structural Analysis of Monuments and Historical Constructions is allowed to store and make available electronically the present MSc Dissertation.

University: Universitat Politècnica de Catalunya

Date: 17/07/19

Signature: 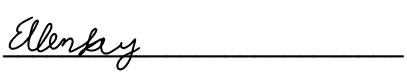

This page is left blank on purpose.

To Carolyn Clarke Nuite, the greatest citizen of San Francisco, and quite possibly, the world.

July 13, 1933 ~ February 28, 2019

This page is left blank on purpose.

ACKNOWLEDGEMENTS

First, I must thank my supervisors, Professor Pere Roca and Professor Luca Pelà. Their availability, input and guidance has been instrumental in developing this thesis.

I would like to express my gratitude to the MSc Consortium for the financial support I was granted throughout this year.

I am indebted to my family at home in California, for letting me live so far away from them for so long. They always support me in my academic endeavors and I am very grateful.

This year as a SAHC student has been full of adventure and hard work. I would like to thank all of the professors who taught my classmates and me. I would also like to thank my classmates, who not only encouraged me during our studies but also shared new cultural experiences with me. This year has been a fun and memorable experience.

This page is left blank on purpose.

ABSTRACT

The behavior of heritage structures, particularly churches, in unpredictable events such as earthquakes is continuously under study in order to find better ways of safeguarding them. Catalunya, the northeast region of Spain, has thousands of historical masonry churches, many of which are from the Romanesque period. The monasteries of Sant Miquel de Cruïlles and Santa Maria de Poblet contain examples of Romanesque churches from the 11th and 12th centuries, respectively, and will be considered as case studies for this thesis. The spacious church of the monastery of Santa Maria de Poblet is part of an imposing monastic complex, near the town of L'Espluga de Francolí. In contrast, the church of Sant Miquel de Cruïlles is much smaller and more modest, located in a rural area near Bisbal d'Empordà and lacking the surrounding monastery that was once present.

Churches are usually much more impacted by earthquakes than other buildings. Studies have shown that churches of different typologies often present similar failure mechanisms after every seismic event (De Matteis et al., 2016; Penna et al., 2019; Sorrentino et al., 2014, among others). Noting the local behavior of independent parts of the church, engineers developed macroelement-based analysis methods. This report uses two such methods to analyze the vulnerabilities of the two case studies. The first is the vulnerability index method, which requires a keen assessment of the geometry of the structure. It quantifies a qualitative observational analysis in order to give a sense of the building's vulnerability, damage state, and possible damage expected from a seismic event. This report found that the two case studies would reach the damage limit state in a seismic event of the reference ground acceleration in the Eurocode 8 and Spanish seismic code (*Norma de Construcción Sismorresistente*).

The next analysis method is the kinematic limit analysis, which individually considers macroelements according to a given failure mechanism to determine the capacity of the element. Since overturning is a very common collapse mechanism in churches, many macroelements have been analyzed for overturning in this paper: 15 cases are considered for Poblet and 13 cases for Sant Miquel de Cruïlles. Evaluation of the structure's performance point is carried out based on well-known guidelines and codes (ATC, 1996; FEMA, 1997; NTC, 2018, 2019). The most vulnerable elements of Santa Maria de Poblet were found to be the transept facade, main facade and bell tower, while for Sant Miquel de Cruïlles they were the wall of the bell tower, main facade, and south transept facade. Based on the analysis considering the response spectra of the two codes used, these elements could reach "moderate" or "extensive" levels of damage in the next earthquake.

Finally, this paper also compares these two analysis methods, discussing how the results compare and contrast and weighing their advantages and disadvantages. It draws conclusions about the state of these churches and how they might reflect the state of other Romanesque Catalonian churches.

This page is left blank on purpose.

RESUMEN

El comportamiento de las estructuras del patrimonio, particularmente las iglesias, en eventos impredecibles como los terremotos, se estudia continuamente para encontrar mejores formas de salvaguardarlas. Cataluña, la región noreste de España, tiene miles de iglesias históricas de mampostería, muchas de las cuales son de época románica. Los monasterios de Sant Miquel de Cruïlles y Santa Maria de Poblet contienen ejemplos de iglesias románicas de los siglos XI y XII, respectivamente, y se considerarán estudios de caso para esta tesis. La espaciosa iglesia del monasterio de Santa Maria de Poblet es parte de un imponente complejo monástico, cerca de la ciudad de L'Espluga de Francolí. En contraste, la iglesia de Sant Miquel de Cruïlles es mucho más pequeña y más modesta, está ubicada en una zona rural cerca de Bisbal d'Empordà y carece del monasterio circundante que estaba presente en el pasado.

Las iglesias suelen ser mucho más afectadas por los terremotos que otros edificios. Los estudios han demostrado que las iglesias de diferentes tipologías a menudo presentan mecanismos de falla similares después de cada evento sísmico (De Matteis et al., 2016; Penna et al., 2019; Sorrentino et al., 2014, entre otros). Al observar el comportamiento local de las partes independientes de la iglesia, los ingenieros desarrollaron métodos de análisis basados en macroelementos. Este informe utiliza dos de estos métodos para analizar las vulnerabilidades de los dos estudios de caso. El primero es el método del índice de vulnerabilidad, que requiere una evaluación aguda de la geometría de la estructura. Cuantifica un análisis de observación cualitativo para dar una idea de la vulnerabilidad del edificio, el estado de daño y el posible daño esperado de un evento sísmico. Este informe encontró que los dos estudios de caso alcanzarían el estado límite de daño en un evento sísmico de la aceleración del terreno de referencia en el Eurocódigo 8 y la Norma de Construcción Sismorresistente de España.

El siguiente método de análisis es el análisis de límite cinemático, que individualmente considera los macroelementos de acuerdo con un mecanismo de falla para determinar la capacidad del elemento. Ya que el vuelco es un mecanismo de colapso muy común en las iglesias, muchos macroelementos se han analizado en este documento: se consideran 15 casos para Poblet y 13 para Sant Miquel de Cruïlles. La evaluación del punto de desempeño de la estructura se realiza en base a directrices y códigos bien conocidos (ATC, 1996; FEMA, 1997; NTC, 2018, 2019). Los elementos más vulnerables de Santa María de Poblet fueron la fachada del crucero, la fachada principal y el campanario, mientras que para Sant Miquel de Cruïlles fueron la pared del campanario, la fachada principal y la fachada sur del crucero. Según el análisis que considera los espectros de respuesta de los dos códigos utilizados, estos elementos podrían alcanzar niveles de daño "moderados" o "extensos" en el próximo terremoto.

Finalmente, este documento también compara estos dos métodos de análisis, discutiendo cómo se comparan y contrastan los resultados y sopesando sus ventajas y desventajas. Presenta

conclusiones sobre el estado de estas iglesias y cómo pueden reflejar el estado de otras iglesias románicas catalanas.

TABLE OF CONTENTS

LIST OF FIGURES

LIST OF TABLES

1. INTRODUCTION

1.1. Background

Historical buildings are essential to a region's history and identity. Though they may have been constructed centuries ago, they are often still frequently-used structures in today's society and symbolize the pride of a community in the artistic and structural accomplishments of their forebears. For these reasons, their conservation should be a priority.

As buildings age, they naturally decay and are subject to occasional natural hazards such as earthquakes. In regions that experience frequent earthquakes, some civilizations developed seismically resistant building techniques. However, many historical structures have few, if any, anti-seismic measures in place. They are therefore vulnerable, or at risk of damage, should an earthquake occur. One of the most vulnerable structural typologies is churches, due to their large open naves with high ceilings and lack of intermediate diaphragms. They often have weak components that are susceptible to overturning or other modes of failure in an earthquake.

Spain, a country whose history is inextricable from Christianity, is home to thousands of churches. This thesis will focus on those of the Romanesque period, which took place in the 11th to 12th centuries in Europe (Pladevall i Font & Gurri i Serra, 2014). Catalonia, a region in the northeast of Spain, accepted and implemented the Romanesque style of art and architecture which is characterized by solid and sober lines. Many monasteries and churches from that period still survive today. Although Catalonia is a region of low seismicity, it is interesting to examine the seismic vulnerability of Romanesque churches of the area.

1.2. Objectives

The objective of this paper is to implement and evaluate two known methods for analyzing historical masonry buildings, specifically in the area of seismic vulnerability. The first of these methods is the vulnerability index method, which considers the vulnerabilities and anti-seismic measures present within a structure and determines its level of vulnerability. The second is the kinematic limit analysis method, which determines the vulnerability of individual structural elements in relation to a given failure mechanism. Essentially, the former assesses the structure globally, while the latter provides local assessments.

These methods can be applied with limited information about the church; in fact, after just a simple geometrical survey lacking extensive knowledge about the material properties. This means that they can be used to analyze many churches expediently in order to determine the most vulnerable ones, for which interventions should be prioritized.

This paper also aims to compare the two analysis methods and evaluate whether the methods yield similar results. It will weigh the advantages and disadvantages of each method and discuss their performances with regard to the two churches on which they are applied. It will propose improvements to the methods when possible.

The churches of the monasteries of Santa Maria de Poblet and Sant Miquel de Cruïlles, both located in the region of Catalonia in northeastern Spain, are the subjects of this analysis. They are Romanesque masonry churches in a region of modest seismicity; like many historical structures, they were not designed for seismic action. This report will conclude on the vulnerability of these two churches and their major structural components. It will provide possible strengthening interventions to be considered in future conservation works, with the goal of keeping these churches and others like them standing for many more years.

1.3. Methodology

Churches are gathering places for people and therefore their vulnerability represents a high risk for loss of life. They have cultural value and often house important artistic works that should be saved, such as the carved alabaster altar in the monastery of Santa Maria de Poblet (Figure 1.3.1). In addition, they are of economic interest to the region because they attract tourists. The churches of the Santa Maria de Poblet and Sant Miquel de Cruïlles monasteries were selected for this report because they are considered representative of Catalonian Romanesque churches. They each have at least one additional reason for study: Poblet Monastery holds high importance as a UNESCO World Heritage site, and the church of the monastery of Sant Miquel de Cruïlles is significantly damaged and thus deserves to be investigated.

To begin, a historical review was conducted to obtain all relevant information about the churches' construction. Of special interest were past earthquakes, fires, or structural alterations which may have contributed to the state of the structure today. Books, websites, and previous studies were consulted.

Next, it was necessary to review previous research that analyzed masonry churches on a regional or an individual scale. Many of these studies were conducted after disastrous earthquakes and aimed at improving the seismic resistance of the structures.

(a)

(b)

Figure 1.3.1. (a) Carved alabaster altar and (b) royal tombs of the monastery of Santa Maria de Poblet (Baldiri, 2019)

Also, building codes with provisions for existing structures were consulted, such as the Italian code *Norme tecniche per le costruzioni* and its instructions for application, herein called the Circolare (NTC, 2018, 2019). Also very important were the Italian Guidelines for evaluation and mitigation of seismic risk to cultural heritage, which explain a vulnerability index method for evaluating existing structures (G.U. no. 47, 2011).

From the literature review, the vulnerability index method and kinematic limit analysis methods were chosen as they are methods that have been widely used in the past and they are relatively simple. They are not often used in tandem, so this paper takes the opportunity to compare their results.

With these two methods in mind, site visits were performed. Visual inspections were performed with a checklist for the vulnerability index method, to note down relevant features of the structure. Damages were carefully recorded to create crack maps. Two-dimensional plan, elevation and section drawings of the churches were already available from prior studies and aided in the damage mapping. The inspections helped to obtain a general understanding of how each structure functioned, taking into account such factors as connections and masonry quality which are not displayed in plans.

After reviewing the churches, the vulnerability index method was carried out. Many assumptions had to be made during the analysis and they are detailed later in this report. For each element deemed to be at risk of local failure by overturning, the kinematic limit analysis method was performed. Comparing the results to each other and to other studies in which these methods were used enabled a full analysis of the churches and the methods.

1.4. Outline

As is customary, this thesis begins with a review of the state of the art in the study of masonry churches and seismic vulnerability. This includes a discussion of the seismic behavior of masonry; a summary of established seismic guidelines and building codes; and previous studies in seismic vulnerability of masonry buildings, especially those in Italy, a land of high seismicity and many churches. Then, it presents the vulnerability index method and kinematic limit analysis method, including the background of the methods and detailed explanations of the calculations. Next, it introduces the region of Catalonia, followed by an introduction to both churches. Information is provided on the churches' location, history, geometry, condition, and any past studies done on the church.

Subsequently, the analysis methods are applied to the churches. First, any assumptions made during the analysis are explained. Then the results are displayed and analyzed. Finally, taking all of the history, damage state, and vulnerability results into account, possible strengthening interventions are recommended.

2. STATE OF THE ART

2.1. Seismic behavior of masonry

Masonry comes in many forms: it is composed of units of brick, stone, adobe or other materials stacked with or without mortar. Its behavior depends on the material of the units, dimension and shape of the units, presence or lack of mortar and its properties, and geometry of the construction. Mortar is elastic-fragile under tension and has relatively low compressive strength, whereas the units are stronger in compression than in tension (G.U. no. 47, 2011). The low tensile strength of masonry as a whole makes it much weaker out-of-plane than in-plane. When masonry cracks, strength and stiffness degrade in what is called softening.

Problems may arise in masonry buildings for many reasons. When subjected to out-of-plane acceleration in the case of an earthquake, it is essential that the walls be properly sized, sufficiently compact (i.e. without voids) and that there are strong connections between horizontal and vertical load-bearing elements. In the case of churches, which usually lack intermediate floors, this means that the walls and roof should have good connections. The term "box behavior" is often used to describe the desired behavior of a building with solid wall-to-wall connections, causing horizontal acceleration to be resisted in-plane by the walls parallel to the motion. This prevents the walls perpendicular to the ground motion from taking out-of-plane loading that could lead to overturning. If horizontal elements are sufficiently stiff and well-connected to the walls, they can restrict out-of-plane displacement of the walls. If they are not well-connected or too heavy, as has been the case with some poor reinforced concrete interventions, the roof may separate and shear off (Modena et al., 2011). Another possible scenario is delamination in multi-leaf walls, where only one of the outer leaves overturns. Clamping, tie rods, metal connections and the proper fitting of the wall and floor elements all improve the behavior under lateral actions (G.U. no. 47, 2011). Other elements that often see damage in earthquakes are arches and vaults. The thinness of vaults makes them particularly susceptible. These elements induce thrust which must be counteracted by tie rods, buttresses or other solutions (Modena et al., 2011).

Historical masonry buildings were built not with design rules but with rules of thumb and experiential knowledge. Most of the time they were built for only gravity loads (Valente et al., 2017). In studying their earthquake resistance, it is important to remember that they may never have experienced strong ground motions or may have been structurally modified since they last were damaged. Thus, they may not show the damage that might be expected. There may be damage still present in the building that has been hidden by interventions. There may be lasting local effects from past earthquakes. Over generations, in areas of high seismicity, building typologies generally evolved to include anti-seismic measures such as buttresses and tie-rods. These technologies have shaped the seismic building codes of the modern age. In areas of low seismicity, people sometimes added anti-seismic measures when rebuilding after

earthquakes, but after years, when the risk of earthquakes was no longer on the mind of the public, these measures were forgotten (G.U. no. 47, 2011).

Before the 1990s, many engineers thought that the complexities and uniqueness of cultural heritage buildings made global evaluation by a simplified model too unrealistic (Lagomarsino, 2012). Plus, masonry has nonlinear behavior which makes it rather difficult to model. However, some kind of evaluation was extremely necessary because of the high threat to historical structures.

Nowadays, the seismic vulnerability assessment of historical structures is generally classified as either empirical models, based on observations of damage after an earthquake, or analytical models based on sophisticated structural and hazard analysis such as time-history analysis (Kazantzidou-Firtinidou et al., 2016; Milutinovic & Trendafilosk, 2004). For churches, specifically, simplified empirical models have been found to be sufficient to represent the typical damage scenarios (Lagomarsino, 2012). Therefore, complex global models are not always necessary. Besides, it should be noted that if local transfer from one element to another is weak, as may be the case for a structure that has seen many structural changes throughout its life, the weakness may not even be apparent in a global model.

2.2. The development of seismic analysis guidelines for existing structures

As studies began to be performed on post-earthquake damage, rules and guidelines developed for seismic analysis of existing structures starting approximately in the 1990s. Methods developed for the calculation of capacity and demand of a structure for horizontal actions. The N2 method was developed and formulated in (Fajfar, 2000). This method will be discussed in Section 2.5.3.

In the United States, the Applied Technology Council and California Seismic Safety Commission began to investigate seismic retrofitting and seismic risk of concrete structures in California. They developed a version of the capacity spectrum method which will be discussed in Section 2.5.3. The Federal Emergency Management Agency set out to develop nationally applicable guidelines for the seismic rehabilitation of buildings (FEMA, 1997). They laid out the nonlinear static procedure which compares a pushover analysis to a response spectrum, essentially another version of the capacity spectrum method. In fact, the ATC and FEMA approaches are actually just more complex versions of the N2 method.

The Risk-UE project in Europe set out to develop vulnerability models, fragility models and damage probability matrices and propose a damage survey and building inventory for representative typologies of European buildings (Milutinovic & Trendafilosk, 2004). Based on six vulnerability classes defined by (Grünthal, 1998), this report proposes plausible behavior for each vulnerability class. Their first proposal was similar to the analysis methods that had arisen from many Italian studies, calculating a vulnerability index, damage probability matrix and vulnerability curves. The second method was a displacement-

based method to compare the capacity (from time history or pushover analysis) to the elastic or inelastic response spectrum in a variation of the capacity spectrum method. It should be noted that the Risk-UE capacity curves were developed for southern European buildings; some researchers have evaluated their application to other regions and made proposals for adjustment when necessary (Kazantzidou-Firtinidou et al., 2016).

When a disastrous earthquake strikes and extensive damages occur, it is necessary to define suitable speedy vulnerability assessment methodologies at a large scale which are able to explain damage scenarios and enable prioritization of interventions. A study of the 1995 earthquake in Lunigiana and Garfagnana, Italy, prompted the development of a 16-mechanism checklist including the most common damage mechanisms, based on macroelements (Angeletti et al., 1997). This checklist was used in surveys after the Umbria and Marches earthquake of 1997 and revised to include 18 mechanisms (Lagomarsino & Podestà, 2004a). The Italian survey form was approved in 2001 by the Italian Civil Protection (Lagomarsino et al., 2019). It has since been used internationally (Leite et al., 2013). In 2006 the current 28-mechanism form used in the more recent earthquakes in Italy was developed by the Italian Ministry for Cultural Heritage and Activities (G.U. no. 47, 2011). Based on years of study and outcomes of thousands of survey forms, this Italian body developed the Italian Guidelines for evaluation and mitigation of seismic risk to cultural heritage, hereafter referred to as the Italian Guidelines (G.U. no. 47, 2011; Cecchi & Calvi, 2006). This document lays out a system for prevention of damage to historic constructions because until it was written, prevention of damage in seismic events had been only rarely successful and several inadequate strengthening campaigns had led to irreparable damage. Thus, this document suggested a procedure for categorizing and assessing buildings that may need seismic interventions in order to reach higher safety levels.

The Italian Guidelines lays out the three seismic evaluation levels based on the depth of study: LV1, LV2, and LV3. The first is a "qualitative analysis and evaluation with simplified mechanical models", the second is an "evaluation of individual elements (local collapse mechanisms)", and the third is a "global evaluation of seismic response of the building" (G.U. no. 47, 2011). The vulnerability analysis performed in this report falls into category LV1 and the kinematic limit analysis is considered LV2. The final level, LV3, requires in-depth, complex analysis and is not within the scope of this study.

2.3. Studies on the seismic behavior of masonry churches

Italy is a seismically active region with a plethora of masonry churches. With each significant earthquake, new studies have been performed, beginning with the Fruili earthquake of 1976 (Doglioni et al., 1994), and followed by: Lunigiana and Garfagnana earthquake in 1995 (Angeletti et al., 1997), Umbria-Marche earthquake in 1997 (Lagomarsino & Podestà, 2004a, 2004b), L'Aquila earthquake in 2009 (Brando et al., 2017; De Matteis et al., 2016; Lagomarsino, 2012), Emilia earthquakes in 2012 (Cattaneo, 2014;

Sorrentino et al., 2014; Valente et al., 2017), Central Italy earthquakes in 2016-2017 (Penna et al., 2019).

These studies have all found that churches are more vulnerable than ordinary buildings to seismic events. (Lagomarsino & Podestà, 2004b) analyzed the most significant factors in the vulnerability of the churches in the Umbria-Marche earthquake. They tried to make generalizations about church behavior based on their classification by architectonic typology, dimensions, and age; however, they could not find a significant correlation. What has been discovered through the studies of damage after all of these earthquakes, however, is that although churches can be quite disparate, damage mechanisms in churches have certain recurring characteristics. Churches almost always experience local failures in macroelements; that is, structural elements that may behave independently from the rest of the church. Out-of-plane overturning of macroelements such as the facade, gable, or belfry are some of the most common failures seen after earthquakes (Penna et al., 2019). Examples of macroelements overturning are provided in Figure 2.3.1.

As mentioned in Section 2.2, Italian authorities developed a survey form for use in every post-earthquake investigation, which originated with 16 and evolved to include 28 of the most common failure mechanisms. (Lagomarsino et al., 2019) recently evaluated the Italian survey form currently in use and proposed a new more complex method for the damage inspection. The goal is to obtain more practical values of the damage index (a value calculated to indicate the structure's relative level of damage, based on certain observations). This new form is called the *Church Assessment Form - Damage,* or *CAF-D.* It addresses some of the limitations or problems with the current damage index calculation, which will be discussed later in Section 3.3. In New Zealand after the 2010-2011 Canterbury earthquakes, both this new method and the current method were conducted (Leite et al., 2013). This new method was shown to better approximate the actual damage levels, whereas the existing methodology underestimated them.

Many papers were written on the L'Aquila earthquake of April 2009 using some form of damage survey (Brando et al., 2017; De Matteis et al., 2016; Lagomarsino, 2012). Lagomarsino, 2012 selected certain interesting cases and commented on the behavior of the facade, roof, apse, and belfries. He called attention to damage that had been induced by structural interventions, and concluded on their effectiveness in a positive or negative way. In fact, this study was rather like the present thesis, since it evaluated churches individually, with the exception being that it directly followed the destruction of an earthquake.

(a) (b)

(c) (d)

Figure 2.3.1. Examples of damage due to overturning in church macroelements, observed in the 2009 L'Aquila earthquake (Lagomarsino, 2012):
(a) overturning of the facade in Santa Maria degli Angeli church, in Civita di Bagno, L'Aquila,
(b) overturning of the gable in Madonna dei Raccomandati church in San Demetrio né Vestini.
(c) delamination and collapse of the outer leaf of the apse of S. Eusanio Martyr church in Sant'Eusanio Forconese,
(d) overturning of the gable belfry in S. Michele Arcangelo church in Villa Sant'Angelo.

(De Matteis, Brando, Corlito, et al., 2019) focused on the dioceses of L'Aquila and Sulmona-Valva, which were the most affected by the 2009 seismic event. Sixty-four churches (about 10% of all of those in the area) were identified as representative typologies and having three naves. They found that medieval churches built from the 11th to 14th centuries generally had low seismic vulnerability. The most common damage types included diagonal cracking due to in-plane mechanisms. Barrel vaults saw longitudinal cracks, and some columns were crushed vertically. When macroelements were not tied properly, out-of-plane mechanisms occurred. The study used a visual and descriptive damage grading scheme from (De Matteis et al., 2016) and presented later in this paper as Figure 2.4.3, in which the European Macroseismic Intensity (Grünthal, 1998) was applied to churches.

(De Matteis, Brando, Corlito, et al., 2019) concluded that their findings should be used to make strategic interventions that are cost effective and the most necessary in order to protect the most vulnerable

churches, which is backed up with an example of the effect of certain interventions on reducing the vulnerability index in (De Matteis, Brando, & Corlito, 2019).

Finite element models should not be forgotten as an option for analysis of a masonry structure, although they are time-consuming and thus not often used in post-disaster plans. As an example, three medieval churches were studied after the Emilia earthquake, and finite element models were created which accurately emulated the damage experienced (Valente et al., 2017).

It follows that this current work with two Spanish Romanesque churches is being performed with equations calibrated for Italian churches from a range of historical eras, which is not ideal. It must be assumed that the similarity of the churches is close enough to enable the use of the same equations. This has been shown to be a good assumption for similar historical city centers (Brando et al., 2017), and relatively similar even for churches of different countries (Lagomarsino et al., 2019).

Another consideration is that many past studies benefitted from the fact that the churches were analyzed immediately after an earthquake and it was easy to see the degree of effectiveness of the anti-seismic measures and other important factors. The churches examined in this paper have not recently suffered an earthquake, so their observation could not always lead to such clear conclusions.

2.4. The vulnerability index method

2.4.1. Background of the vulnerability index method

Vulnerability is defined as the degree of damage to one or more elements due to a certain hazard; thus, the seismic vulnerability of a building is a measure of the damage the building will likely experience due to ground motion of a certain intensity (Milutinovic & Trendafilosk, 2004).

The vulnerability analysis method under study is based on (Lagomarsino & Podestà, 2004b) and the Italian Guidelines for evaluation and mitigation of seismic risk to cultural heritage (G.U. no. 47, 2011) and was developed to quickly analyze a multitude of structures with a checklist-based approach. This method is considered an LV1 study because it evaluates collapse accelerations by a simplified method, using qualitative data from a visual inspection. Section 5.4 of the Italian Guidelines breaks down the evaluation process by the type of structure. This thesis deals with the church typology, which the guidelines acknowledge to be a wildly diverse group of structures. The main distinguishing feature about this typology is the lack of intermediate diaphragms in halls that are typically large. In addition, the macroelements may be large and have quite independent behavior.

It becomes necessary to define macroelements (mentioned previously in Section 2.3) in order to elaborate this analysis. The macroelements are architectonic parts of a structure which can be said to have certain general behaviors with respect to the rest of the building, such as the bell tower, apse, nave, etc. These macroelements have a number of possible collapse mechanisms, and thus a vulnerability level can be assigned to each one (G.U. no. 47, 2011).

The vulnerability index method is a widely popular method for quick observation of vulnerability and damage; variations have been implemented by a multitude of authors including (Brando et al., 2017; De Matteis, Brando, Corlito, et al., 2019; Ferreira et al., 2013; Lagomarsino et al., 2019; Penna et al., 2019). The method has some flexibility: not only can it be applied to countries other than Italy, but also when studying a large population of churches after a disaster, the vulnerability and damage indices can be derived for the entire population of churches, or for only the churches that experienced a certain seismic intensity, or for all examples of a certain macroelement (De Matteis, Brando, Corlito, et al., 2019). It has been observed that this procedure can be used to calculate the damage resulting from any earthquake intensity, therefore this procedure can be used as a predictive tool for future events rather than as a retroactive observational analysis.

2.4.2. Objectives of the vulnerability index method

The vulnerability analysis method does not aim to achieve an extremely accurate picture of structural failure. Rather, it uses simple indicators that have been observed in many structures to make predictions about the church under study. It aims to provide an idea of the level of vulnerability after just a geometric survey of the building.

The method calculates a vulnerability index and a damage index, which will be explained in the next section, to quantify the vulnerability and damage state and allow comparison between churches. The method also finds the acceleration required to reach the damage limit state and ultimate limit state, which will also be described later. Then it calculates the mean damage level for a given earthquake intensity, from an equation developed by the study of many Italian churches. This equation can be used to make fragility curves, which predict the damage level for the church in any earthquake intensity.

The ultimate objective of this method is to apply it to a group of structures and identify quickly which are the most vulnerable ones. Then, these can be investigated with LV2 or LV3 analyses to determine the necessary interventions. Alternatively, if it is applied to just one or two structures as is done here in this report, it can give a general idea of how a church will be affected by a seismic event it is likely to experience.

2.4.3. Explanation of the vulnerability index method

As mentioned before, there are one or more collapse mechanisms associated to each macroelement; for fifteen macroelements, there are twenty-eight collapse mechanisms (Table 2.4.1).

Table 2.4.1. Mechanisms included in the vulnerability index analysis method

Macroelement	**Mechanism**
Facade	1. Overturning of the facade
	2. Damage at the top of the facade
	3. Shear mechanisms in the facade
	4. Narthex
Nave	5. Transversal vibration of the nave
	6. Shear mechanisms in the side walls
	7. Longitudinal response of the colonnade
	8. Vaults of the nave
	9. Vaults of the aisles
Transept	10. Overturning of the transept facade
	11. Shear mechanisms in the transept walls
	12. Vaults of the transept
Triumphal arch	13. Triumphal arches
Dome, drum and tiburio	14. Dome, drum and tiburio
	15. Lantern
Apse	16. Overturning of the apse
	17. Shear mechanisms in the presbytery and the apse
	18. Vaults in the presbytery and the apse
Roof	19. Roof mechanisms: side walls of nave and aisles
	20. Roof mechanisms: transept
	21. Roof mechanisms: apse and presbytery
Chapels	22. Overturning of the chapels
	23. Shear mechanisms in the chapel walls
	24. Vaults of chapels
Adjacent buildings	25. Interactions with adjacent buildings
Projections	26. Projections (gable belfry, spires, pinnacles, statues)
Bell tower	27. Bell tower
	28. Belfry

For example, the three mechanisms for the facade (overturning, damage at the top of facade or gable, and shear) are shown in Figure 2.4.1. The complete list of collapse mechanisms, provided in the Italian Guidelines, is found in Appendix A.1.

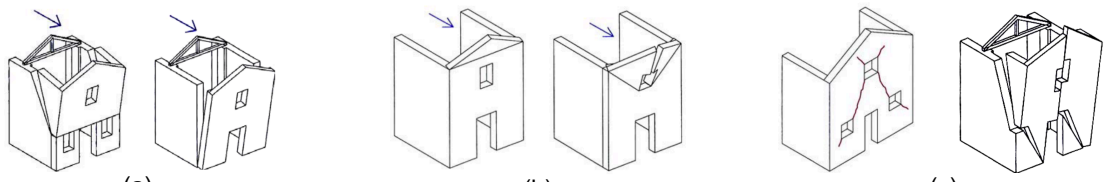

(a) (b) (c)

Figure 2.4.1. Collapse mechanisms for the facade: (a) overturning, (b) damage to the top/gable, (c) shear

- **Vulnerability Index**

For each mechanism, a vulnerability index i_v can be calculated. The vulnerability index is a parameter that describes the vulnerability of the structure, on a scale of 0 to 1, taking into account the significance of vulnerability indicators and anti-seismic measures and the importance of each macroelement with respect to the rest of the structure.

Through visual inspection, the presence of vulnerability indicators or anti-seismic measures are identified. Vulnerability indicators are specific to the mechanism in question, but in general include the presence of inadequate interventions or alterations, presence of concentrated loads, weakness due to openings such as windows, or the geometry of the element (e.g. thin element) (see Figure 2.4.2(a)). The anti-seismic measures include effective devices such as tie-rods, clamps at corners, braces, lightweight tie-beams, and buttresses, which may have been original constructions or later additions (see Figure 2.4.2(b)). They can also include positive construction characteristics such as monolithic masonry construction, stockiness of elements, or quality connections. As an example, the vulnerability indicators and anti-seismic measures for mechanism one, overturning of the facade (described as detachment of the facade from the walls or evident out of plumb) are:

Vulnerability Indicators:
- presence of thrusting elements (roof rafters, vaults, arches)
- presence of large openings in side walls near corners

Anti-seismic Measures:
- presence of longitudinal tie-rods
- presence of effective elements of contrast (buttresses, leaning buildings)
- good quality clamping between the facade and side walls of the nave

All of the vulnerability indicators and anti-seismic measures for the twenty-eight mechanisms are tabulated in Appendix A.1.

(a)

(b)

Figure 2.4.2. Examples of (a) a vulnerability indicator: the large rose window above the organ in the main facade of the church of Poblet Monastery; and (b) an anti-seismic measure: buttresses in Sant Miquel de Cruïlles

After the presence of vulnerability indicators and anti-seismic measures is determined for each mechanism, their importance is given a numerical value v_k as suggested by Table 2.4.2 (G.U. no. 47, 2011). For example, if the first mechanism has large openings in the side walls near corners, and they are judged to be of a moderate contribution to the facade's likelihood of overturning (one indicator, effectiveness level two), then the vulnerability score may be $v_{kv} = 2$. For the anti-seismic measures, if buttresses support the facade and there are longitudinal tie-rods considered to be of moderate effectiveness (two measures, effectiveness level two), then the anti-seismic score may be $v_{ka} = 3$.

Table 2.4.2. Judgement of v_k (G.U. no. 47, 2011)

Number of vulnerability indicators or anti-seismic measures	Effectiveness	$\boldsymbol{v_k}$
≥ 1	3	3
≥ 2	2	
1	2	2
≥ 2	1	
1	1	1
0	0	0

The assignment of v_k is the first of a few very subjective steps that are part of this method; engineering judgment was used to yield the best results and it should be noted that the best attempt was made to be consistent throughout the analysis. In cases of uncertainty, a low and a high value were considered, in order to calculate a range of values of the vulnerability index and acknowledge its subjectivity.

Next, it is necessary to assign weights to the mechanisms based on the importance of the macroelement in relation to the geometry of the entire structure and to global stability. Most of the mechanisms have a weight of $\rho_k = 1$ except for those of the narthex and the lantern, for which $\rho_k = 0.5$; and those of the transept, vault of the apse, chapels, adjacent buildings, and projections, for which the value must be decided, $0.5 \leq \rho_k \leq 1$. This decision of how much a certain macroelement contributes to the structure is another subjective step in this method. The size of the macroelement relative to the other macroelements was the main factor in determining which value to take, as was also done by (Lagomarsino et al., 2019). To simplify the matter, if the element was large its weight was taken as 1, and if it was small its weight was taken as 0.5. If the macroelement was not present in the church, its weight was set at zero.

Finally, the value of the vulnerability index i_v for each church could be calculated with Equation 2.4.1 (G.U. no. 47, 2011).

$$i_v = \frac{1}{6} \frac{\sum_{k=1}^{28} \rho_k (v_{kv} - v_{ka})}{\sum_{k=1}^{28} \rho_k} + \frac{1}{2}$$ Equation 2.4.1

where ρ_k is the weight of mechanism k,
v_{kv} is the vulnerability of mechanism k,
v_{ka} is the score of the anti-seismic measures of mechanism k.

- **Damage Index**

Moving on, the damage index is an evaluation of the overall level of damage of the church, based on the level of damage present in each macroelement. The damage d_k visible with respect to each mechanism is taken as a discrete value between 0 and 5, based on the Grünthal approach and the adaptation by De Matteis et al. seen in Figure 2.4.3 (De Matteis, Brando, Corlito, et al., 2019; De Matteis et al., 2016; Grünthal, 1998).

It should be commented that this method of quantifying qualitative damage assessments can be subjective; the difference between slight and moderate damage or between moderate and substantial damage may be a difficult distinction in some cases.

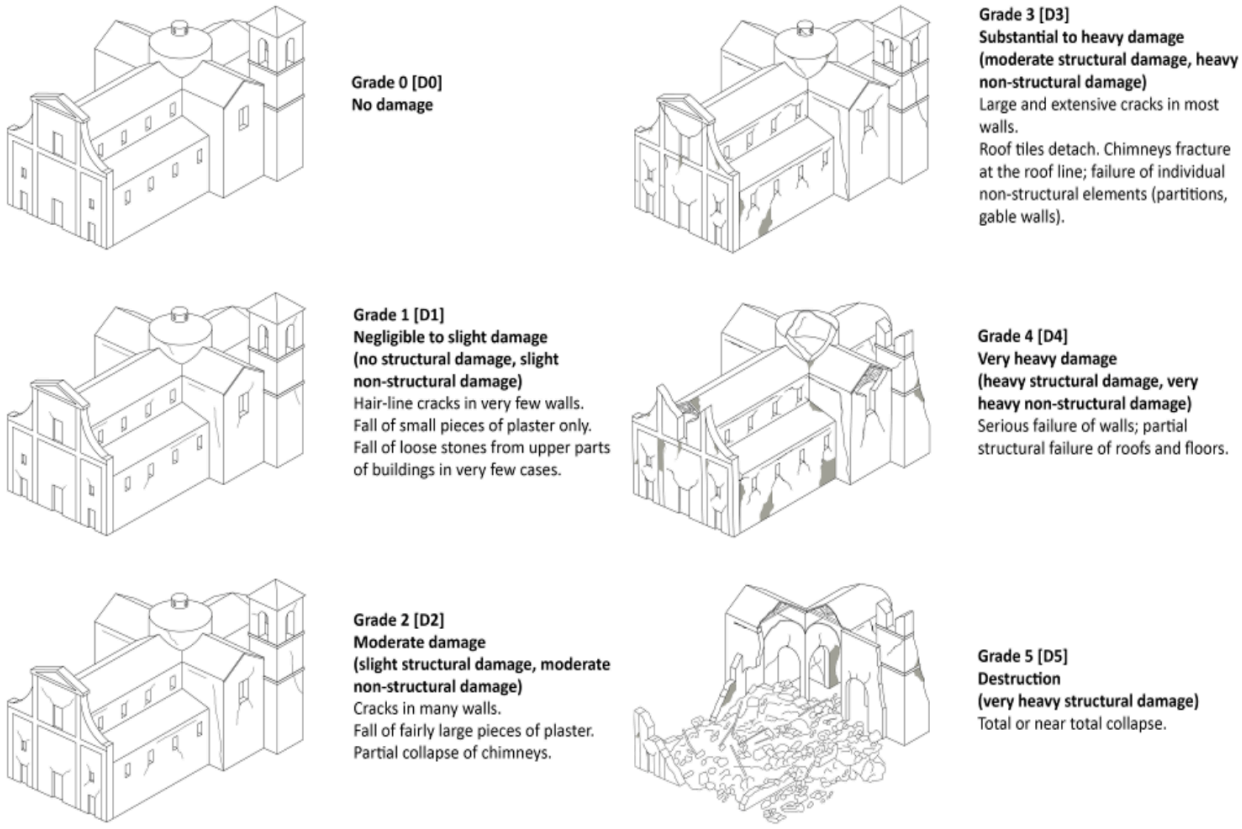

Figure 2.4.3. Damage grades applied to churches (De Matteis, Brando, Corlito, et al., 2019)

The damage state of each macroelement with regard to each mechanism was evaluated and the damage index was calculated by Equation 2.4.2. The result is a damage index between 0 and 1, where 0 indicates no damage and 1 indicates full damage or collapse. Usually, when the damage index is greater than 0.3, the church is not fit for use (Lagomarsino, 2012).

$$i_d = \frac{1}{5}\frac{\sum_{k=1}^{28}\rho_k d_k}{\sum_{k=1}^{28}\rho_k} \qquad \text{Equation 2.4.2}$$

where d_k is the visible damage corresponding to mechanism k, from 0 to 5 per Figure 2.4.3.

- **Ground accelerations for ultimate and damage limit states**

The final step presented by the Italian Guidelines is the calculation of the ground acceleration corresponding to the ultimate limit state (ULS) and the damage limit state (DLS) of the structure. The ULS intends to safeguard human lives in a rare, high-intensity quake. Structural damage experienced is grave, but the building maintains a residual resistance and stiffness when confronted with lateral shifting and the entire load capacity when under vertical stress. The damage limit state limits structural damage for a lower-intensity earthquake that has a major probability of occurrence relative to the ULS

earthquake. The building on the whole is not greatly damaged in a way that justifies the interruption of use following an earthquake (G.U. no. 47, 2011).

After statistical analysis of the damage sustained in historical buildings, it was possible to define a direct correlation between seismic input and revealed vulnerability. Equation 2.4.3 and Equation 2.4.4 calculate a ground acceleration value for each church which causes the DLS and the ULS respectively (G.U. no. 47, 2011).

$$a_{DLS} = 0.025 \cdot 1.8^{2.75-3.44i_v} \quad \text{Equation 2.4.3}$$

$$a_{ULS} = 0.025 \cdot 1.8^{5.1-3.44i_v} \quad \text{Equation 2.4.4}$$

- **Damage prediction and fragility curves**

Eventually, the desired goal is to make predictions about the possible behavior of the structure in future earthquakes. The damage index calculated per Equation 2.4.2 can be related to a damage score 0 to 5 for the entire church. (De Matteis, Brando, Corlito, et al., 2019) studied the damage scores for single elements and for a group of Italian churches as a whole. Damage probability matrices were obtained which give the frequency of occurrence of different damage levels. A binomial probability distribution function (BPDF) from (Lagomarsino & Podestà, 2004b) was found to describe the probability of each damage level in the churches and in the macroelements. The adopted BPDF is:

$$p_k = \frac{5!}{k!(5-k)!}\left(\frac{\mu_D}{5}\right)^k\left(1-\frac{\mu_D}{5}\right)^{5-k} \quad \text{Equation 2.4.5}$$

where μ_D is the mean damage level (Equation 2.4.6).

The mean damage level can be calculated based on the vulnerability index. It should be noted, as was mentioned in Section 2.3, that the curve was calibrated for three-nave Italian churches, but the churches studied herein are considered sufficiently similar. With Equation 2.4.6, also from (Lagomarsino & Podestà, 2004b), we can plot the mean damage expected for each earthquake intensity and vulnerability level.

$$\mu_D = 2.5\left[1 + tanh\left(\frac{I+3.4375\cdot i_v-8.9125}{3}\right)\right] \quad \text{Equation 2.4.6}$$

where I is the intensity of the earthquake, on the European Macroseismic Scale EMS-1998.

Finally, fragility curves can be created. They demonstrate the probability of a certain damage level being attained or exceeded given a certain seismic intensity. For each damage level D_k, using the probability

function discussed before, these curves can be derived as per (De Matteis, Brando, Corlito, et al., 2019). This means graphing the probability of attaining a certain level of damage [$P(D = D_k);\ 1 \leq D_k \leq 5$] or exceeding a certain level of damage [$P(D \geq D_k);\ 1 \leq D_k \leq 5$] as a function of the macroseismic intensity, considering the value of expected mean damage given by Equation 2.4.6. Fragility curves can be used to strategically compare building vulnerabilities based on the expected intensity for the region, and by recalculating the vulnerability index for the structure after a proposed intervention, one can see how the expected damage would decrease.

2.5. The kinematic limit analysis method

2.5.1. Background of the kinematic limit analysis method

Many times, churches are globally stable but possess some weak structural elements that will fail before an overall structural failure occurs. Therefore, it is useful to find the capacity of these elements individually. The kinematic limit analysis method is based on the analysis of local collapse mechanisms of macroelements. For this reason, it is considered as a Level 2 (LV2) analysis method in the Italian Guidelines (G.U. no. 47, 2011). The calculations for this method derive from the Circolare of the NTC-2018, chapter 7: "Design for Seismic Actions" (NTC, 2019).

This thesis focuses on the overturning mechanism, since out-of-plane overturning has been seen to be the most frequent mechanism in previous earthquakes (Penna et al., 2019).

Many studies have used the kinematic limit analysis method, including (Cattaneo, 2014). The basic idea of the method is assuming a portion of the structure acts as a rigid body, with plastic hinges forming at the edges. Of course, the element may not exactly follow rigid body movement, but the assumption suffices since the masonry is not an elastic, isotropic or homogeneous material. A capacity curve will be developed and then evaluated in relation to the demand spectrum.

It is important to consider the weight of the wall and the compression resistance of the masonry in the calculation, because by excluding them in simplified calculations Cattaneo, 2014 performed for the transverse vibration of the nave, he obtained values differing by over 30%. He found the slenderness to be a key indicator in the capacity of elements. The more slender elements had lower activation accelerations. He found this trend to be clear even for churches of different typologies.

2.5.2. Objectives of the kinematic limit analysis method

The kinematic limit analysis method is a way to analyze specific macroelements of a structure which may be its most vulnerable components. In this way, the structure's susceptibility to local failures can

be characterized. After calculating the capacities of all possible failure mechanisms for a macroelement, the governing collapse mechanism is the one for which the activation acceleration is the smallest.

The method essentially involves a calculation of the seismic capacity of one macroelement according to a given failure mechanism, i.e. the capacity of the facade in relation to out-of-plane overturning. The capacity curve is obtained in terms of the relation between the base shear of the structure and the displacement of a chosen control point. Then, this capacity curve can be evaluated against the seismic demand, represented by the appropriate response spectrum. The goal is to determine the ground acceleration necessary to activate each mechanism and assess the level of performance achieved by way of finding a performance point (NTC, 2019). From the performance point (described further in the following section), the expected level of damage can be attained based on (Milutinovic & Trendafilosk, 2004).

2.5.3. Explanation of the kinematic limit analysis method

The considered collapse mechanisms are the same as those evaluated in the vulnerability analysis method and proposed in the Italian Guidelines (G.U. no. 47, 2011). For each mechanism, some structural element of the macroelement is identified as undergoing rigid body motion. For example, consider the wall in Figure 2.5.1. The entire wall is undergoing rigid body motion, and it is considered as a single block with weight P_1; width b_1; and the following forces acting on it: roof or vault load N_1, horizontal thrust component from the vault N_{1o}, and tie rod T_1. The multiplier α_0 is found by applying $\alpha_0 P_1$ as a horizontal force at the center of gravity, to activate the kinematic mechanism.

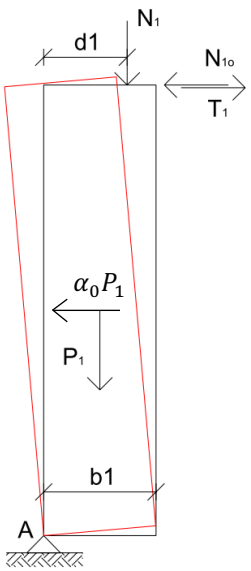

Figure 2.5.1. Diagram of wall overturning kinematic mechanism (Benincà et al., 2009)

- **Capacity curve**

Following the Circolare section C7.3.4.2 for nonlinear static analysis, this analysis begins with determining the capacity curve of the structure (NTC, 2019). The capacity curve is usually expressed by the relation $F_b - d_c$, where F_b is the base shear and d_c is the displacement of any chosen control point, usually the mass center of the highest block involved in the mechanism. For ease of calculation, the capacity curve here will be dealt with in terms of base acceleration α instead of base shear. The base shear can be obtained from α by multiplying by the weight of the elements taking part in the mechanism.

To perform a rigid body analysis of local mechanisms, Circolare section C8.7.1.2.1 will be used (NTC, 2019). First, the $\alpha - d_c$ curve is obtained through nonlinear kinematic analysis; it represents the capacity curve for the real system. The theory of virtual work is applied to obtain the multiplier α_0 (Equation 2.5.1), where the horizontal force $\alpha_0 P_1$ activates the mechanism. Displacement is normalized considering the maximum displacement of the mass center of the highest block to be 1. Then, increasing displacements are assumed and the value of α calculated for each one until $\alpha = 0$. This is the inelastic portion of the capacity curve.

$$\alpha_0 = \frac{\sum_{k=1}^{N} P_k \delta_{Py,k} - \sum_{k=1}^{m} F_k \delta_{F,k} + L_i}{\sum_{k=1}^{N} (P_k + Q_k) \delta_{PQx,k}} \qquad \text{Equation 2.5.1}$$

where N is the number of blocks making up the macroelement;

m is the number of external forces, assumed independent of seismic actions, applied to different blocks;

P_k is the weight force of the k-th block, applied at its mass center;

Q_k is the resultant of the weight forces not weighing on the k-th block but whose mass generates on it a horizontal seismic force, not effectively transmitted to other parts of the building;

F_k is the generic external force applied to one of the blocks; these forces can favor the activation of the mechanism (for example thrusts of vaults) or hinder it (for example, arcs of contrast, or attraction forces that develop in the presence of parts of the building not involved in the mechanism);

$\delta_{Py,k}$ is the vertical virtual displacement of the center of gravity of the self-weight P_k forces, acting on the k-th block, assumed positive if upward;

$\delta_{F,k}$ is the virtual displacement of the point of application of the external force F_k, projected in the same direction (of positive or negative sign depending on whether it acts with or against the mechanism);

$\delta_{PQx,k}$ is the horizontal virtual displacement of the mass center of horizontal forces $\alpha(P_k + Q_k)$ acting on the k-th block, assuming as positive direction that of the seismic action that activates the mechanism;

L_i is the total work of any internal forces (e.g. lengthening of a chain or tie-rod).

In the end the real structure must be associated to an equivalent one with a single degree of freedom. To determine the force - displacement curve of the equivalent system, the nonlinear kinematic approach can be used (NTC, 2019). The following equations (Equation 2.5.2, Equation 2.5.3) convert the acceleration and displacement to those of the equivalent nonlinear single degree of freedom oscillator. They assume the wall is infinitely rigid before the mechanism forms.

$$a = \frac{\alpha(d_c)}{e^* FC} \qquad \text{Equation 2.5.2}$$

$$d = d_c \frac{\sum_{k=1}^{N}(P_k+Q_k)\delta_{PQx,k}^2}{\delta_{Cx}\sum_{k=1}^{N}(P_k+Q_k)\delta_{PQx,k}} \qquad \text{Equation 2.5.3}$$

where FC is the confidence factor given in Equation 2.5.5,

δ_{Cx} is the virtual horizontal displacement of the control point, like $\delta_{PQx,k}$, starting from the initial undeformed configuration;

and e^* is the fraction of mass participation which, in the first approximation, can be evaluated considering the virtual displacements relating to the kinematic mechanism (starting from the undeformed configuration) as representative of the mode of vibration of the local mechanism:

$$e^* = \frac{\left[\sum_{k=1}^{N}(P_k + Q_k)\delta_{PQx,k}\right]^2}{\left[\sum_{k=1}^{N}(P_k + Q_k)\right]\left[\sum_{k=1}^{N}(P_k + Q_k)\delta_{PQx,k}^2\right]} \qquad \text{Equation 2.5.4}$$

where $P_k, Q_k, \delta_{PQx,k}$ are as defined for Equation 2.5.1.

The confidence factor per Table 4.1 of the Italian Guidelines is calculated based on the level of knowledge. For the geometric survey, the availability of drawings and development of a crack map led to partial confidence factor $F_{C1} = 0$, but the level of research was low for material and construction survey ($F_{C2} = 0.12$), mechanical properties ($F_{C3} = 0.12$), and terrain and foundations ($F_{C4} = 0.06$). Equation 2.5.5 yields the value of $FC = 1.3$ for the cases studied (G.U. no. 47, 2011).

$$FC = 1 + \sum_{k=1}^{4} F_{Ck} \qquad \text{Equation 2.5.5}$$

where F_{Ck} are the partial confidence factors for different aspects of the structure.

The above equations will give the inelastic portion of the curve, which is valid if the body is assumed completely rigid prior to the mechanism forming. However, an elastic branch can be calculated if there is assumed to be some elastic deformation before the mechanism begins. For kinematic analysis,

Circolare section C8.7.1.2.1.2 describes the method of obtaining the elastic portion of the curve (NTC, 2019).

$$a_e = \frac{4\pi^2}{T_0^2} d \qquad \text{Equation 2.5.6}$$

$$T_0 = k\lambda L \sqrt{\frac{W}{Eg}} \qquad \text{Equation 2.5.7}$$

where k is a coefficient of the value 6.2 for cantilevered elements and 2.2 for mechanisms undergoing vertical bending;

L is the height of the element;

λ is the slenderness of the element (ratio between length L and thickness b);

W is the specific weight of the masonry;

E is the modulus of elasticity of the masonry.

The elastic and inelastic curves are combined to give the full capacity curve of the nonlinear SDOF equivalent system. The inelastic curve undergoes a displacement shift to meet the elastic curve at the yield point (d_y, a_0), where $a_0 = \frac{\alpha_0}{e^* FC}$ is the activation acceleration of the mechanism. Thus, the yield point is the point at which the kinematic mechanism forms. Per Circolare section C7.3.4.2, the capacity curve should be truncated when $a = 0.85 a_y$. Also, it is useful to have a bilinear capacity curve, and this method of obtaining the capacity curve already yields a bilinear one (NTC, 2019).

Finally, some operation must be performed to analyze structural performance. The capacity of a structure and the seismic demand for that structure are not independent. One reason is that as demand increases, the structure eventually yields, decreasing its stiffness and lengthening its period. The seismic acceleration depends on the period, so the seismic demand changes as the structure yields. Second, a building yielding due to seismic action dissipates energy with hysteretic damping. The energy dissipates from the structure and this effective damping diminishes the displacement demand. There is a point at which the capacity of the structure matches the reduced demand for the specific earthquake. This point is called the performance point (ATC, 1996). The performance point lies on both the capacity spectrum and on a reduced spectral demand curve representing the nonlinear demand (Milutinovic & Trendafilosk, 2004). By noting the position of the performance point on the capacity curve, it can be determined whether the structure meets the required performance objectives. There are two methods to obtain the performance point of the structure, defined in the Circolare: Method A and Method B (NTC, 2019).

- **Method A: equal energy (N2) method**

The first method of finding the performance point is Method A, commonly called the N2 method and also laid out by (Fajfar, 2000). It should be noted that the method underwent a few changes from the NTC-2008 to NTC-2018 codes.

Method A of the Circolare suggests using a capacity curve that is bilinear with the first part elastic and the second part perfectly plastic. However, since a bilinear elastic - inelastic curve was derived in the previous section, analysis will proceed with this curve. The elastic period of the bilinear system is given by Equation 2.5.8.

$$T^* = 2\pi\sqrt{\frac{m^*}{k^*}} \qquad \text{Equation 2.5.8}$$

where $m^* = \Phi M \tau$ (Φ being the vector representing the first vibrational modal displacements, M being the mass matrix, τ being the vector corresponding to the direction of the earthquake considered);

k^* is the stiffness of the elastic section of the bilinear curve.

Now the maximum displacement demand, and the performance point of the equivalent system, d^*_{max}, can be found. If $T^* \geq T_C$, the displacement demand of the inelastic system is assumed to be equal to that of an elastic system of the same period ($d^*_{e,max}$):

$$d^*_{max} = d^*_{e,max} = S_{De}(T^*) \qquad \text{Equation 2.5.9}$$

where $S_{De}(T^*)$ is the displacement demand for the period T^*, obtained from a response spectrum defined later in this section.

For $T^* < T_C$, the displacement demand for the inelastic system is greater than that of the elastic system of the same period and is obtained by:

$$d^*_{max} = \frac{d^*_{e,max}}{q^*}\left[1 + (q^* - 1)\frac{T_C}{T^*}\right] \geq d^*_{e,max} \qquad \text{Equation 2.5.10}$$

where $q^* = S_e(T^*)m^*/F^*_y$;

F^*_y is the yield force of the equivalent system.

- **Method B: equivalent damping or capacity spectrum method**

Method B has been explained in many sources, including the ATC-40 and FEMA-273 (ATC, 1996; FEMA, 1997). In Method B, the performance point is obtained with an iterative process. It is necessary to present the demand spectrum in the spectral ordinates (ADRS) format, or the $a - d$ plane with the

spectral acceleration S_e represented in functions of the spectral displacements S_{De}, obtained by Equation 2.5.11 from the NTC-2018 (NTC, 2018).

$$S_{De}(\mathrm{T}) = S_e(\mathrm{T})\left(\frac{T}{2\pi}\right)^2 \qquad \text{Equation 2.5.11}$$

where T is the period of the structure.

A first assumption for the performance point is that the displacement d^*_{max} is equal to the displacement of an elastic structure of the same initial stiffness of the analyzed structure, d_e. However, ATC-40 states that any point may be used based on engineering judgment (ATC, 1996). For the most part, Equation 2.5.12 was used for the first assumption during the analysis performed in this paper.

$$d^{*(0)}_{max} = d_e = S_{De}(T^*) \qquad \text{Equation 2.5.12}$$

The capacity curve of the equivalent system $F^* - d^*$ is substituted by a bilinear equivalent curve (using energy terms), if the curve is not already bilinear. It is obtained by setting the first section with a slope equal to the initial stiffness of the structure, identifying the F^*_y force and the slope of the $F^*_y - d^*_{max}$ tract, and imposing equality of the area subtended by the two curves.

The associated equivalent viscous damping ξ_{eq} is expressed as a percent (Equation 2.5.13).

$$\xi^{(1)}_{eq} = k\frac{63.7\left(F^{*(0)}_y d^{*(0)}_{max} - F^{*(0)}_{max} d^{*(0)}_y\right)}{F^{*(0)}_{max} d^{*(0)}_{max}} + 5 \qquad \text{Equation 2.5.13}$$

where k is a coefficient that takes into account the dissipative capacity of the material and its hysteresis characteristics whose values are given in Circolare Section C7.3.4.2 (NTC, 2019).

Then the damping correction factor η is modified by Equation 2.5.15 and updated in the equations of the demand spectrum to reduce it.

$$\eta = \sqrt{\frac{10}{\xi^{(1)}_{eq} + 5}} \qquad \text{Equation 2.5.14}$$

The intersection, in the $a - d$ plane, of the reduced demand spectrum and the capacity curve of the equivalent system is the new performance point, shown in Figure 2.5.2. If the new performance point is characterized by a displacement $d^{*(1)}_{max}$ relatively close to that of the previous iteration, $d^{*(0)}_{max}$, the iterative procedure is complete and the solution has been reached. If not, the bilinear curve is recalculated for

the displacement $d_{max}^{*(1)}$ and damping $\xi_{eq}^{(1)}$ and the procedure is repeated. The final answer is the performance point $(F_{max}^{*}, d_{max}^{*})$ (NTC, 2019). For this analysis, "relative closeness" of the displacements is chosen to be 0.001 m.

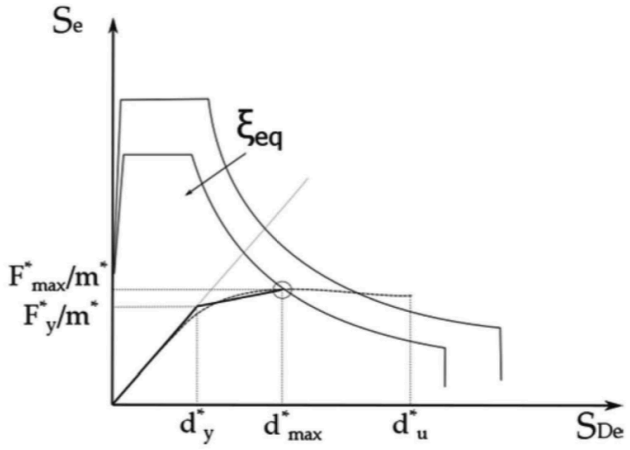

Figure 2.5.2. Reduction of the demand spectrum

- **Response spectra**

The seismic code of Spain, Norma de Construcción Sismorresistente (NCSE-02), and Eurocode 8 both provide a response spectrum for the location of the churches studied.

Chapter 2 of NCSE-02 provides the response spectrum for calculations in the Spanish territory (Álvarez-Cascos Fernández, 2002). The calculated seismic acceleration a_c (Equation 2.5.15) is first calculated and then used to scale the response spectrum given by Equation 2.5.16 and Equation 2.5.17.

$$a_c = S \cdot \rho \cdot a_b \qquad \text{Equation 2.5.15}$$

where a_b is the basic seismic acceleration, from Annex 1 of NCSE-02;
ρ is the nondimensional risk coefficient based on the importance of the structure;
S is the terrain amplification coefficient, from Section 2.2 of NCSE-02.

The normalized elastic response spectrum for horizontal accelerations corresponding to a simple linear oscillator with 5% damping is defined by:

$$\begin{aligned} T < T_A \qquad & \alpha(T) = (1 + 1.5 \cdot T/T_A) \\ T_A \le T \le T_B \qquad & \alpha(T) = 2.5 \\ T > T_B \qquad & \alpha(T) = K \cdot C/T \end{aligned} \qquad \text{Equation 2.5.16}$$

where $\alpha(T)$ is the normalized value of the elastic response spectrum;

T is the natural period of the oscillator [s];

K is the coefficient of contribution based on the type of earthquakes expected, and varies by region. (Values are given in Annex 1 of the NCSE-02);

T_A, T_B are characteristic periods of the response spectrum, of the values:

$$T_A = K \cdot C/10$$

$$T_B = K \cdot C/2.5$$

where C is the terrain coefficient dependent on the type of soil, from section 2.4 of NCSE-02 (Álvarez-Cascos Fernández, 2002).

Finally, the elastic response spectrum $S_e(T)$ is given by Equation 2.5.17.

$$S_e(T) = \alpha(T) \cdot \ a_c \cdot \eta \qquad \text{Equation 2.5.17}$$

where η is the damping correction factor, equal to $\eta = \sqrt{10/(5+\xi)} \geq 0.55$, where ξ is the viscous damping ratio of the structure [%].

Eurocode 8 gives a slightly different elastic response spectrum (CEN, 1998). It is given by the following expressions (Equation 2.5.18 - Equation 2.5.21).

$0 \leq T \leq T_B$ $\quad S_e(T) = a_g \cdot S \cdot \left[1 + \frac{T}{T_B}(2.5\eta - 1)\right]$ Equation 2.5.18

$T_B \leq T \leq T_C$ $\quad S_e(T) = \ a_g \cdot S \cdot \eta \cdot 2.5$ Equation 2.5.19

$T_C \leq T \leq T_D$ $\quad S_e(T) = a_g \cdot S \cdot \eta \cdot 2.5 \left[\frac{T_C}{T}\right]$ Equation 2.5.20

$T_D \leq T \leq 4s$ $\quad S_e(T) = a_g \cdot S \cdot \eta \cdot 2.5 \left[\frac{T_C T_D}{T^2}\right]$ Equation 2.5.21

where $S_e(T)$ is the acceleration value of the elastic response spectrum;

a_g is the design ground acceleration on type A ground:

$$a_g = \gamma_I \cdot a_{g,R}$$

where γ_I is the importance factor from EC8 Table 4.3 and the Spanish National Annex ;

$a_{g,R}$ is the peak reference ground acceleration for soil type A from Annex 5 of the Spanish National Annex;

S is the terrain amplification coefficient, from Table AN/2 of the Spanish National Annex;

T is the natural period of the oscillator [s];

T_B, T_C, T_D are characteristic periods of the response spectrum, according to Table AN/2 of the Spanish National Annex. ("Anejo Nacional AN/UNE-EN 1998-1," 1998; CEN, 1998).

For elements that are "secondary structures" or nonstructural elements, as defined in the NTC-2018 section 7.2.3, a modified elastic demand should be used per Circolare C7.2.3. The modification increases the demand in order to account for the high position of the element and consequential amplification of the seismic acceleration. The acceleration demand in the j-th plane of the structure relative to the i-th mode for nonstructural element a is provided by Equation 2.5.22 (NTC, 2019).

$$S_{aij} = \varphi_{ij}\Gamma_i S_i(T_i)R \qquad \text{Equation 2.5.22}$$

where $S_i(T_i)$ is the seismic demand at ground level for the structure, corresponding to the i-th mode;

Γ_i is the modal participation factor of the ith mode, given by:

$$\Gamma_i = \frac{\varphi_i^T M \tau}{\varphi_i^T M \varphi_i}$$

where φ_i is the normalized modal shape of the i-th mode, M is the mass matrix of the element, τ is the vector corresponding to the direction of the earthquake considered;

and R is the amplification factor for the nonstructural element a with damping ξ_a and period T_a supported on an element with period T_i:

$$R = \left[\left(2\xi_a \frac{T_a}{T_i}\right)^2 + \left(1 - \frac{T_a}{T_i}\right)^2\right]^{-\beta}$$

where $0.4 \leq \beta \leq 0.5$ is a factor relating to the coupling of the modes of the structure with the mode of the element, taken as 0.5 to be conservative.

- **Analyzing the performance point**

The Risk-UE method developed spectral displacement limits for the building drift ratios at the threshold of damage states (Milutinovic & Trendafilosk, 2004). The location of the performance point with a given spectral displacement determines the expected damage grade for the structural element. Table 2.5.1 presents the spectral displacements Sd_k at which each damage grade is expected to be evident in the structure.

Table 2.5.1. Threshold spectral displacement for each damage grade

Damage Grade k	**Threshold Spectral Displacement Sd_k**
0 - No damage	-
1 - Slight damage	$Sd_1 = 0.7D_y$
2 - Moderate damage	$Sd_2 = 1.0D_y$
3 - Extensive damage	$Sd_3 = D_y + 0.25(D_u - D_y)$
4 - Very heavy damage	$Sd_4 = D_u$

2.6. Catalonia

Catalonia is a region in the northeast of Spain, bordering France and Andorra (Figure 2.6.1). Geographically, it reaches the Pyrenees Mountains in the north and the Mediterranean Sea on its eastern and southeastern coast. Its capital is Barcelona. When the County of Barcelona rose in power in the 11th century, the region of Catalonia gained prominence. In the 12th century it was united under the same crown as Aragon and became a strong naval power. In the 15th century with the marriage of King Ferdinand and Queen Isabella, Catalonia became part of Spain (BBC, 2018).

Figure 2.6.1. Map of Catalonia with the locations of the monasteries (BBC, 2018)

2.6.1. Romanesque Catalonia

The 11th century in Catalonia, the beginning of the Romanesque era, was an age of prosperity when noble families were organizing a feudal society. The Carolingian empire was breaking up and European nations were forming. Christians were gradually conquering New Catalonia from the Muslims until the mid-12th century, and so the Romanesque style slowly spread from the north to the south. This explains the prevalence of Romanesque buildings in the northern regions. Lasting into the 13th century in

Catalonia, Romanesque architecture consisted of solid and sober lines, with churches mainly made of massive masonry walls upholding a barrel vault, semi-circular apses with arcatures and Lombard bands which look like pilasters (Figure 2.6.2) (Pladevall i Font & Gurri i Serra, 2014).

Figure 2.6.2. Lombard bands and arcatures on the apse of the church of the monastery of Sant Miquel de Cruïlles

There are almost 2,000 Romanesque churches in Catalonia. In total throughout the area's long Catholic history, six hundred monasteries were built (Baldiri, 2019).

Several monastic orders contributed to the plethora of churches and monasteries in the region. The Benedictine order, which took hold of Latin western Europe in the 9th century, maintained many monasteries that stimulated education, owned farms or villages, and held political and social importance in their communities (Oliver & Gresko, n.d.).

In the 12th century, a new monastic order, the Cistercian order, came about to reject the wealth and status the Benedictines had garnered. To repopulate the land that Catalonia overtook from Muslim occupation, the monks created settlements and built many churches throughout Catalonia (“The Cistercian Route,” 2019). Local nobles and royals of Catalonia and Aragon often chose to be buried in these great monasteries, and thus they often financed their construction and served as patrons. The Cistercian monastic order was disciplined and performed manual labor. The architecture reflected the monks' lifestyle; it is characterized by purity, austerity and refinement. Santa Maria de Poblet, along with Santa Maria de Vallbona de les Monges and Santa Maria de Santes Creus, today form what is called the Cistercian Route. They are part of the "second Romanesque" or "full Romanesque" style because they were built with neatly carved ashlar stones.

2.6.2. Seismicity of Catalonia

Catalonia is a land of low seismicity, reaching basic seismic acceleration values of less than 0.12g per the Spanish seismic code NCSE-02 (Álvarez-Cascos Fernández, 2002). As can be seen in Figure 2.6.3, the intensity values on the MSK scale range from V to VIII in the region, for an earthquake with a return period of 500 years.

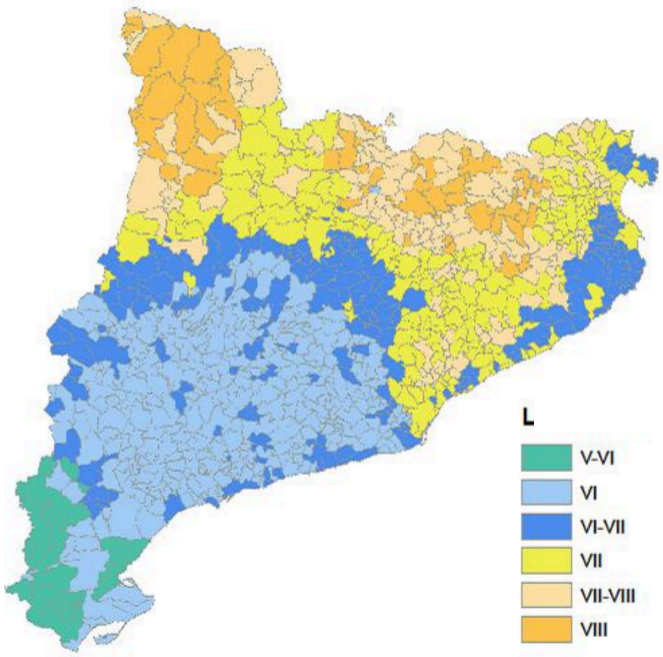

Figure 2.6.3. Intensity of earthquakes with a return period of 500 years, per municipality, considering soil effects (Generalitat de Catalunya, 2014)

2.6.3. Historic earthquakes

The most damaging earthquakes recorded in Catalonia occurred in the 14th and 15th centuries. The first series of quakes in 1373 affected the Ribagorça area. In 1427-1428 there was a series of more than a dozen earthquakes in the province of Girona. Five were rated with an epicentral intensity higher than VII. (Susagna i Vidal & Goula i Suriñach, 1999).

Three strong quakes damaged the city of Amer, Girona in March 1427, which is a city about 34 km west of Sant Miquel de Cruïlles. One severe earthquake in May 1427 has been classified with an epicentral intensity of IX and destroyed the town of Olot and registered as a V-VI in Girona, which is just 16 km west of Sant Miquel de Cruïlles. Another in February 1428 that damaged primarily the Pyrenees area was still felt at a level of VI-VII in Cruïlles and V in Vimbodí i Poblet, based on an intensity map of the event (Susagna i Vidal & Goula i Suriñach, 1999).

Over the centuries there have been many small earthquakes but not many have recorded damage. It is rather impossible to know which small earthquakes may have damaged these historic churches; for example, in June 1930 there was an intensity V earthquake in Espluga d'Francoli, close enough to harm Poblet, but damages were not noted in the Seismic Atlas of Catalonia (Susagna i Vidal & Goula i Suriñach, 1999). Only those earthquakes that were large enough to cause recordable damage are marked in Figure 2.6.4.

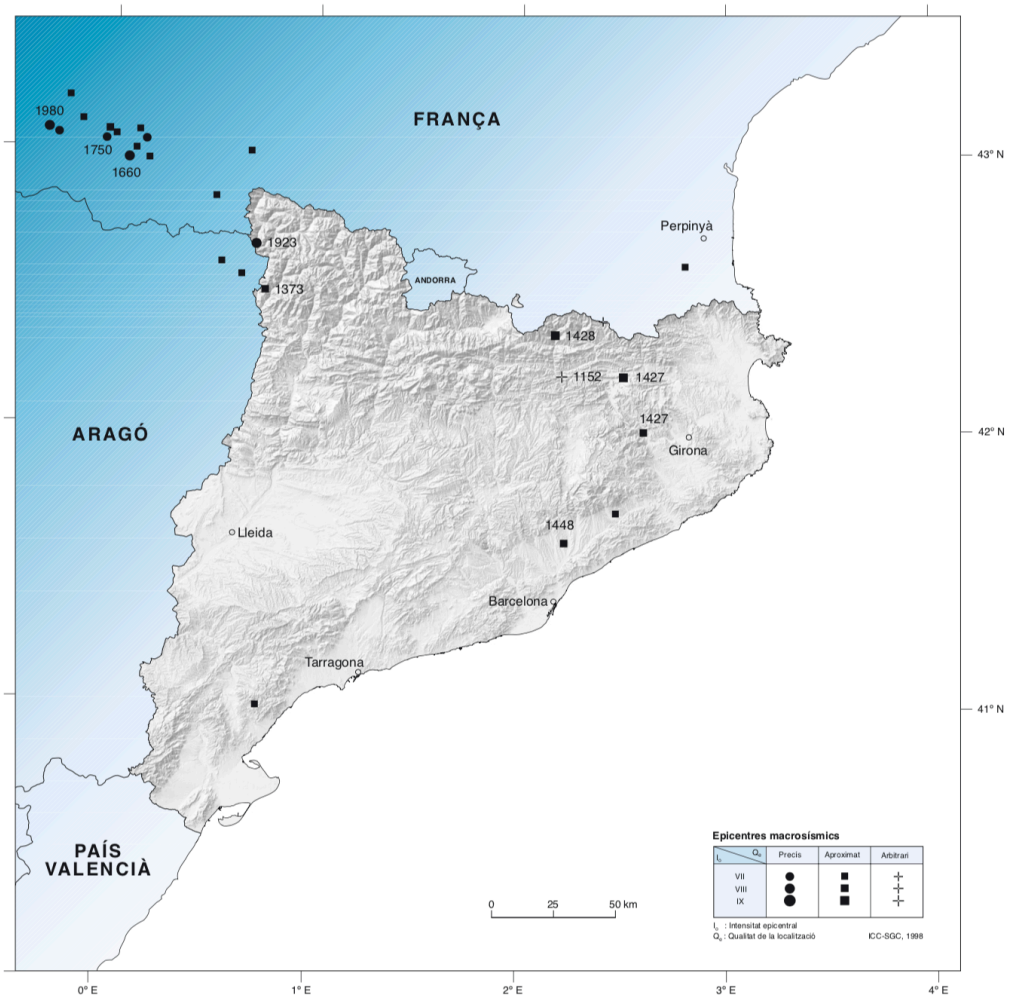

Figure 2.6.4. Epicenters of damaging earthquakes from historical times to the present in Catalonia, $I_o \geq$ VII (Susagna i Vidal & Goula i Suriñach, 1999)

2.7. Monastery of Santa Maria de Poblet

The first case study considered in this report is the church of the well-preserved Cistercian monastery of Santa Maria de Poblet, referred to as Poblet from here on. This monastery boasts a grand complex, which had many uses throughout history for the military and nobles, as a royal palace, residence and pantheon hosting the tombs of several Aragon royals. Today it is a UNESCO World Heritage site.

2.7.1. Location

The monastery of Santa Maria de Poblet is located in the region of Conca de Barberà, province of Tarragona, town of Vimbodí i Poblet. Figure 2.7.1 pinpoints its location east of Barcelona and north of Tarragona. It lies in a rural area at the feet of the Prades mountains, near the river Sec. The soil is considered a soft deposit 5 to 20 meters deep, in contact with hard rock (Generalitat de Catalunya, 2018).

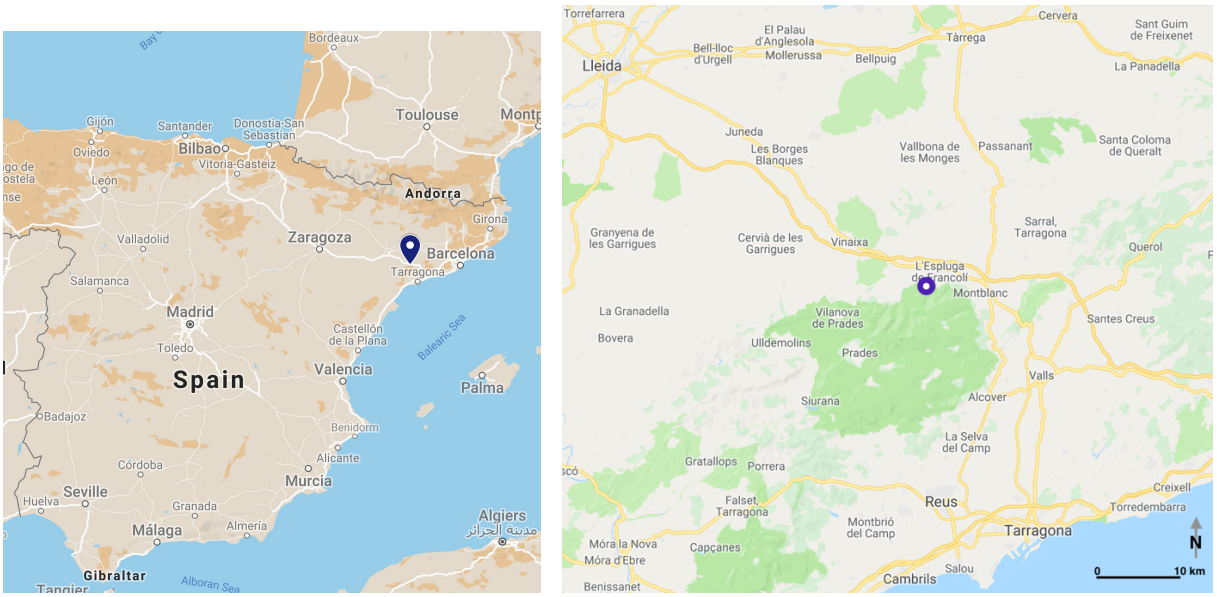

Figure 2.7.1. Location of the Monastery of Santa Maria de Poblet (“Google Maps,” 2019)

2.7.2. History

The first documented reference to Poblet monastery is in 1150, when Ramon Berenguer IV, Count of Barcelona, donated land and brought monks from Fontfroide to Poblet (Cobreras, 2003; Vigué, 1995). Ramon de Cardona and other local nobles gave a large donation in 1151. In 1166 the order was given to start construction. Construction of the church began in 1170 with the apse, which was completed in 1196. Then construction progressed to the transept, the nave and the aisles, which were finished in 1276 (Saloustros, 2013). In 1180 the chapel of Esteve and the infirmary were built, and probably the refectory (Godes & Adell, 2001; Vigué, 1995).

In the 13th century construction continued on the rest of the buildings: sacristy, capitular roof, monk dormitories, cloister. The years of the abbot Ponç de Copons, 1316 - 1348, were a time of prosperity when the library grew, the monastery held significant control in the region, and new constructions were added (Cobreras, 2003; Godes & Adell, 2001; Vigué, 1995). Abbot Ponç constructed the atrium of the entry (north of the church) and started the cimborio (Godes & Adell, 2001). During this era, King Pere

III created the royal pantheon, which elevated the status of the monastery in the region (Vigué, 1995). The southern aisle was demolished and rebuilt during this time, possibly to create side chapels for wealthy families. The aisle was rebuilt in the Gothic style with a rectangular massive ribbed vault. It was either completely demolished and reconstructed, with or without a timber stabilizing structure; or, it was taken down and rebuilt one bay at a time (Saloustros et al., 2015).

In the late 14th century King Pere III went to war with Castille and felt the need to fortify important areas of Catalonia. So, he built a wall and moat at Poblet, as well as the towers of Armes and Sant Esteve. The walls are impressive – two meters thick, about 11 m tall and with a perimeter of 608 m (Vigué, 1995). The Porta Reial was the only door in the wall and was finished in 1399 (Godes & Adell, 2001). The church was thus closed off to the outside until the end of the 18th century when the current Baroque church door was built and connected to the church portal via the gallery (Vigué, 1995).

Poblet experienced some significant seismic events in the 14th and 15th centuries. The fifteenth century saw the construction of the chapel of Saint Jordi and the Porta Daurada, now the main entrance to the monastic complex. In 1575, fire damaged the choir and the organ, and damaged the first vault from the transept. In 1666-68 Pere Antoni d'Aragó, viceroy of Naples, donated to the library and financed the bell tower (Vigué, 1995). An earthquake in 1792 is reported to have produced damage to the church as well as other parts of the monastery, like the dormitory located at the northern part of the transept (Saloustros et al., 2015).

In 1809 the monastery was sacked by the French (Godes & Adell, 2001). In 1813 the monks returned, but obligatory secularization and abandonment of the monastery occurred in 1822. Fires burned the organ, which sat in the high choir, and there was damage to the bay farthest from the transept (Vigué, 1995). In 1823-1830 there were major strengthening works, including three flying buttresses added to support the vault of the main nave from the south side, at the 4th, 6th, and 7th bays (from the transept) and the facade (Saloustros, 2013).

In 1835 the monastery was abandoned, exploited and dismantled by the surrounding villages, and the royal tombs were moved (Godes & Adell, 2001). The land was put up for sale in 1847. Ten years later, the first attempts were made to conserve the ruins, but it wasn't until the Royal Patronage of Poblet was created in 1930 that some progress was made (Cobreras, 2003; Vigué, 1995). Poblet became a national monument in 1921 (Saloustros, 2013). During the Spanish civil war the monastery was sacked and tombs were desecrated (Cobreras, 2003). But in the 1940s and 50s, monks returned. Some works were done, including a restoration in 1941 that probably repaired the crack in the northern aisle (Saloustros et al., 2015).

The 1970s saw the restoration of the library and cimborio and towers of Armes and Saint Esteve. In the 1980s, the abbot's palace was rebuilt and the sacristy restored. The monastery became a UNESCO

world heritage site in 1991 (“The Cistercian Route,” 2019). Recent restoration works have included closing the cracks in the last bay from the transept, and repairing lost material in piers using mortar, as well as preventative interventions (Generalitat de Catalunya, n.d.-b; Saloustros, 2013). Metal elements were added in open joints, cracks and the southern piers. Now, the corrosion of these elements has caused more damage to the church. Finally, the rose window was reconstructed and some damaged voussoirs were replaced with bricks (Saloustros et al., 2015).

2.7.3. Geometry and Structure

The church of the monastery of Poblet is part of a large, beautiful monastic complex. This report will only discuss the geometry of the church. It is a large three-nave church of basilical plan. The church is made of limestone, probably of three-leaf construction with an internal rubble leaf. The original mortars are lime with gypsum and calcareous aggregates (Saloustros et al., 2015).

Plan and section views are provided in Figure 2.7.2, Figure 2.7.3 and Figure 2.7.4.

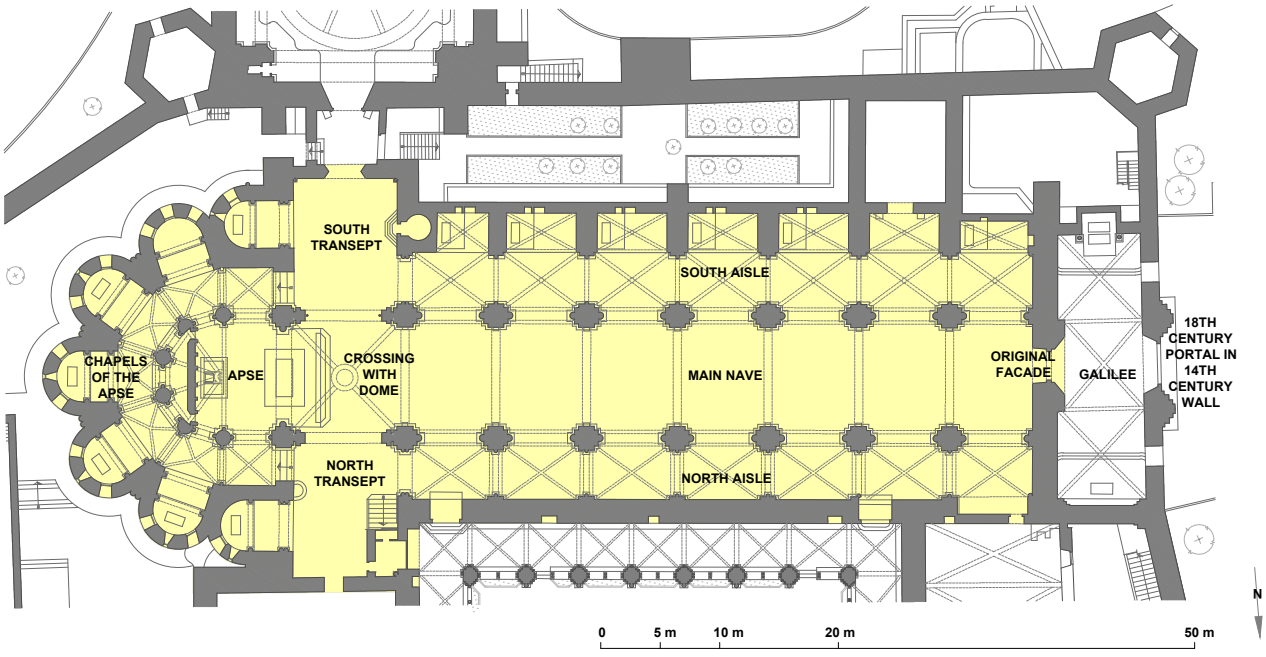

Figure 2.7.2. Plan view of the church of Poblet

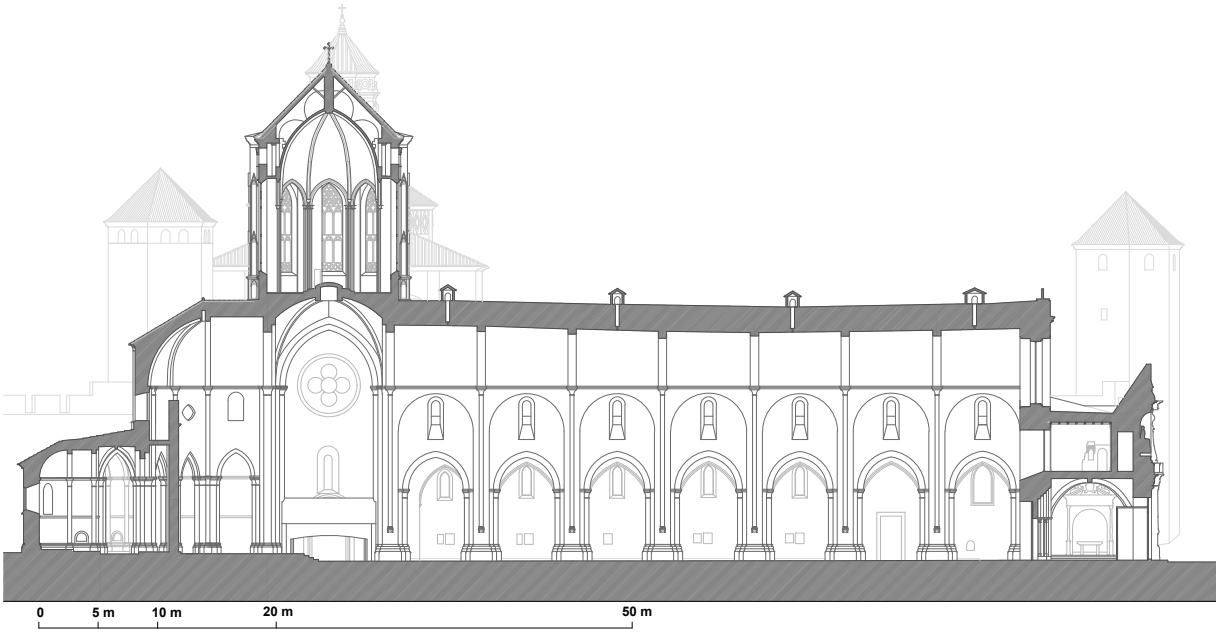

Figure 2.7.3. Longitudinal section of the church of Poblet

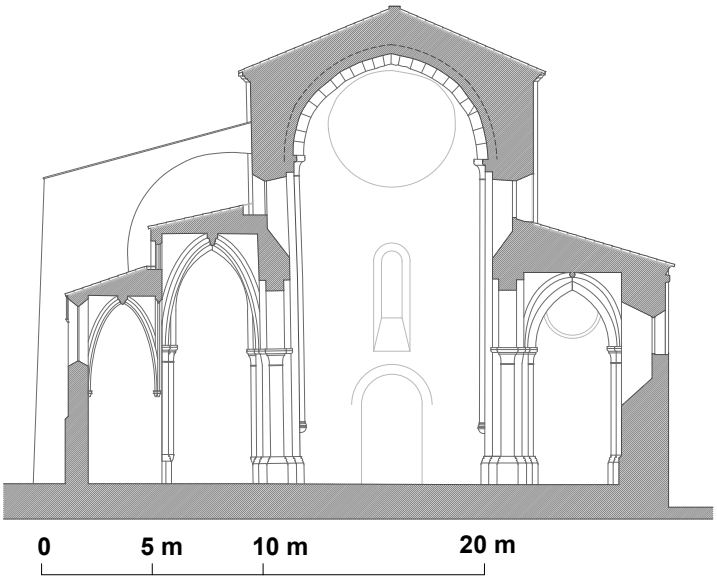

Figure 2.7.4. Transverse section of the 7th bay from the transept, which has a buttress on the south side

- **Main Nave**

Poblet has slightly pointed barrel vaults in the main nave, which is twenty meters high and has seven bays (Figure 2.7.5(a)). It has cross vaults in the lateral naves and a dome at the crossing (Figure

2.7.5(b)). Arcades of slightly pointed arches atop cruciform pillars separate the naves. Looking west, the great rose window of the main facade is visible behind the large organ. Looking east, one finds the apse.

(a) (b)

Figure 2.7.5. (a) Main nave, looking toward the facade and (b) Dome at crossing and vault of apse

- **Apse**

The apse is composed of a slightly pointed barrel vault in combination with a veined Gothic semi-dome, surrounded by an ambulatory and five chapels of the same vault configuration (Figure 2.7.6(b)). The altar is 16th-century carved alabaster (Figure 2.7.6(a)). The apse has the same height as the main nave, but the surrounding chapels are only half as tall (about 9 m).

(a) (b)

Figure 2.7.6. Poblet, (a) Renaissance altar and (b) one of the chapels surrounding the apse

- **Transept**

The transept is considerable in size. The north transept adjoins the monk dormitories and the south transept supports a small bell tower. The transept facades have a decorative window at the top. The north side appears to have a small section in the middle that was once an opening but was later filled in (Figure 2.7.7).

Figure 2.7.7. Poblet north transept facade, from the interior

On the north transept there is a large gable belfry, about 12.5 m high and 1.9 m thick (Montaner, 1925). This is noteworthy because the thickness of the wall is estimated at 1.2 m from the drawings. Thus, the gable belfry seems to be partially supported over the vault of the transept, which is not designed to take additional concentrated loads (Figure 2.7.8). Additionally, if it were to fall onto the transept it could cause damage to the vault of the transept.

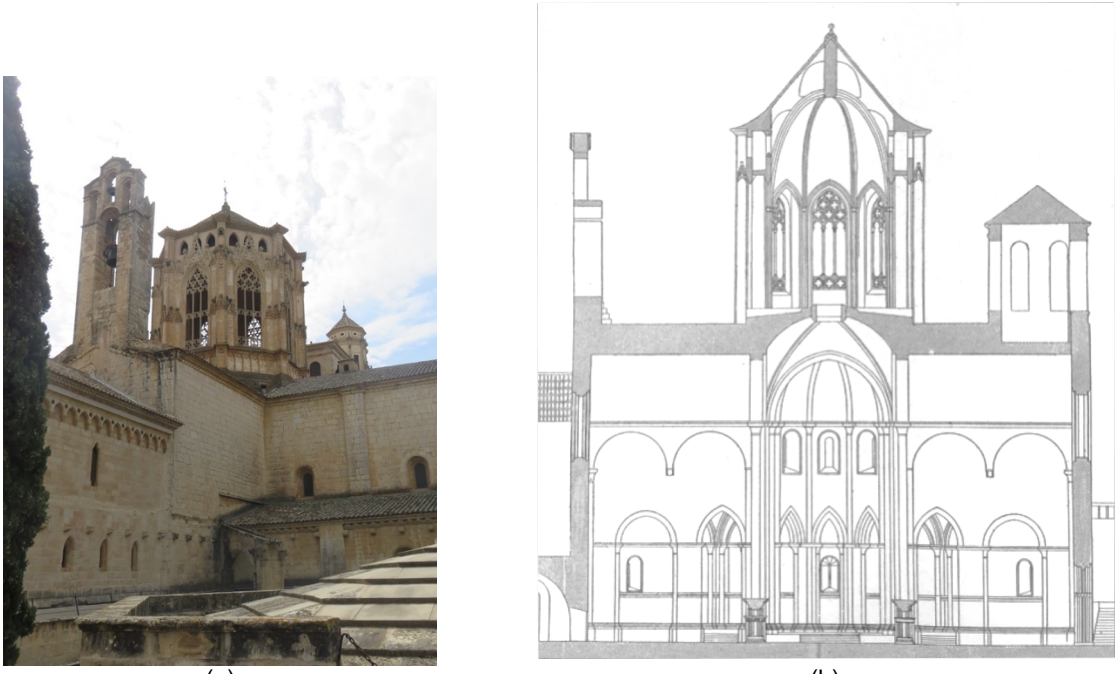

(a) (b)

Figure 2.7.8. Poblet, (a) North transept with gable belfry and (b) Transverse section of the transept (Montaner, 1925)

- **Exterior**

An interesting feature is the church's facade. A second facade was built in front of the original one in the 14th century, so there is a galilee that connects the two facades (Figure 2.7.9). This galilee is composed of cross vaults between two small chapels. However, since it is lower in height than the main nave, it may not be considered to act as bracing to the original facade in a seismic event.

The church has three flying buttresses on the south side of the main nave, rising from the south aisle. They are not evenly spaced, and they are not mirrored on the north side. They can be seen in Figure 2.7.10.

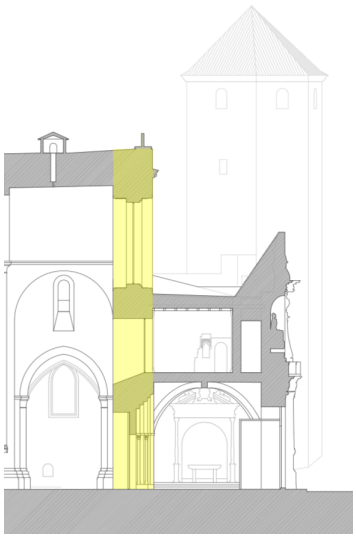

Figure 2.7.9. South-facing longitudinal section of Poblet showing original facade (highlighted) with galilee and new facade in front

(a)

(b)

Figure 2.7.10. (a) Aerial view of Poblet, looking northeast, (b) View of buttresses, looking northeast

2.7.4. Present Condition and Damage State

In the church of Poblet, deformation and some cracks were observed (**Error! Reference source not found.**). Cracks have been reported since the 16th century when they were attributed to a fire in the church. There is also a crack in the center of the main nave (Figure 2.7.12) expected to be from an earthquake in the 18th century, plus another fire that afflicted the monastery in 1822. Soil settlement could also be an issue causing some cracking. Cracks in the bay farthest from the transept are related to the separation or overturning of the facade.

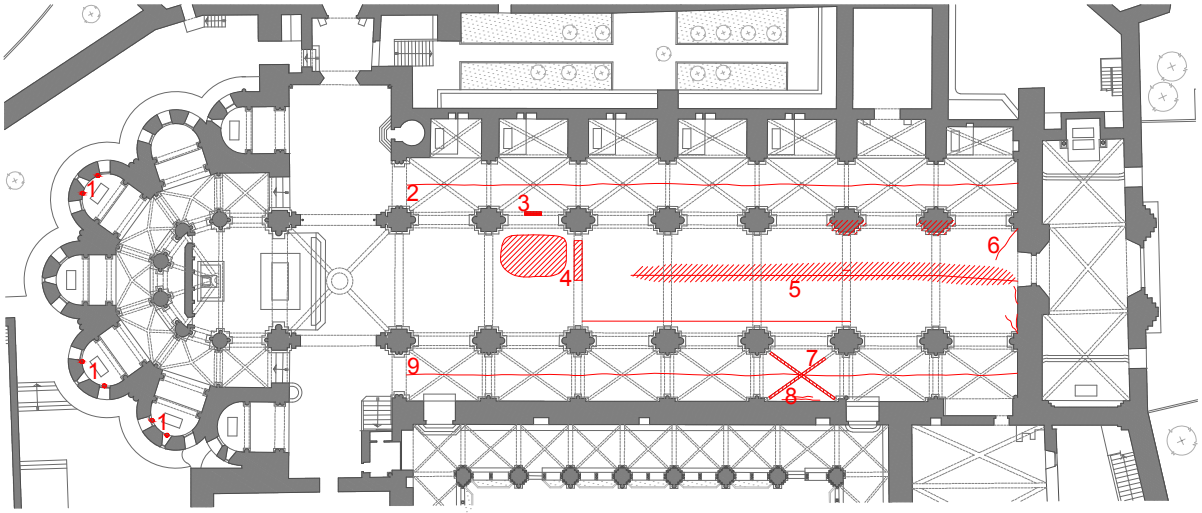

1. Hairline cracks in the chapels surrounding the apse
2. Crack in vault along south aisle
3. Exterior diagonal crack above window of main nave
4. Out-of-plane bulging of vault of the 2nd bay and deformation of adjacent arch
5. Crack and deformation along the key in the main barrel vault
6. Diagonal cracks in vault near the facade
7. Twisting deformation of vault of the 5th bay of the north aisle
8. Sabouret cracks near the window in the 5th bay of the north aisle
9. Crack in vault along north aisle

Figure 2.7.11. Damage map of the church of Poblet

Deformation can be seen in the main nave. First, out-of-plane bulging is visible in the bay second from the transept (Figure 2.7.12). The entire vault is actually deflecting downwards by as much as 50 cm, as can be seen in Figure 2.7.13. As found by Saloustros et al., this must be due to more than just the self-weight of the structure (Saloustros et al., 2015). The highest deflection is at the 5th bay from the transept. The sinking of the key of the vault is related to the outward movement of the upper walls that support the barrel vault. They deflect 14 cm horizontally at the springing of the vault in the south, and 10 cm in the north.

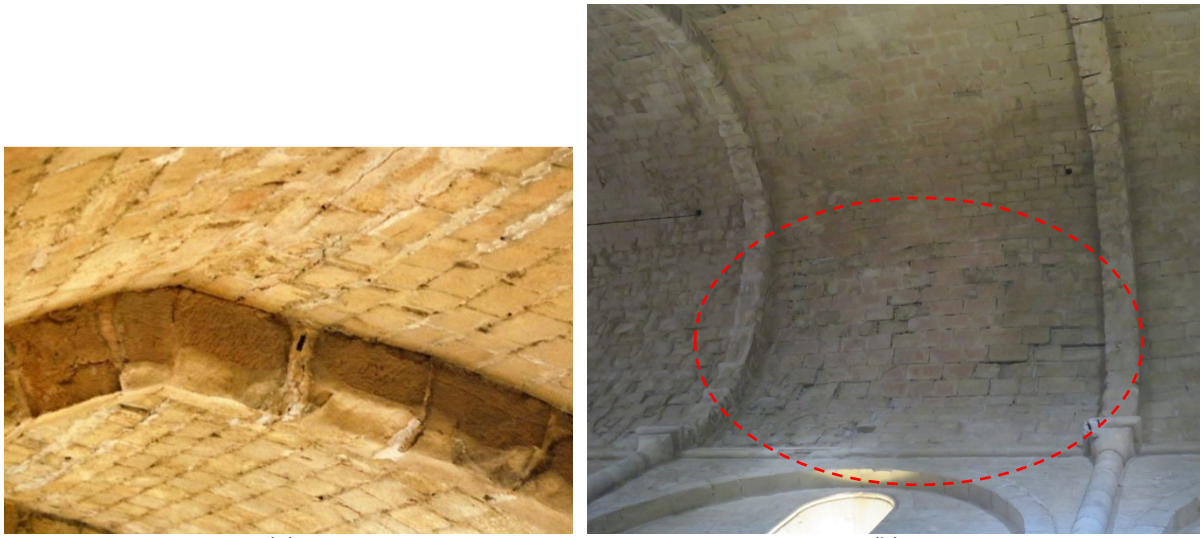

(a) (b)

Figure 2.7.12. (a) Main crack near the key of the main nave with metal element in the joint of an arch (number 5 in Figure 2.7.11); (b) second bay from transept, showing bulging deformation (number 4)

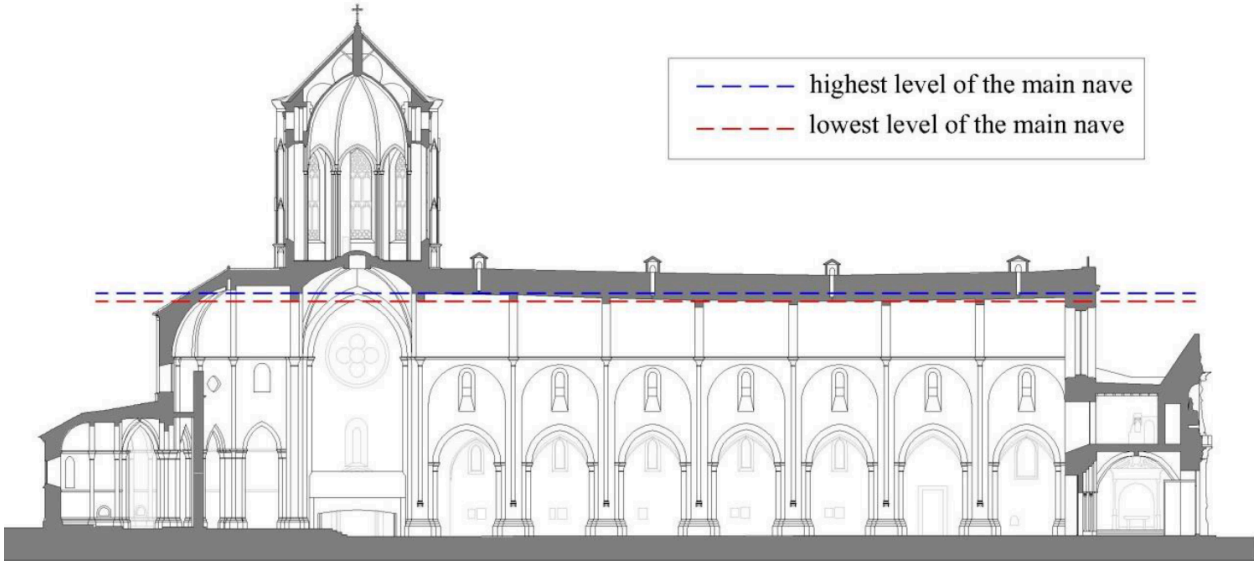

Figure 2.7.13. Deflection of the main nave of Poblet (Saloustros, 2013)

In the vaults of the main nave shown in Figure 2.7.14, there is deformation of the barrel vaults in what seems to be a four-hinge mechanism. A crack runs longitudinally along the south side of the nave, just one or two voussoirs away from the keystone. These voussoirs are misaligned in a few places. There is another longitudinal crack along the north side of the vault, just about six stones above the springing. This appears to be an area of stone crushing corresponding to hinge two in Figure 2.7.15. Hinge four would tend to push out the point of springing of the arch, which does occur, as leaning can be seen at the top of the sixth and seventh columns from the transept. Hinge formation could be caused by a factor other than asymmetric loading, such as an earthquake or foundation settlement. Savvas Saloustros examined these possibilities, which will be discussed in the next section.

Figure 2.7.14. Vaults of the main nave of Poblet

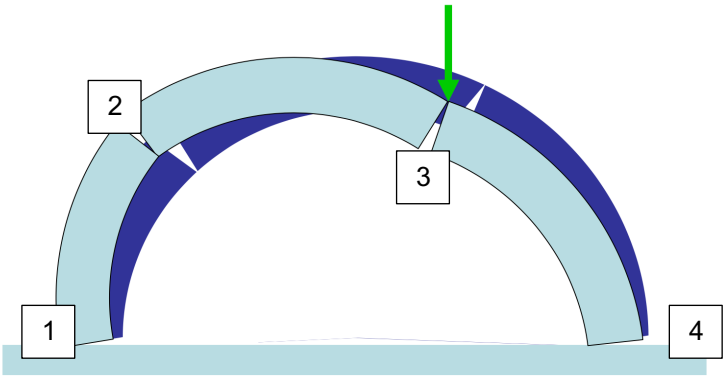

Figure 2.7.15. Typical four-hinge mechanism of an arch subjected to asymmetric geometry and/or loading

Deformation was also noticed in one of the vaults of the north aisle, in which the ribs appear to be twisting (number 7 in Figure 2.7.11). Sabouret cracks are also visible at this vault, where the vault is separating from the wall above the window (Figure 2.7.16, number 8 in Figure 2.7.11).

Figure 2.7.16. Fifth vault from transept, north aisle

There are also many thin cracks in the chapels surrounding the apse. Each crack location is marked by a dot in Figure 2.7.11 (number 1). Figure 2.7.17 shows one example of cracking in a chapel wall, which seems to have even led to the spalling of a thin layer of the stone.

Figure 2.7.17. Thin cracks in chapel wall and spalling of stones

2.7.5. Past studies on Poblet Monastery

A graphic statics analysis was performed for three bays of the church (the deformed 5th and 7th bays and a typical non-deformed bay) (Dominguez A. C., 2012). Modified assumptions had to be made in order to fit a thrust line inside the base of the piers for the 5th deformed bay.

An extensive study was performed by Savvas Saloustros et al. (Saloustros, 2013; Saloustros et al., 2014, 2015) to perform numerical analysis on the church. This was the first structural or seismic analysis to study the state of stresses and the damage causes.

In Saloustros 2013 (Saloustros, 2013), he analyzes a quarter of the fifth bay and half of the fifth bay using finite element modeling. He found possible explanations for the damage visible in the church:

- Cracking near the key of the main nave: The self-weight alone may be responsible for this tensile damage; in its present state there is a tensile stress concentration along this crack. It could also be due to removal and reconstruction of a lateral bay during the works in the early 14th century, which could have caused large deflection. It could also be due to an earthquake. It is most evident in the results of the analysis if the infill over the lateral vaults is considered to have low mechanical properties.
- Crushing in barrel vault from 3rd to 5th bays: This can be correlated to an earthquake and is probably not because of the structure's self-weight.
- Horizontal displacement of the tops of the piers and clerestory walls: Likely due to the demolition and reconstruction of the southern aisle, either one bay at a time or all at once.
- Diagonal cracks in the bay adjacent to the facade and over the southern window of the second bay: Damage caused by an earthquake caused the facade to tend to separate.
- Cracking in vaults of lateral aisles: Tensile damage could have resulted from self-weight but these cracks probably also propagated with an earthquake or settlement.
- Crushing in the lateral vaults: Due to self-weight or earthquake.

He concluded it is unlikely that settlement of the piers occurred. However, as mentioned, earthquakes could have contributed to the damage. Pushover analyses revealed that earthquakes could have led to crushing in the main and lateral naves (Figure 2.7.18). In pushover in the north direction, a hinge formed at the southern part of the main nave where a crack can be seen today. Saloustros derived four collapse mechanisms from the pushover analysis and from visible damage in the church (Figure 2.7.20). He concluded by using the pushover curve and Eurocode response spectrum that the church would resist an earthquake "with the cost of some moderate and reparable damage". In addition, a graphic statics analysis coordinated with the finite element model results found a thrust line within the bounds of the typical bay.

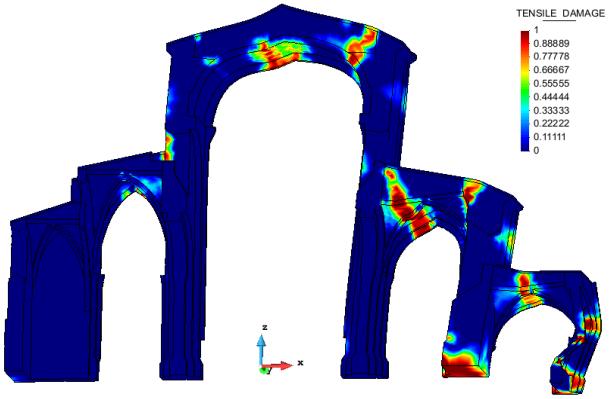

Figure 2.7.18. Tensile damage with deformation (×29) for deflection for the pushover analysis towards the north (+X), a_g=0.135g (Saloustros, 2013).

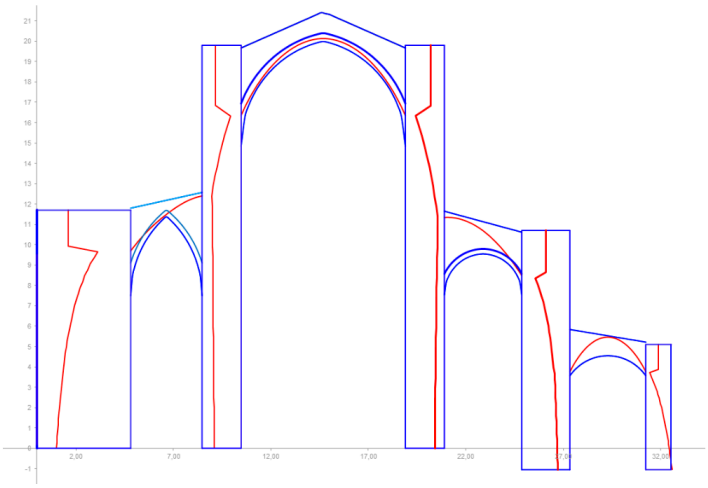

Figure 2.7.19. Graphic statics for typical bay of Poblet, performed by Pere Roca (Saloustros, 2013)

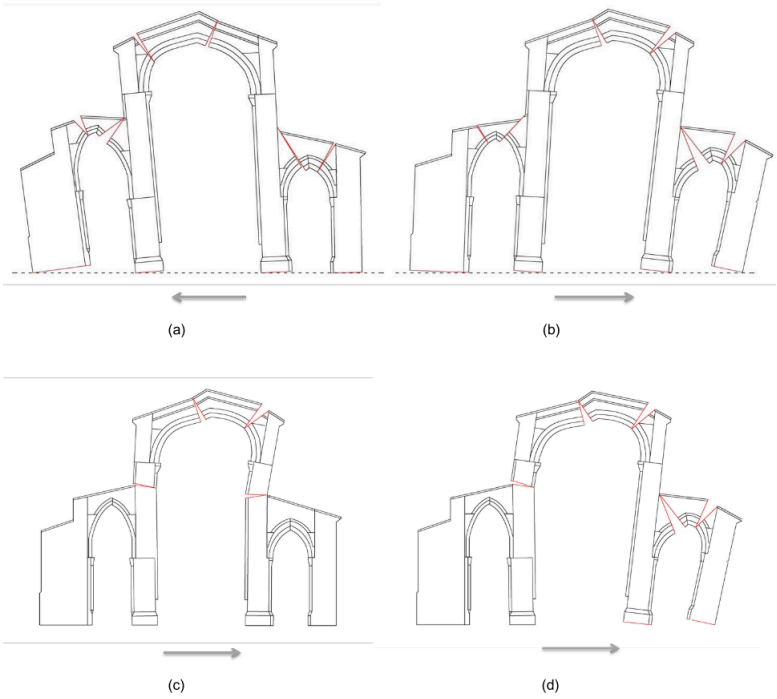

Figure 2.7.20. Possible mechanism for the arches of the main nave of Poblet (Saloustros, 2013)
(a) Pushover analysis towards south, global mechanism;
(b) Pushover analysis towards north, global mechanism;
(c) Pushover towards north, local mechanism 1;
(d) Pushover towards north, local mechanism 2.

Further research refined this model slightly and extended its analyses (Saloustros et al., 2014, 2015). It was found that if settlement occurred, the most likely case was below the northern external wall, which would have spread cracking near the key of the main nave and caused cracking at the middle height of the arch on both sides. They estimated that the reconstruction during the 14th century increased horizontal displacement of the springing of the barrel vault by 210% and the deflection at the key increased by 37% because of lack of thrust.

2.8. Monastery of Sant Miquel de Cruïlles

Not much remains today of the monastery of Sant Miquel de Cruïlles. This Benedictine monastery was much smaller in size and influence than Poblet, but home to pieces of beautiful Romanesque art including wall paintings of which fragments still remain. Today the church can only be visited by appointment.

2.8.1. Location

In the region of Baix Empordà, this monastery is located just 1 kilometer from the village of Cruïlles, on the road from Bisbal d'Empordà to Cacà de la Selva. It is in a quiet rural area near the river Daró. It is a

region of high relative humidity. The soil type in the region is soft rock or stiff soil with a depth less than 100 m (Generalitat de Catalunya, 2018). Figure 2.8.1 shows a map of the monastery's location.

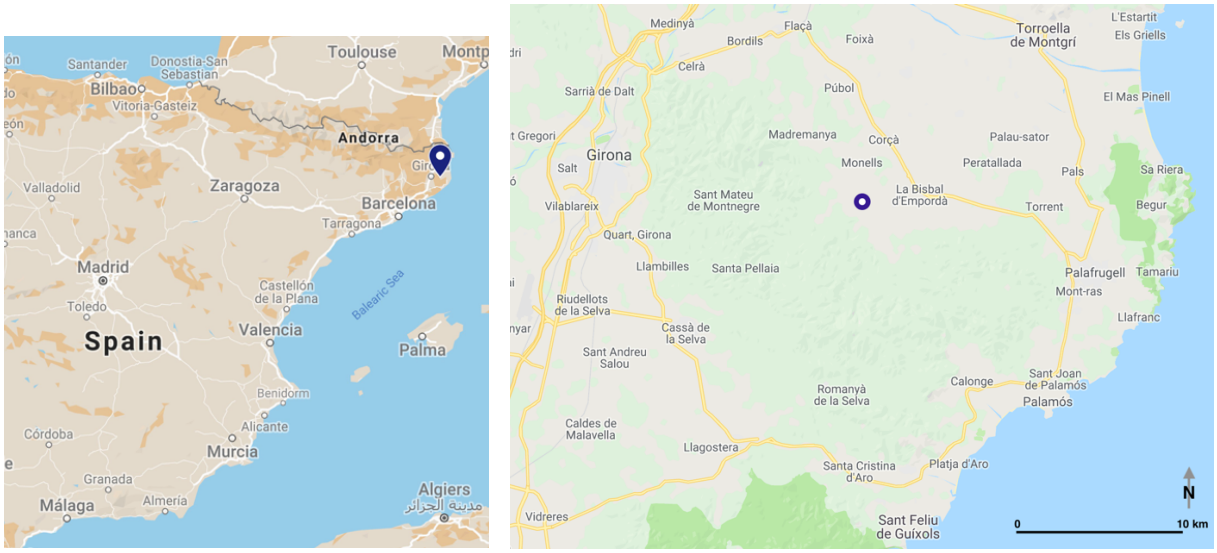

Figure 2.8.1. Location of the Monastery of Sant Miquel de Cruïlles

2.8.2. History

The age of the monastery is not precisely known, so evidence of its establishment must be searched for in historical texts. The church of Sant Miquel de Cruïlles was consecrated in 904. The building itself dates to the end of the 11th century; it was built on top of another older temple. The lords of Cruïlles donated to its construction between 1031 and 1057 (Generalitat de Catalunya, n.d.-a). In the year 1037, Countess Ermessenda of Barcelona left 30 *mancusos* to the monastery at a time when the monks were dependent on an Italian monastery. In 1102 and 1121, Berengues Amat mentioned the monastery as a primary beneficiary of his donations (Vigué, 1989). It was a Benedictine monastery (Pladevall i Font & Gurri i Serra, 2014).

In 1485 the church was sacked by the *remences*, or the serfs of Catalonia (Rotger, 2011). In 1592 Pope Climent VIII united it with Sant Pere de Galligants as a priory. (Vigué, 1989)

In 1835 the monastery was secularized, as were many churches and monasteries of Catalonia in this period, and became private (Generalitat de Catalunya, n.d.-a).

- **Construction History**

In the 11th century the construction began on the church. It is believed that the church was planned to be a single-nave church without a dome but the plan changed later on (Generalitat de Catalunya, n.d.-a; Vigué, 1989).

Construction started at the church's east corner and south arm of the transept. But before the construction of the north arm of the transept was finished, there was a change of plans in the work which altered the design to a three-nave church. Evidence for this is found in the fact that the window of the north transept was blocked by the wall of the aisle. The walls that divide the aisle from the north transept is original, built with the church. (Vigué, 1989)

The small tower at the intersection of the south transept and the nave was of the late Romanesque period (twelfth to thirteenth century), which seems to have been the base of a belfry that remains unfinished (Vigué).

In the sixteenth century, a new facade was constructed at the level of the first arch, leaving the old facade to rest in ruins. Also in this century, large buttresses were built against the lateral walls (Vigué, 1989). In the sixteenth and seventeenth centuries, the bell tower seen today was constructed. Walls were built in the arches of the aisles to form side chapels. There were probably reforms made to the small drum above the crossing (Generalitat de Catalunya, n.d.-a).

In probably the 17th century, the pavement of the central nave was lowered (Generalitat de Catalunya, n.d.-a).

The interior saw many changes throughout the years, finally being covered with plaster likely in the 18th century. In the same century, part of the southern transept was converted into a sacristy by the construction of a transverse wall (Generalitat de Catalunya, n.d.-a).

- **Recent Interventions**

In 1972 - 1974 there were restoration works that excavated the subsoil at the apse of the church, which revealed old constructions and foundations of previous presbyteries (Generalitat de Catalunya, n.d.-a; Vigué, 1989). In 1981, structural repairs were made. The massive sixteenth and seventeenth century buttresses were shortened and lowered, the arches of the main nave were stiffened and the roof was repaired. In 1995 the roof of the north transept, crossing and apse was resurfaced. In 2006, paintings were restored, and from 2008 - 2014 many archaeological restorations were done. These included raising the flooring of the nave and lowering the ventilation channels. However, more work had to be done in 2018 to treat humidity by capillary action (Generalitat de Catalunya, n.d.-a).

2.8.3. Geometry and Structure

The church was originally part of a monastic complex, of which almost nothing else remains today. One wall with arches has been preserved next to the sacristy; it used to belong to the capitular room. The monastery spread from the south of the church and was probably centralized around a cloister.

As mentioned, the church was likely planned as a single-nave church but was eventually built with lateral naves. It is easy to see from Figure 2.8.2 that there were once four bays in the nave, but today there are only three because the 16th-century facade was created by filling in the arch between the first set of columns. This arch can be seen by observing the facade (Figure 2.8.3(a)). The church measures 26.7 m from the door to the end of the apse. As can also be seen from the plan view, the exterior is marked by buttresses (Figure 2.8.2, Figure 2.8.3(b)).

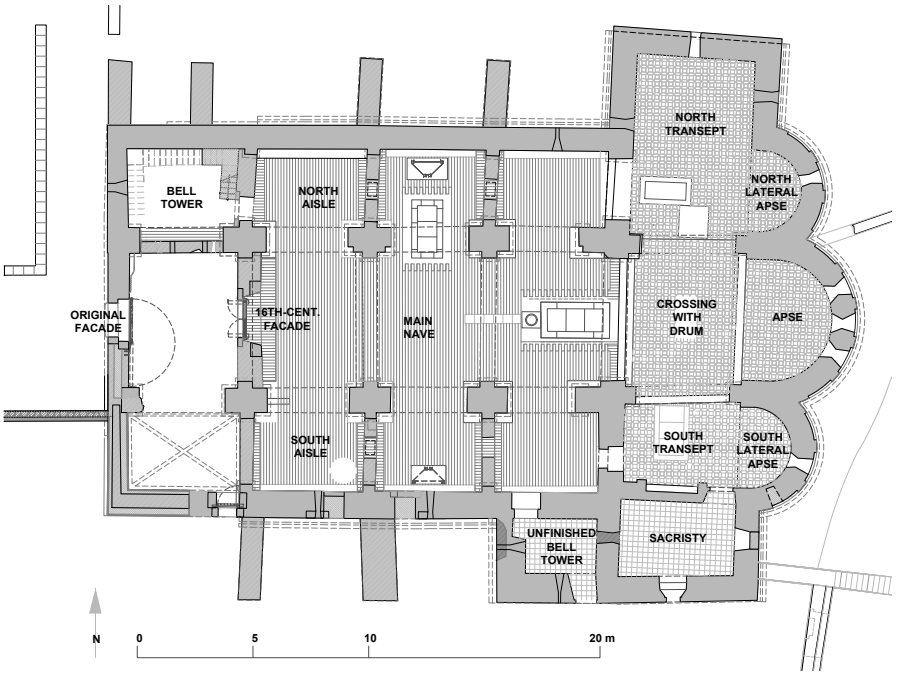

Figure 2.8.2. Plan of the church of Sant Miquel de Cruïlles

(a) (b)

Figure 2.8.3. (a) 16th-century (present-day) facade and (b) exterior buttresses on north side of Sant Miquel de Cruïlles

The church entrance opens into the barrel-vaulted main nave, where tie-rods can be seen between the second and third sets of columns, counting from the transept (Figure 2.8.4(a)). The nave is about 10 m tall. The aisles also have barrel vaults and are about 7 m tall. They are broken up into chapels by the transverse dividing walls at each column, which can be seen in Figure 2.8.4(b). There is a central apse and two lateral apses, all semi-circular with a half dome vault (Figure 2.8.5). The transept houses a barrel vault and on the south side leads to the sacristy. It is about 8 m tall. At the crossing of the transept and the nave there is a dome with squinches (Figure 2.8.6). The dome has a drum around it visible from the exterior.

(a) (b)

Figure 2.8.4. Interior of Sant Miquel de Cruïlles: (a) nave; (b) transverse wall in south aisle

(a) (b) (c)

Figure 2.8.5. (a) North lateral apse, (b) apse, and (c) south lateral apse of Sant Miquel de Cruïlles

Figure 2.8.6. Dome at the crossing, which is covered by a drum

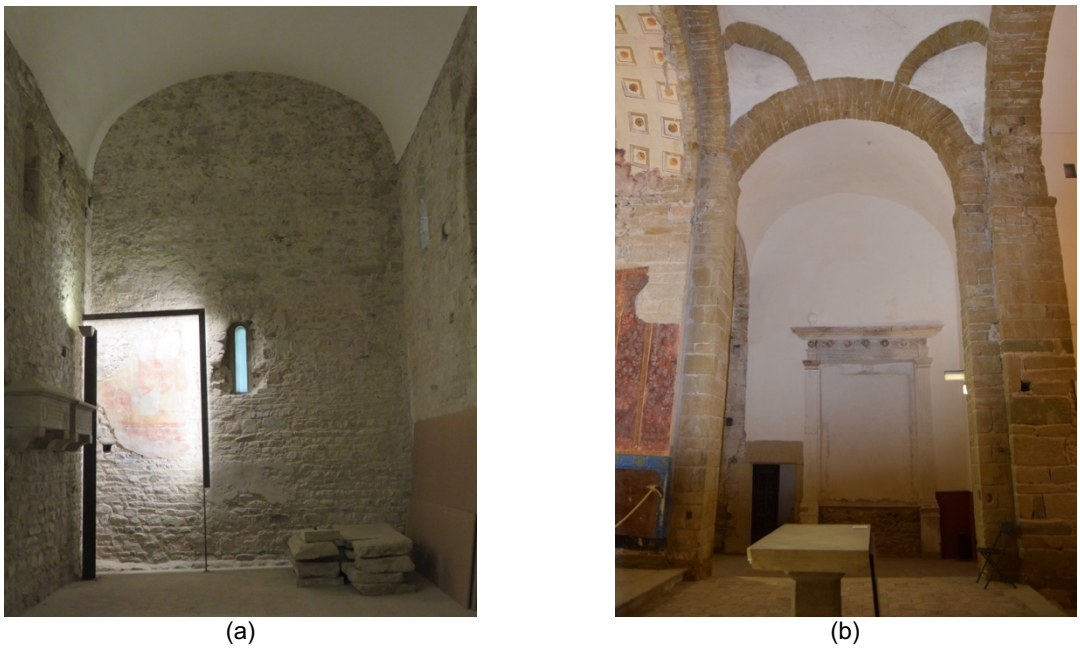

(a) (b)

Figure 2.8.7. North branch of transept (a) and south branch of transept (b) of Sant Miquel de Cruïlles

At the northwest corner of the church rises the 16th- or 17th-century bell tower. It is 15.7 m tall and square in plan, with sides about 5.5 m long. The tower was clearly built in several phases, given the stratification of the varying masonry types (Figure 2.8.8). Stairs lead from the ground floor into the belfry, whose floor is made of concrete and where a thick concrete beam can be found around two walls (Figure 2.8.9(b)). A single steel beam lies beneath this floor (Figure 2.8.9(a)). The odd construction configuration of this tower is not specifically analyzed in this report, but since it is clear that it has undergone many changes over time which likely lack sufficient connections, including some concrete of incompatible stiffness, it probably has high seismic vulnerability.

Figure 2.8.8. Bell tower of Sant Miquel de Cruïlles (south side)

(a)

(b)

Figure 2.8.9. (a) Underside and (b) top of the floor of the bell tower of Sant Miquel de Cruïlles

2.8.4. Present Condition and Damage State

The vaults and many of the side walls and dividing walls are covered with plaster, which makes damage inspection difficult. In addition, the irregularity of the masonry makes it hard to distinguish cracks in some cases.

- **Cracks**

In general, cracks are seen in the apse and chapels, with some cracks in the transept and drum also. The apse vault has severe radial cracking (Figure 2.8.10(a)). In the walls of the north side chapel can be seen diagonal cracks appearing to indicate the formation of an overturning mechanism (Figure 2.8.10(b)). In the south side chapel the cracks are vertical and less apparent. In the north transept there are some diagonal cracks that may indicate possible activation of an overturning mechanism in the transept facade (Figure 2.8.11). A few columns inside the church show vertical cracks, which could be indicative of compressive stresses that are too high. Crack maps for the interior of the building are provided in Figure 2.8.12.

(a) (b)

Figure 2.8.10. (a) Apse vault cracking and (b) north side chapel wall cracking in Sant Miquel de Cruïlles

Figure 2.8.11. Diagonal cracking in east wall of north transept

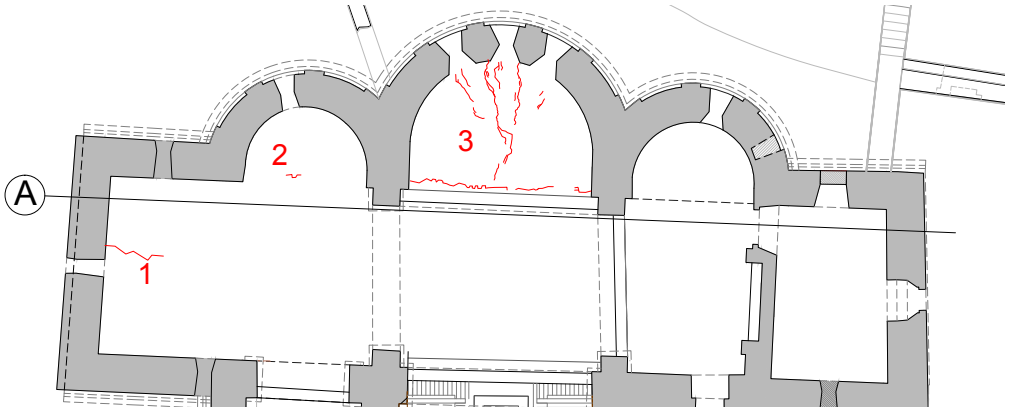

(a)

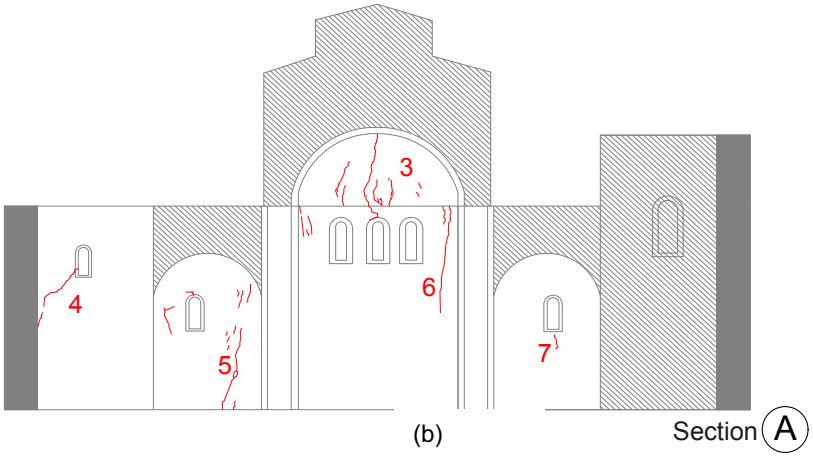

(b)

1. Crack in the vault of the north transept
2. Cracks in vault of apse
3. Crack in arch of north lateral apse
4. Diagonal crack in transept wall, possibly due to overturning of the transept facade
5. Cracks in north lateral apse due to overturning
6. Crack in wall of apse due to overturning
7. Crack in south lateral apse

Figure 2.8.12. (a) Plan and (b) section crack map of apse, transept and side chapels of Sant Miquel de Cruïlles

Moving to the exterior of the building, more cracks can be found that aren't necessarily apparent on the interior. There are cracks on the north transept facade, specifically one above the window and in the upper east corner (Figure 2.8.13) and a crack in the drum (Figure 2.8.14).

Figure 2.8.13. Cracks in exterior of north transept facade of Sant Miquel de Cruïlles

Figure 2.8.14. Crack in drum of Sant Miquel de Cruïlles

- **Other damage**

The north column embedded in the facade was built with some very granular sandstones that are now deteriorating in the moist air. Compression cracks in the column have become rather severe, and at the base, the column has lost a sizable amount of its section (Figure 2.8.15(a) and (b)). The humidity is now

monitored and regulated in the church in order to limit the amount of water absorbed by the stone. Deterioration of the stone is also visible in a few other places, including just outside the main door of the church (Figure 2.8.15(c)).

(a)

(b)

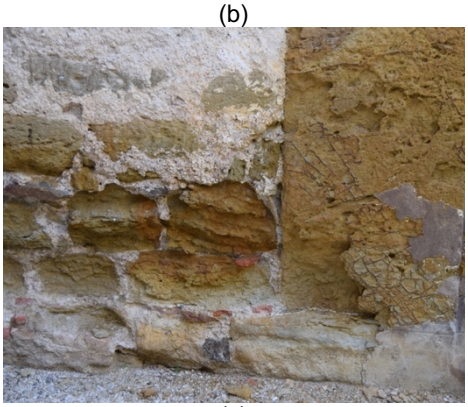

(c)

Figure 2.8.15. (a) and (b) Deteriorating column between main nave, north aisle, and bell tower; (c) deteriorating stones just outside the main door to the church

There is also some slight deformation visible in the arches of the nave (Figure 2.8.16).

Figure 2.8.16. Slight deformation of the key of the first arch from the crossing

3. VULNERABILITY INDEX ANALYSIS

3.1. Vulnerability analysis of Poblet

3.1.1. Assumptions

- **Vulnerability index**

The church of Poblet had a few key features that determined its vulnerability index. Beginning with the main facade, Poblet has an interesting structure. There was a secondary facade and galilee built in the 14th to 18th centuries. The facade considered for the vulnerability analysis is the original one. This original facade has an extremely large rose window that occupies a large part of the facade. The door of the facade is also quite a large opening; these weaknesses are two of the vulnerability indicators considered in the analysis.

The north transept has a large gable belfry, which is both thick and tall. It is taken into account as a projection (mechanism 26) as well as a "towering gable" and "concentrated load" on the transept facade and vault, respectively (mechanisms 10 and 12). The south transept has a short bell tower rising from it, which can be seen in the transverse section in Figure 2.7.8(b). The bell tower is analyzed as a bell tower with belfry (mechanisms 27 and 28) and considered as a "concentrated load" on the transept facade and vault (mechanisms 10 and 12).

It is interesting to note that the apse has five chapels surrounding it at the bottom; however, the apse overturning mechanism may still be possible in the higher portion of the apse that rises above the chapels.

As far as adjacent buildings, the monk living quarters are considered to be leaning against the north transept facade. The wall thicknesses seem to be relatively similar (on the order of 2 m) but there is a clear difference in construction periods due to the lack of connection between the masonries. Thus, the stiffnesses are assumed significantly different between the church and this adjacent building.

- **Weights of the mechanisms**

The transept is small relative to the size of the rest of the church, so mechanisms 10-12 have weight $\rho = 0.5$. The apse is quite large, with a webbed vault, so it has weight $\rho = 1$. The chapels are small and not relevant to most of the church's structure, so they have weight $\rho = 0.5$. The adjacent building, the monks' dormitories, is not substantially connected to the church so it is given $\rho = 0.5$ also. The gable belfry projecting above the north tower, on the other hand, is quite vulnerable and could fall on to the transept in an earthquake, causing damage to the vault, so it is considered with a weight of $\rho = 1$.

- **Damage index**

The mechanisms with associated damage identified in Poblet are: transverse vibration of the nave (5), vaults of the nave (8), vaults of the aisles (9), and overturning of the chapels (22). Cracking and deformation observed in relation to these mechanisms was minor and assigned a damage level of $d_k = 1$.

3.1.2. Results

The results for the vulnerability index method for Poblet are given in Table 3.1.1. A range is provided is because of some uncertainties in the subjective method. However, the difference between the lower and higher values is not large, suggesting that minor uncertainties in the calculation do not greatly affect the numerical results. The uncertainties included considering the weight of the belfry and the bell tower on the transept vault as $v_{kv} = 1\ or\ 2$, considering the openings and thrusting vault as $v_{kv} = 2\ or\ 3$, considering the windows of the apse in affecting shear behavior as $v_{kv} = 0\ or\ 1$, and considering the asymmetric support of the belfry as $v_{kv} = 1\ or\ 2$.

The vulnerability index i_v is within the range found in (De Matteis, Brando, Corlito, et al., 2019) for 64 damaged Italian churches, but above the mean of $i_v = 0.57$. The low damage index of Poblet reflects the relatively low level of damage, which is only apparent in a few cracks throughout the large church.

Table 3.1.1. Vulnerability Analysis Results for Poblet

Vulnerability index, $\boldsymbol{i_v}$	0.62 - 0.65
Damage index, $\boldsymbol{i_d}$	0.038
$\boldsymbol{a_{DLS}}$ [g]	0.034 - 0.036
$\boldsymbol{a_{ULS}}$ [g]	0.13 - 0.14

Comparing the acceleration required for the limit states to the reference ground acceleration for the region, 0.04g per the Spanish code and 0.051g per the National Annex to the Eurocode, the church would be expected to reach the damage limit state for the reference ground motion (Álvarez-Cascos Fernández, 2002; “Anejo Nacional AN/UNE-EN 1998-1,” 1998). However, it would not be expected to collapse.

The vulnerability index was used to create the following fragility models (Figure 3.1.1 and Figure 3.1.2). The first shows the probability of any given damage level occurring for a certain seismic intensity, based on the European Macroseismic Scale previously explained in Section 2.4.3 (Grünthal, 1998). From Figure 2.6.3, an intensity 6 earthquake is the earthquake of return period 500 years for Poblet, so for

intensity 6 the church would be most likely to attain damage level $D_k = 2$ (moderate damage), with probability 35%, and would have a 30% chance of exceeding that damage level. It would be extremely likely to experience at least damage level $D_k = 1$ (91%). Therefore, it is possible to conclude that the church will suffer moderate damage in the next strong earthquake but should be reparable. Furthermore, since the earthquake of intensity 6 has probability of 0.2% exceedance per year, in the near future it is more likely that there would be a smaller earthquake that would only cause minor damage (level $D_k = 1$).

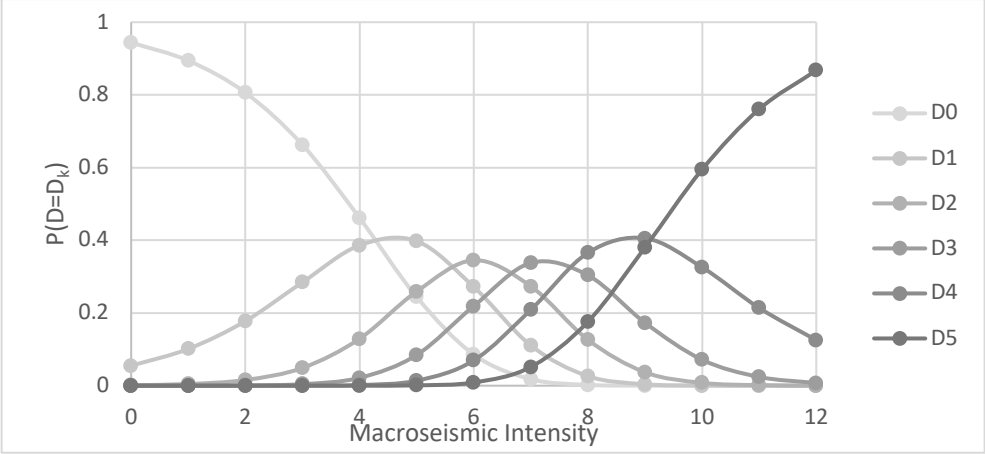

Figure 3.1.1. Poblet fragility model 1: probability of each damage level

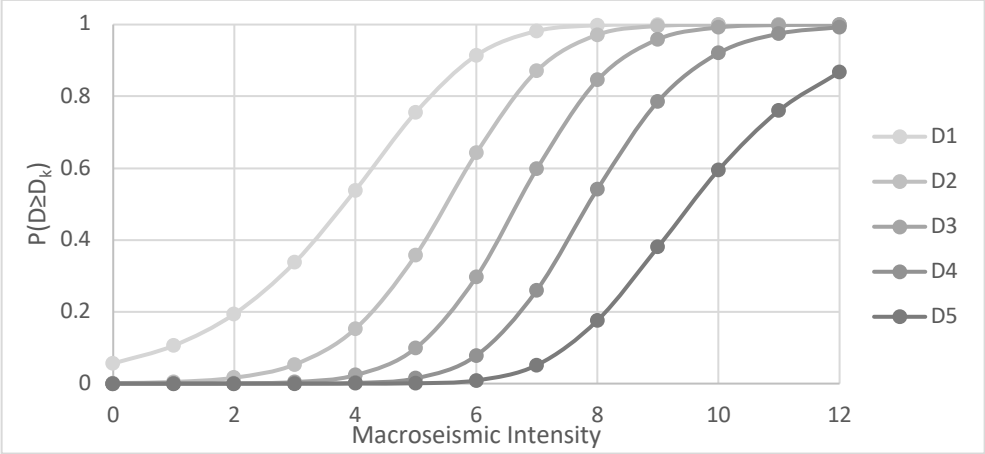

Figure 3.1.2. Poblet fragility model 2: probability of reaching or exceeding each damage level

3.2. Vulnerability Analysis of Sant Miquel de Cruïlles

3.2.1. Assumptions

- **Vulnerability index**

The windows of Sant Miquel de Cruïlles are relatively small; however, due to the low quality of most of the masonry, the load transfer may not be adequate around the openings and thus they are considered to be significant weaknesses.

The tower houses some undesirable reinforced concrete interventions. The floor slab in the tower is concrete, about 15 cm thick, and there is a concrete beam within only two of the concrete walls. Therefore a "significant weight" is considered to be present in the bell tower.

The bell tower has large openings that are given a low vulnerability score although they are not of different heights (Figure 3.2.1). The support at the tower base is irregular due to the irregular masonry, the presence of a single steel beam within the tower, and the archway on one side which leads between the church and the tower.

Figure 3.2.1. Inside the belfry of the Cruïlles bell tower

- **Anti-seismic measures**

The tower and buttresses are considered to prevent lateral contrast against the transverse vibration of the main nave (mechanism 5). The arches and vaults of the three naves are actually quite adequately reinforced; the transverse walls in the aisles and the exterior buttresses provide lateral stiffness against transversal movement. The tower also provides stiffness in the longitudinal direction against movement of the nave's colonnade (mechanism 7).

This church has two transverse tie-rods in the main nave, between the second and third sets of columns from the transept. These are considered to be effective anti-seismic measures to resist the spreading of the vaults.

- **Weights of the mechanisms**

The vault of the apse is quite large (and significant to the structure), and the chapels are of a size comparable to the apse, so the weights of mechanisms 18, 22 - 24 are taken as $\rho = 1$. The transept is small relative to the size of the rest of the church, so mechanisms 10 - 12 have weight $\rho = 0.5$.

- **Damage index**

Sant Miquel de Cruïlles has notable visible damage. The apse and side chapels, in particular, have widespread cracking. The mechanisms considered with non-zero damage levels were: transverse vibration of the nave (5), nave colonnade (7), aisle vaults (9), overturning of the transept facade (10), drum (14), overturning of the apse (16), vaults of the apse (18). Most of the mechanisms were assigned damage level $d_k = 1$ with the exception of the nave colonnade and the apse mechanisms, which had higher damage, $d_k = 2$. This is because several columns of the nave have compression cracks or loss of cross section, and the cracking in the apse is moderate in severity.

3.2.2. Results

As in the case of Poblet, the results for Sant Miquel de Cruïlles (Table 3.2.1) show that small variations in the vulnerability index calculation are not very consequential. These variations were considering the thrusting vault and windows of the apse as $v_{kv} = 1\ or\ 2$, considering the openings and irregular support of the bell tower as $v_{kv} = 1\ or\ 2$, and considering the concrete in the belfry as $v_{kv} = 1\ or\ 2$.

Table 3.2.1. Vulnerability Analysis Results for Sant Miquel de Cruïlles

Vulnerability index, $\boldsymbol{i_v}$	0.50 - 0.53
Damage index, $\boldsymbol{i_d}$	0.103
$\boldsymbol{a_{DLS}}$	0.043 - 0.047
$\boldsymbol{a_{ULS}}$	0.17 - 0.19

The vulnerability index for Sant Miquel de Cruïlles is about 20% less than that of Poblet, which is very interesting, as the thinner walls of Sant Miquel de Cruïlles and the rubble masonry would at first glance seem to make it more vulnerable. It falls slightly below the mean vulnerability of the churches studied by (De Matteis, Brando, Corlito, et al., 2019).

The seismic risk is higher in Cruïlles than in Poblet, at 0.07g in the Spanish code and 0.113g in the National Annex to the Eurocode (Álvarez-Cascos Fernández, 2002; "Anejo Nacional AN/UNE-EN 1998-1," 1998). The church would be expected to reach a damage limit state for the reference ground acceleration. The ultimate limit state is not expected to be reached.

An earthquake with 475-year return period for Sant Miquel de Cruïlles has intensity 6 to 7 (per Figure 2.6.3). Considering an intensity of 7 with the following fragility models (Figure 3.2.2 and Figure 3.2.3), it can be estimated that the church would be almost equally as likely to experience damage level $D_k = 2$ as it would level $D_k = 3$ (32% versus 30%, respectively). Probability of exceeding level three is only 17%, meaning there is about an 80% probability that the structure achieves minor, moderate or substantial to heavy damage. The probability of damage at least level $D_k = 1$ is 96% and at least level $D_k = 2$ is 79%.

It can be concluded that this structure is more vulnerable than Poblet when taking into account the regions' seismicities. Poblet only had probability of exceeding level $D_k = 2$ of 30%, compared to 47% for Cruïlles. Cruïlles faces a considerable threat of substantial to heavy damage that should not be ignored.

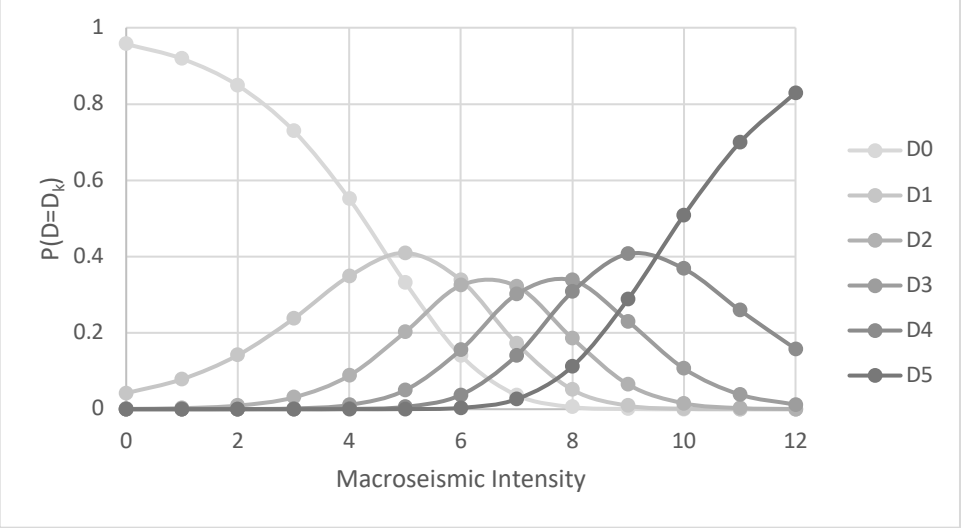

Figure 3.2.2. Sant Miquel de Cruïlles fragility model 1: probability of each damage level

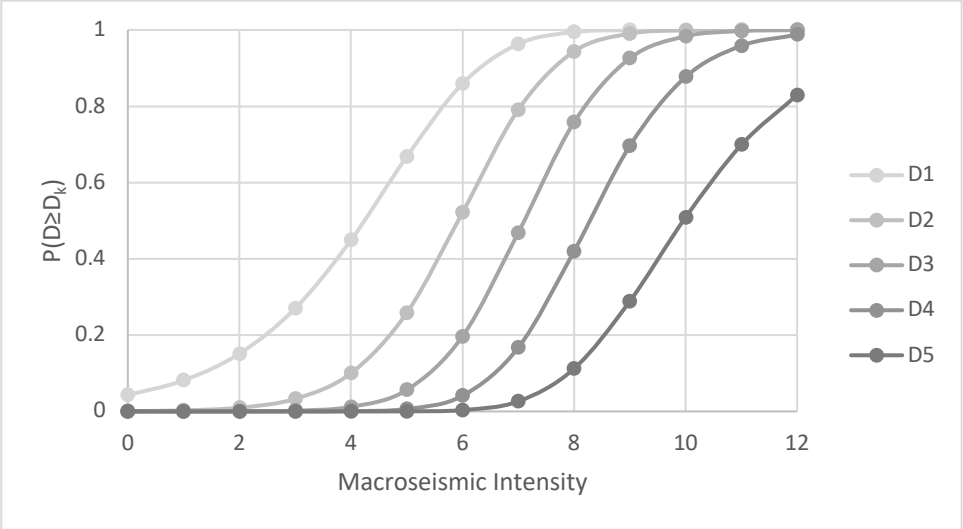

Figure 3.2.3. Sant Miquel de Cruïlles fragility model 2: probability of reaching or exceeding each damage level

With very careful examination, however, an interesting result is noticed: the peaks of the individual fragility curves for Cruïlles in Figure 3.2.2 occur at slightly higher intensities than those for Poblet in Figure 3.1.1. For example, damage level $D_k = 2$ is most likely to occur at an intensity of around 6.5 for Cruïlles, while it is most likely to happen for Poblet at intensity 6. This phenomenon is also visible by comparing the mean damage grade versus intensity for both churches (Figure 3.2.4). According to the vulnerability analysis, Poblet is more likely to attain a higher damage grade than Cruïlles for any given intensity. Comparing Poblet and Cruïlles both at earthquake intensity 6, we see that Poblet would reach damage level $\mu_D = 1.9$ while Cruïlles would only be at $\mu_D = 1.6$. Yet, since Cruïlles may have to withstand an earthquake of up to intensity 7, that brings its expected mean damage level to $\mu_D = 2.4$ for a 475-year earthquake.

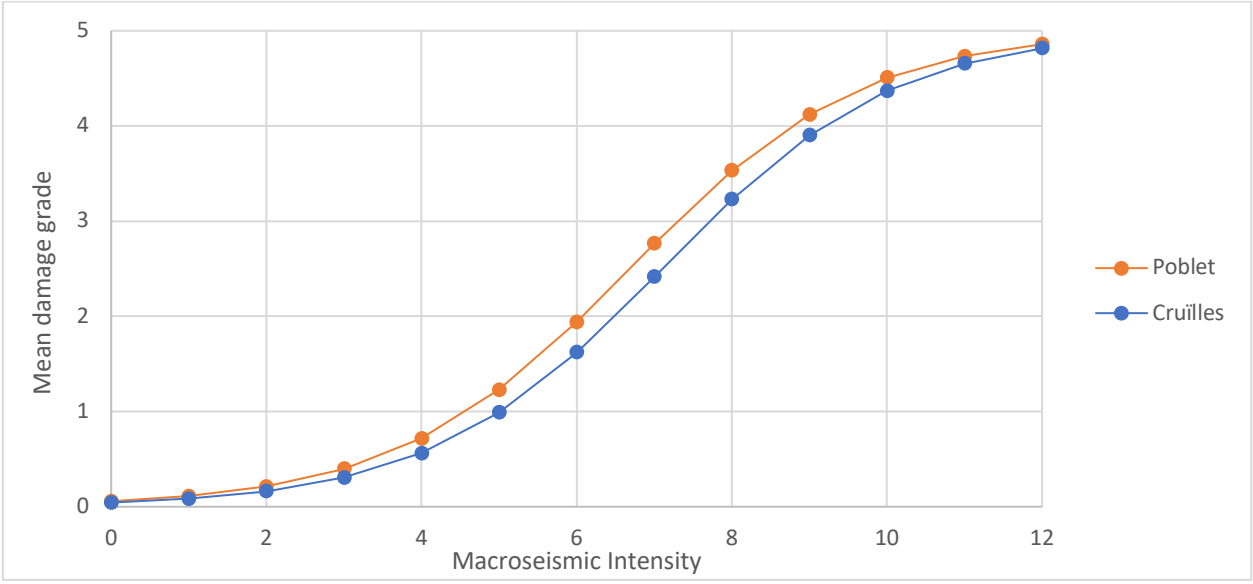

Figure 3.2.4. Poblet and Cruïlles fragility model 3: mean expected damage for a given earthquake intensity

3.3. Evaluation of the method and possible improvements

The vulnerability analysis method is quite subjective, as noted throughout its explanation in section 2.4.3. The subjective steps of the method are: noticing the presence of vulnerability indicators and anti-seismic measures, the assessment of the effectiveness of the measure or the importance of the vulnerability indicator, and the weighting of the macroelements.

The method first depends on an accurate, thorough examination of the structure in order to ensure all of the vulnerabilities and anti-seismic measures are noticed and recorded. Some of the vulnerability and anti-seismic measures are clearly defined so it is easy to state whether they are present or not (e.g. presence of tie-rods, presence of thrusting vaults), but others are vague (e.g. presence of very thin walls, presence of large openings). The more subtle components, such as "good quality masonry" or "good architraves", may not even be identified upon first observation. Furthermore, adjectives like "thin", "large", "heavy", "good" can be subjectively interpreted by the user of this method. This can result in the detection of or failure to detect a vulnerability indicator or anti-seismic measure, which would affect the calculation of the vulnerability index.

The most subjective part is the decision of the effectiveness of the vulnerability indicators or anti-seismic measures. When using Table 2.4.2 to find each v_k value, one notices that the *number* of indicators does not directly help in the decision of v_k, since with just one indicator, v_k can range from 1 to 3 (and the same can be said for the presence of two indicators). The decision of effectiveness for the indicators in the arbitrary range of 1 to 3 (presumably 1 = low, 2 = moderate, and 3 = high effectiveness) is what leads to the evaluation of v_k. The indicators for each mechanism are given an effectiveness score as a group, not individually. This is not an exceptionally clear process, so it should be clarified, for example, whether having two indicators of low effectiveness equates to a group effectiveness of 1 ($v_k = 2$) or 2 ($v_k = 3$).

The third subjective factor is the weighting of the macroelement in its importance for the global stability of the structure. The weights of the mechanisms of the transept, vault of the apse, chapels, adjacent buildings, and projections, are for the user to decide, $0.5 \leq \rho_k \leq 1$. In this paper, only the values 0.5 and 1 were chosen, based on whether the macroelement was of little or high importance, primarily judged by its relative size. It may be hard to tell the structural relationship between the macroelement and others around it, so size is the easiest way to guess the importance of the element. In the case of the gable belfry of Poblet, its failure could lead to damage of the transept, so it was given the maximum weight of 1. There is no clear basis for choosing an intermediate value between 0.5 and 1. In addition, as pointed out by (Lagomarsino et al., 2019), the weight factor does not represent the diversity of architectural configurations one may find in the field. An example is that there may be an occurrence of two of the same macroelement (e.g. bell tower, belfry, chapels), and there is no way in the present method to

distinguish between them. He also noticed that some macroelements (e.g. the nave) have more relevant mechanisms than others, which naturally gives them a greater weight in the calculations.

Methods based on empirical evidence or post-earthquake surveys are most valid when used to evaluate the risk of a group of structures rather than an individual one, since the uncertainties in damage grade evaluation tend to be balanced out when evaluating many structures (Milutinovic & Trendafilosk, 2004). This is an inherent drawback to the vulnerability index method. When evaluating structures individually, a range of vulnerability should be computed to understand the flexibility of the result based on different decisions made in the analysis process. As noted in this paper, there were not large differences in results for a few small uncertainties.

The computation of the damage index may be a way to classify the structural damage currently visible and compare it to other structures analyzed with the same equation, but it should be remembered that the damage may have been repaired over the years or hidden behind plaster or decorative elements.

Several authors have noted the drawbacks of this method specifically in calculating the damage index (Lagomarsino et al., 2019; Penna et al., 2019). For example, the damage index is not robust, that is, it technically can take any value from 0 to 1 but churches above about 0.3 (quite a low value) are usually considered unusable. The damage indices for churches surveyed after an earthquake would be expected to have a strong correlation to their vulnerability indices, but this may not be true (for example in New Zealand in 2011, many churches had high vulnerabilities but low damage indices (below 0.3) (Lagomarsino et al., 2019)).

Furthermore, if only one macroelement has severe damage, the damage index will be low instead of indicating that there is severe damage. Also, it can happen that one church with slight damage on many elements may have the same overall damage index of another church with severe damage to a few elements. Therefore, much caution must be employed if trying to conclude on the safety of the church based on its damage index. Taking into account many issues with the current formulae, (Lagomarsino et al., 2019) proposed a new technique, already mentioned in Section 2.3. Lagomarsino's new method increases the number of available damage mechanisms. It considers an additional macroelement (the high choir), offers a more robust and flexible calculation of the damage index, and deals with the possibility of having two occurrences of the same macroelement. It also offers separate calculations of the damage index for transversal and longitudinal damage, outlines both a rapid and a detailed implementation method, and discusses the option of a damage index specifically for artistic value.

In conclusion, the vulnerability index method is based on a simple visual inspection and model aimed at efficiency, for which it does an adequate job in the analysis of many churches, but it is subject to the eyes of the inspector and analyst and has some flaws for individual church examination.

This page is left blank on purpose.

4. KINEMATIC LIMIT ANALYSIS

4.1. Response spectra for Poblet and Cruïlles

The values obtained from the Spanish seismic code NCSE-02 and Eurocode 8 for the construction of the response spectra are tabulated in Table 4.1.1. The EC 8 spectrum used was the Type 1 spectrum. The soil types were obtained from a seismic mesozonation map of Catalonia developed by the Cartographic and Geologic Institute of Catalonia (Generalitat de Catalunya, 2018). The importance factor for NCSE-02, $\rho = 1.3$, was chosen considering the structures to be of special importance as cultural heritage, thus increasing the return period to 1000 years (CEN, 1998). The other importance factor, γ_I for EC 8, should in theory also be equal to 1.3 for the increased return period. However, EC 8 provided a higher reference ground acceleration than NCSE-02 for both locations. Therefore, a 475-year return period was chosen for the EC 8 analysis (with importance factor $\gamma_I = 1$) in order to have more comparable results between the spectra. Therefore both structures are treated as ordinary (importance class II) according to EC 8, rather than of special importance (importance class III).

The elastic response spectra are displayed in Figure 4.1.1. It is interesting that for Cruïlles, the EC 8 spectrum is higher than that from the NCSE-02, while for Poblet the NCSE-02 spectrum is the higher one.

Table 4.1.1. Parameters for the response spectra

	Santa Maria de Poblet		**Sant Miquel de Cruïlles**	
Parameter	**NCSE-02**	**EC 8**	**NCSE-02**	**EC 8**
S	1.6	1.4	1.04	1.2
C	2	-	1.3	-
K	1	1	1	1
a_b **[g]**	0.04	-	0.07	-
ρ	1.3	-	1.3	-
$a_{g,R}$ **[g]**	-	0.051	-	0.113
γ_I	-	1	-	1

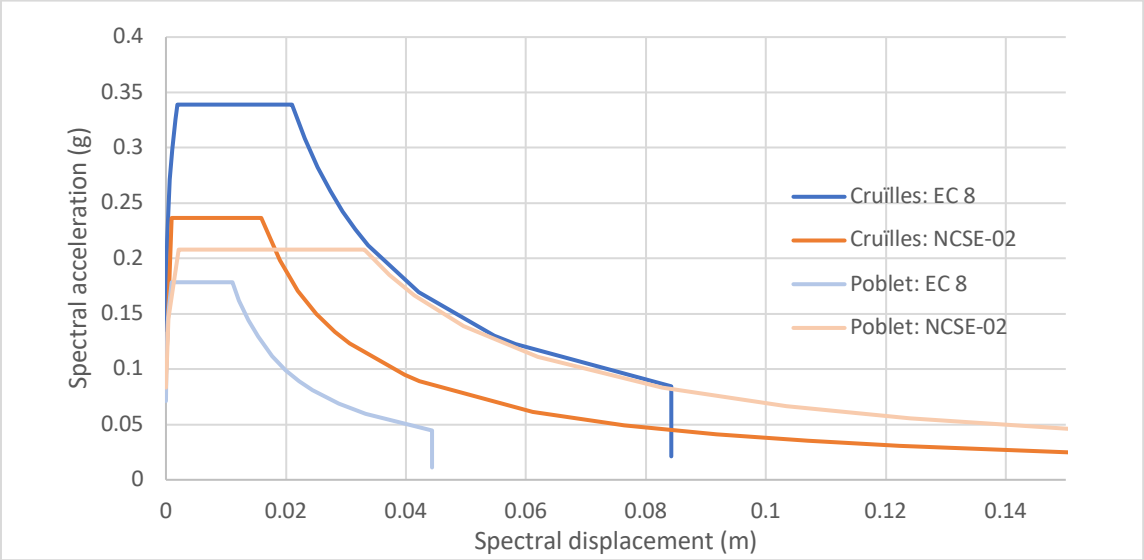

Figure 4.1.1. Elastic response spectra

4.2. Analysis of Santa Maria de Poblet

4.2.1. Assumptions

- **Main Facade**

Once again, the fortifying interventions made to Poblet's facade in the 14th century present an unusual case. The galilee and second facade were added at that time. The galilee is about half as tall as the original facade, so it is not considered as an effective structural support to prevent overturning. The original facade therefore was analyzed for overturning in full, in the portion above the galilee, the upper portion beginning at mid-height of the rose window, and the upper portion exclusively above the rose window.

- **Transept Facades**

The north transept facade adjoins the building known as the monk's living quarters. This building clearly has a different masonry that is not sufficiently connected to the church, but it may restrict the possibility of overturning of the north transept facade. From the top of the north transept facade rises the gable belfry that is possibly the most vulnerable element to overturning. Plane belfries are a vulnerable typology that suffer damage to the arch-pier system and are also susceptible to overturning. The structure they are built upon is more rigid and therefore no amplification of the seismic action occurs in their frequency range (the R factor is close to 1) (Lagomarsino, 2012).

The south transept facade is not adjoining adjacent buildings, so it may overturn. Atop the south transept sits a small bell tower that was also analyzed for overturning.

- **Apse**

The apse is a half cylinder built on columns, surrounded by a vaulted ambulatory and radiating chapels. It has a half dome ribbed vault. The apse for the purpose of analysis, therefore, is considered to be the part only above the level of the roof of the ambulatory.

The apse is most likely comprised of a vault, thickness assumed 0.25 m, with infill above it. The apse infill properties are not well known. The infill may be heavy or light, either partially or completely filling in the space between the half dome vault and the outer wall and roof. Therefore two conditions have been tested for the apse: with zero infill and with a full infill of weight $\gamma = 18\ kN/m^3$ as assumed for the weight of the infill over the main nave in (Saloustros, 2013).

Domes and half domes can be conceived as a collection of arches for static analysis. For this analysis, two distributions of stress were considered: radial arches and transverse arches. When incorporated with the two considered infill cases, there are a total of four cases under study for the apse. They will be described in detail in the next section.

The period T_0 for calculation purposes was approximated by Equation 2.5.7 although the apse is round and not a planar element; the slenderness ratio λ is still taken as the ratio of height to the thickness of the element. The portion of the apse under study is elevated, thus it should have $R > 1$ for the increase of the response spectrum. However, the calculation of R requires the calculation of the period of the structure supporting the elevated element. In the case of the apse, this is a round wall on top of columns. The process of approximating the period of this portion of the structure would be too complex, so for simplicity R is taken as 1.

- **Soil Type**

The soil type is Type E for the Eurocode (Generalitat de Catalunya, 2018). However, the worst soil classification considered in the Spanish code is Type IV, roughly comparable to Type D in the Eurocode. Thus, the EC 8 response spectrum was obtained using soil parameters for Type E, while the NCSE-02 response spectrum was obtained following the Type IV soil parameters.

- **Material properties**

Following Table C8.5.I of the Circolare for ashlar masonry, the compression strength was taken as 6 MPa, the elastic modulus as 2800 MPa, and the weight density as 22 kN/m^3 (NTC, 2019).

4.2.2. Results

The performance points were found with Method A and Method B (Section 2.5.3) using both the Eurocode 8 (EC 8) and Spanish seismic code (NCSE-02). To elucidate the calculation of the performance point using Method B (capacity spectrum method), the reduction of the response spectra is exemplified in Figure 4.2.3 for the overturning of the main facade of Poblet. Since the Eurocode elastic response spectrum intersected the elastic part of the capacity curve, it was not necessary to reduce it, and the performance point was located at the intersection. The performance point for Method A and Method B are overlapping in this case. On the other hand, for the spectrum of the Spanish seismic code, a few iterations were necessary to achieve the reduced response spectrum within satisfactory accuracy.

Besides the graph for the overturning of Poblet's main facade (Figure 4.2.3), provided below are the results for the transept facade (Figure 4.2.4), apse (Figure 4.2.5 and Figure 4.2.6) and gable belfry (Figure 4.2.7). Each macroelement is highlighted in Figure 4.2.1. More mechanisms are provided in Appendix A.2. These are all of the results analyzed for Poblet:

- **Main facade**
- Main facade above galilee
- Main facade above the middle of the rose window
- Gable of main facade
- **Transept facade, case 1: limited by the vault and walls**
- Transept facade, case 2: including the intersection with the transept walls and vault
- Transept facade limited by the vault and walls, above the middle of the rose window
- Gable of transept facade limited by the vault and walls
- Exterior gable of transept facade
- Apse above chapels, case 1: Solid infill with radial distribution of stress
- **Apse above chapels, case 2: No infill with radial distribution of stress**
- **Apse above chapels, case 3: Solid infill with transverse distribution of stress**
- Apse above chapels, case 4: No infill with transverse distribution of stress
- **Gable belfry**
- Bell tower

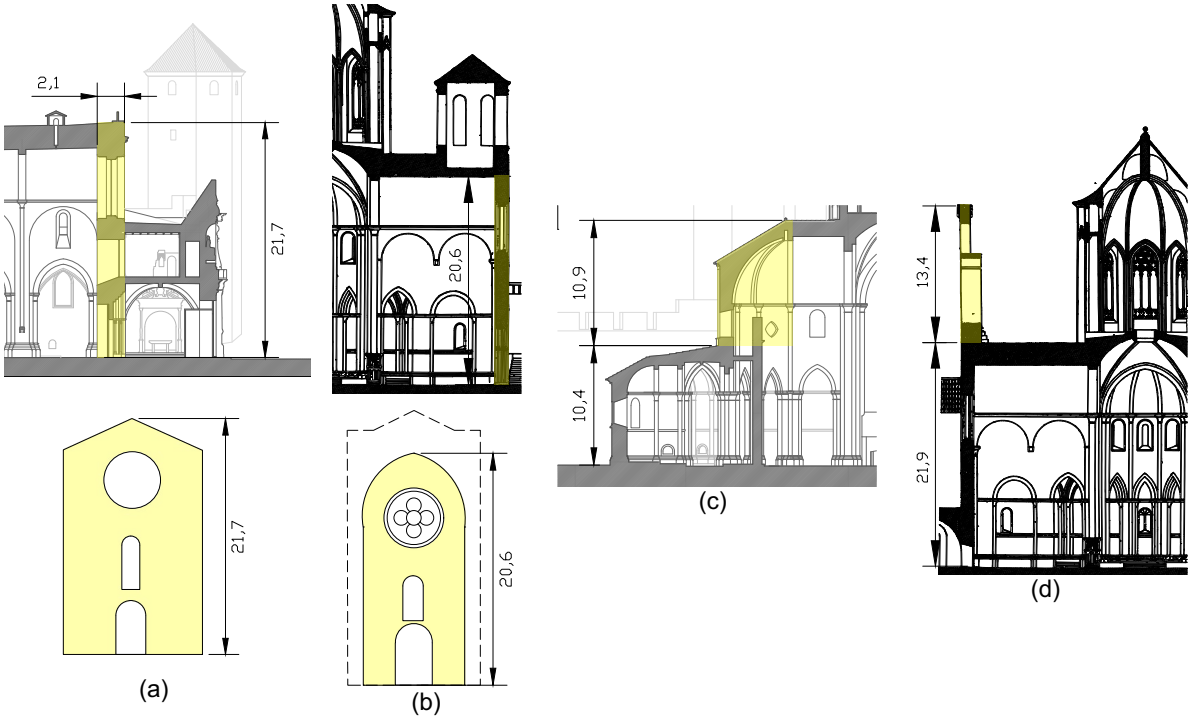

Figure 4.2.1. Mechanisms of Poblet analyzed in this section for overturning: (a) main facade, (b) transept facade, (c) apse, (d) gable belfry

One of the first observations to be made from the following graphs is that the results obtained by the Eurocode and the Spanish seismic code are quite different. Generally, the Eurocode has lower displacements, with the Method A - EC8 always having the lowest displacement. This is interesting because the spectrum corresponding to EC 8 was increased for the poor soil, Type E, while the NCSE-02 did not have comparable parameters for that soil. The increased EC 8 spectrum would be expected to result in larger displacements at the performance point, but clearly they were still below the NCSE-02 displacements.

With regard to the main facade, based on the locations of the performance points, it can be said to expect damage level 1 or 2. Comparing the two facades (main and transept), the results from EC 8 analysis are similar; the performance point is in the elastic region between Sd_1 and Sd_2. But for the main facade, the performance points from NCSE-02 analysis are in the damage level 2 region while the transept facade performance point lies in damage level 3. Method A and B achieved very close results. The transept facade has the lowest activation acceleration and the least stiffness, out of the mechanisms analyzed here.

For the apse, four cases were considered:

(1) Solid infill with radial arch distribution of stress

(2) No infill with radial arch distribution of stress (Figure 4.2.5)

(3) Solid infill with transverse arch distribution of stress (Figure 4.2.6)

(4) No infill with transverse arch distribution of stress

Figure 4.2.2 shows the two ways in which stress may be distributed through this arch. Equilibrium must be attained for the vault to be stable. Figure 4.2.2(a), demonstrating the radial distribution or a series of radial arches, is the most common way to imagine the behavior of a dome (Huerta, 2001). In this case, thrust must be applied at the key of the arches to maintain equilibrium. However, the analysis with case (1) proved the equilibrium to be impossible with a heavy infill which required a large thrust that overturned the apse. Therefore, case (2) with radial stress distribution but no infill was tested (the vault was composed only of masonry of thickness 0.25 m). In this case, $a_0 = 0.20$.

Next, the hypothesis of a transverse arch stress distribution was tested (Figure 4.2.2(b)). In this case, no thrust is needed from the adjoining structure; the vault is stable on its own. For the solid infill case (3), $a_0 = 0.37$ and for the no infill case (4), $a_0 = 0.47$.

In performing these calculations, it was noted that the value of α_0 is quite sensitive to the value of the thrust and to the geometry. This was particularly true for case (1), where decreasing the height of the point of thrust application by 1% would result in a 30% increase in capacity, and halving the thrust value would increase the capacity by 175%.

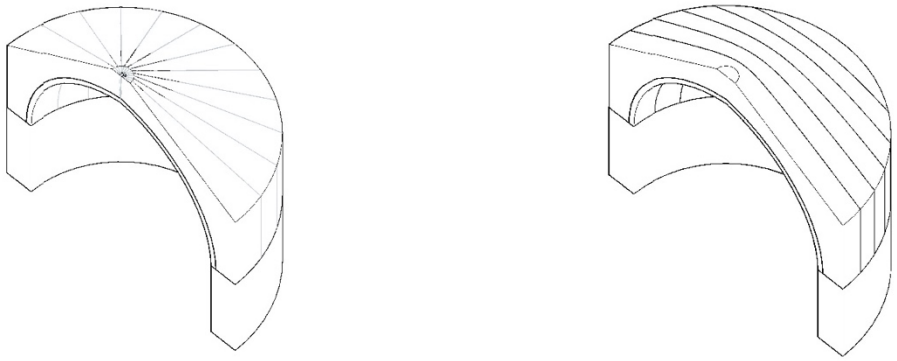

(a) (b)

Figure 4.2.2. (a) Radial distribution of stress for the apse of Poblet, and (b) transverse arch distribution of stress

For the gable belfry, the EC 8 results place the performance point in damage level 2 and the NCSE-02 in level 3. The R factor is low because the stiffness of the belfry and the transept facade are quite different. That the performance points are not in the very heavy damage/collapse region is somewhat surprising since this element appears from a cursory observation to be the most vulnerable. It can probably be explained by the fact that the thickness is rather high (1 to 2 m), so it is not as flexible as it appeared.

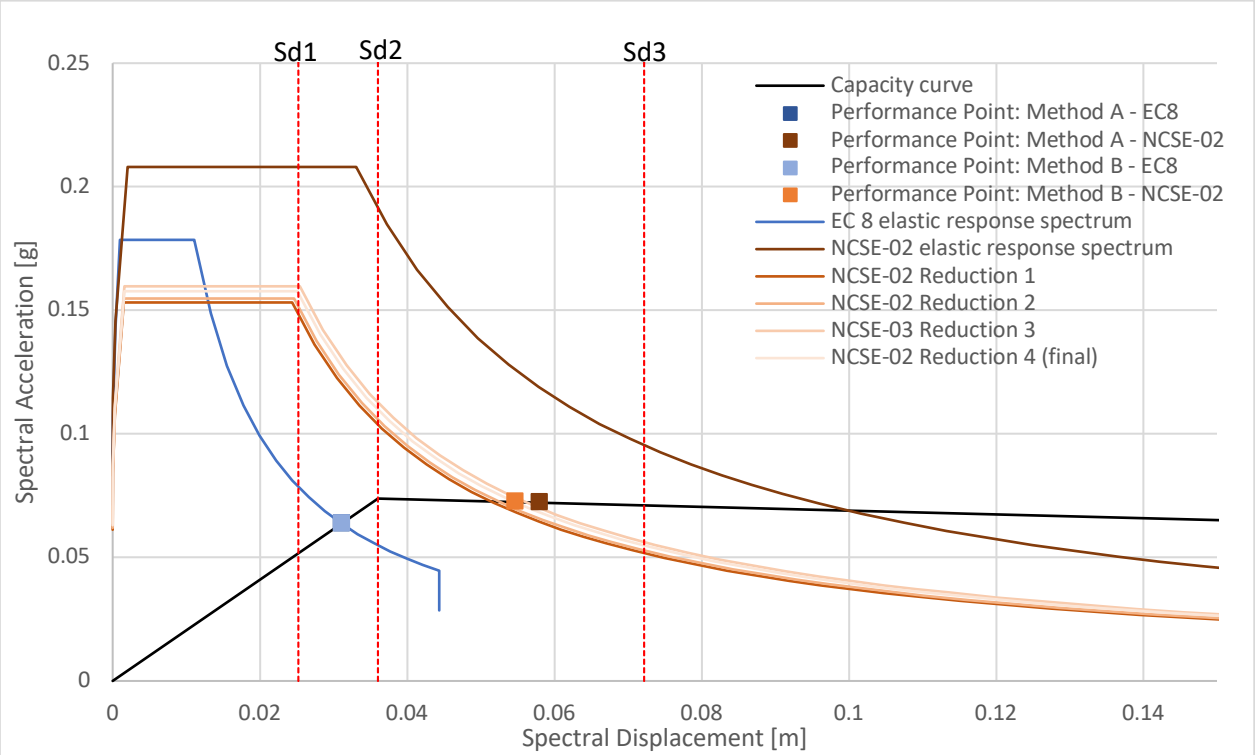

Figure 4.2.3. Performance point derivation for overturning mechanism of the Poblet main facade

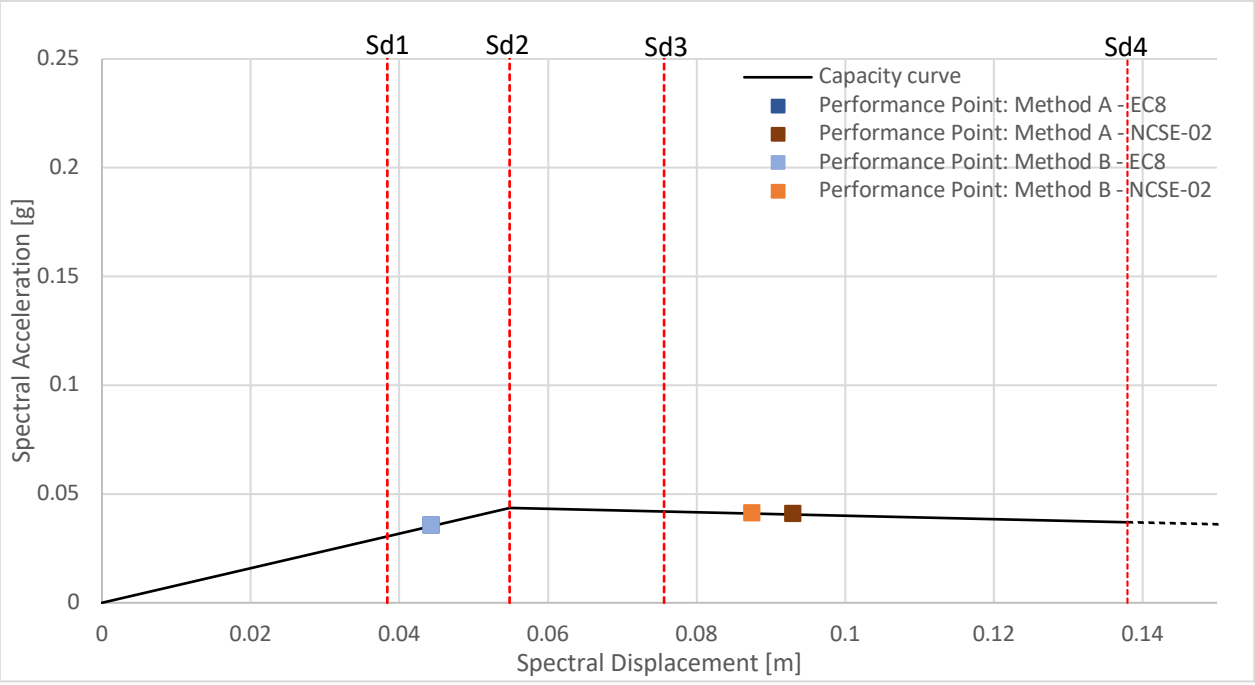

Figure 4.2.4. Poblet transept facade overturning, case 1: limited by the vault and walls

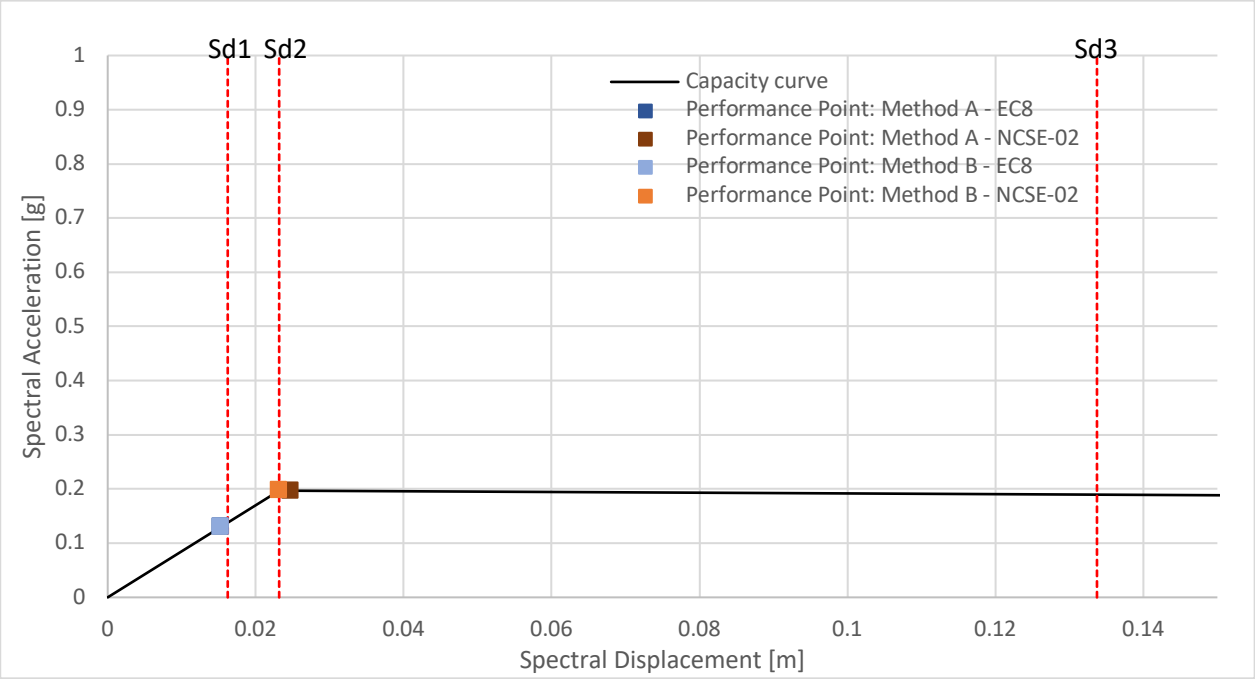

Figure 4.2.5. Poblet apse overturning, case 2: no infill with radial distribution of stress ($R = 1$)

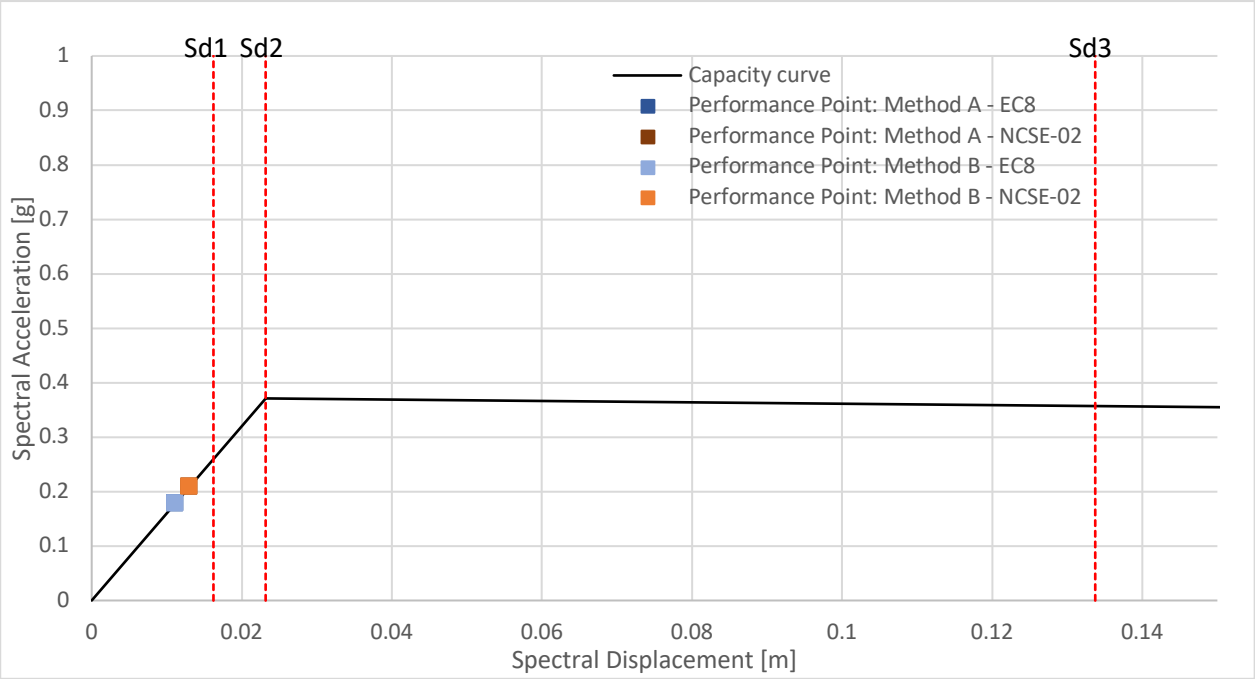

Figure 4.2.6. Poblet apse overturning, case 3: solid infill with transverse distribution of stress ($R = 1$)

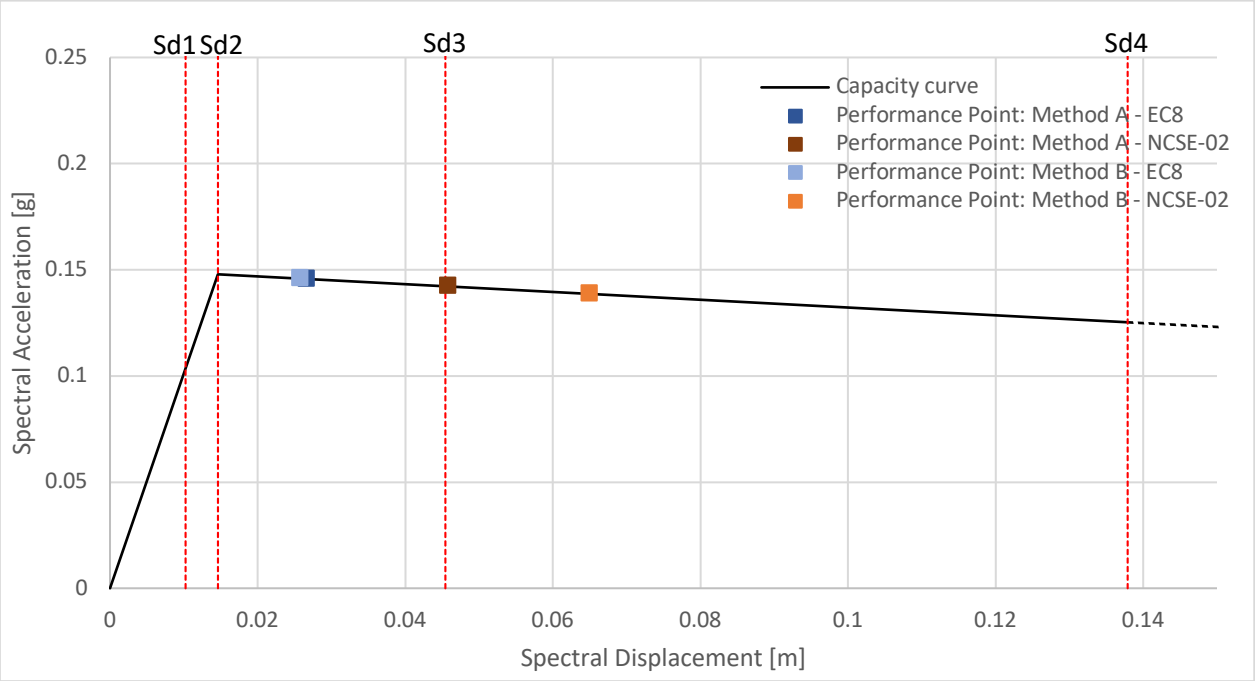

Figure 4.2.7. Poblet gable belfry overturning ($R = 1.4$)

Now the results can be analyzed overall, with Table 4.2.1 of the activation accelerations for all of the analyzed macroelements for Poblet (including the ones graphed in Appendix A.2). The elements with highest capacity are the gables and the apse case 4 with no infill and no thrust (an unlikely case). The other elements have generally sufficient capacities to resist overturning for the reference ground acceleration of 0.04g or 0.051g except for the transept facade, cases 1 and 2. The main facade and bell tower have only slightly higher capacities.

In Table 4.2.2 are displayed the percent differences in the locations of the performance point for calculation presented in this section (the rest can be found in Table A.3.1). The highlighted color indicates the value that was higher in that case, i.e. for the main facade, in the performance point calculation using Method A, the displacement was 60% higher for the NCSE-02 calculation compared to the EC 8 calculation.

From the table it is apparent that the difference between results within one method but between the two different codes is highly variable. The results from Method A were more often more precise than the results from Method B (they had a smaller percent difference between EC 8 and NCSE-02). In looking at the results obtained by the two methods considering a single code, it can be noticed that the variability is very low. For the case of the Eurocode in the analysis of three of the cases, the performance point was in the elastic region, so the two methods obtained exactly the same results. In almost every case, the results of the NCSE-02 were higher than for the EC 8 and in general, Method A results were higher than Method B results.

Table 4.2.1. Activation acceleration for all calculated overturning mechanisms for Poblet

Macroelement	**Overturning activation acceleration a_0**
Main facade	0.07
Main facade above galilee	0.20
Main facade above the middle of the rose window	0.33
Gable of main facade	0.91
Transept facade, case 1: limited by the vault and walls	0.04
Transept facade, case 2: including the intersection with the transept walls and vault	0.03
Transept facade limited by the vault and walls, above the middle of the rose window	0.16
Gable of transept facade limited by the vault and walls	0.38
Exterior gable of transept facade	0.77
Apse above chapels, case 2: No infill with radial distribution of stress	0.20
Apse above chapels, case 3: Solid infill with transverse distribution of stress	0.37
Apse above chapels, case 4: No infill with transverse distribution of stress	0.47
Gable belfry	0.15
Bell tower	0.07

Table 4.2.2. Percent difference in performance points for four select cases of kinematic mechanisms of Poblet

		Percent difference in results (%)			
		Between EC 8 and NCSE-02		**Between Method A and Method B**	
		Method A	**Method B**	**EC 8**	**NCSE-02**
Main facade	**d**	60	55	0	6
	a	12	13	0	0
Transept facade, case 1	**d**	71	65	0	6
	a	14	15	0	1
Apse, case 3	**d**	16	16	0	0
	a	16	16	0	0
Gable belfry	**d**	53	86	3	35
	a	2	5	0	2

4.3. Analysis of Sant Miquel de Cruïlles

4.3.1. Assumptions

- **Main Facade**

The current main facade of the church adjoins the east wall of the bell tower. The overturning calculations were performed for the facade ignoring the presence of the tower. The southern edge of the main facade still retains part of the original wall that existed there, which can now be considered to act as a buttress to this wall (Figure 4.3.1(a)). Therefore, the main facade was analyzed for overturning under two cases: case 1 in which the buttressing wall does not move, and case 2 in which the buttressing wall overturns with the facade.

Another note is that the facade was constructed by filling in an arch of the nave (seen in Figure 4.3.1(b)). Therefore, the connection of this infill section to the rest of the masonry is probably weak; it has also been considered for overturning.

(a) (b)

Figure 4.3.1. (a) Buttressing wall at the southern edge of the main facade of Cruïlles; (b) Arch in main facade

- **Transept Facades**

The walls of Sant Miquel de Cruïlles are primarily irregular masonry; however, the corners of the transepts are marked with larger, more well-cut stones (Figure 4.3.2). Thus, the overturning mechanism was considered for the entire wall to its edges, as well as just the portion of the facade contained between the two strips of better-quality masonry at the corners. This assumption is supported by the damage seen in the L'Aquila earthquake of 2009, where a fracture line occurred in the plane of the facade rather than in the connection with the lateral walls (Lagomarsino, 2012).

(a) (b)

Figure 4.3.2. North transept of Sant Miquel de Cruïlles, exterior (a) from the north, (b) from the west

- **Apses**

For the main apse, since portions of the apse walls intersect with the lateral apses, the most vulnerable case was analyzed, which is the overturning of the portion of the apse that projects beyond the shared walls (as will be seen in Figure 4.3.3(d)). As in Poblet, the cases of radial and transverse arch stress distributions were considered. This will be explained in the next section.

For the lateral apses, due to poor geometrical surveying, a few approximations were made such as the height of the apse (taken as 1.5 m less than the height of the main apse). For this case, a wedge-like portion of the apse was studied, as will be explained in the next section.

For all of the apses the vault was assumed to be of thickness 0.2 m. The period T_0 for calculation purposes was approximated by Equation 2.5.7 although the apse is round and not a planar element; the slenderness ratio λ was still taken as the ratio of height to the thickness of the element.

- **Material properties**

Following Table C8.5.I of the Circolare for irregular masonry, the compression strength was taken as 1 MPa, the elastic modulus as 870 MPa, and the weight density as 19 kN/m^3 (NTC, 2019). In general, for irregular or rubble masonry, localized crushing occurs, causing progressive decay and a low capacity to withstand cyclical loading (Lagomarsino, 2012). This is reflected in the low compression strength taken for this masonry.

4.3.2. Results

The macroelements considered for overturning in this section for the church of Sant Miquel de Cruïlles are shown in Figure 4.3.3. They are overturning of the main facade (Figure 4.3.5), the transept facade (Figure 4.3.6), the entire bell tower (Figure A.2.15) and the lateral apse (Figure 4.3.9). In total, the following mechanisms were analyzed and their results can be found in Appendix A.2:

- **Main facade, case 1: excluding buttressing wall**
- Main facade, case 2: including buttressing wall
- Main facade, case 3: beneath the arch
- Gable of the main facade
- **North transept facade, case 1: including intersection with transept walls**
- North transept facade, case 2: limited by transept walls
- South transept facade, case 1: including intersection with transept walls
- South transept facade, case 2: limited by transept walls
- West wall of bell tower

- **Entire bell tower**
- Main apse, case 1: radial arch stress distribution
- **Main apse, case 2: transverse arch stress distribution**
- **Lateral apse**

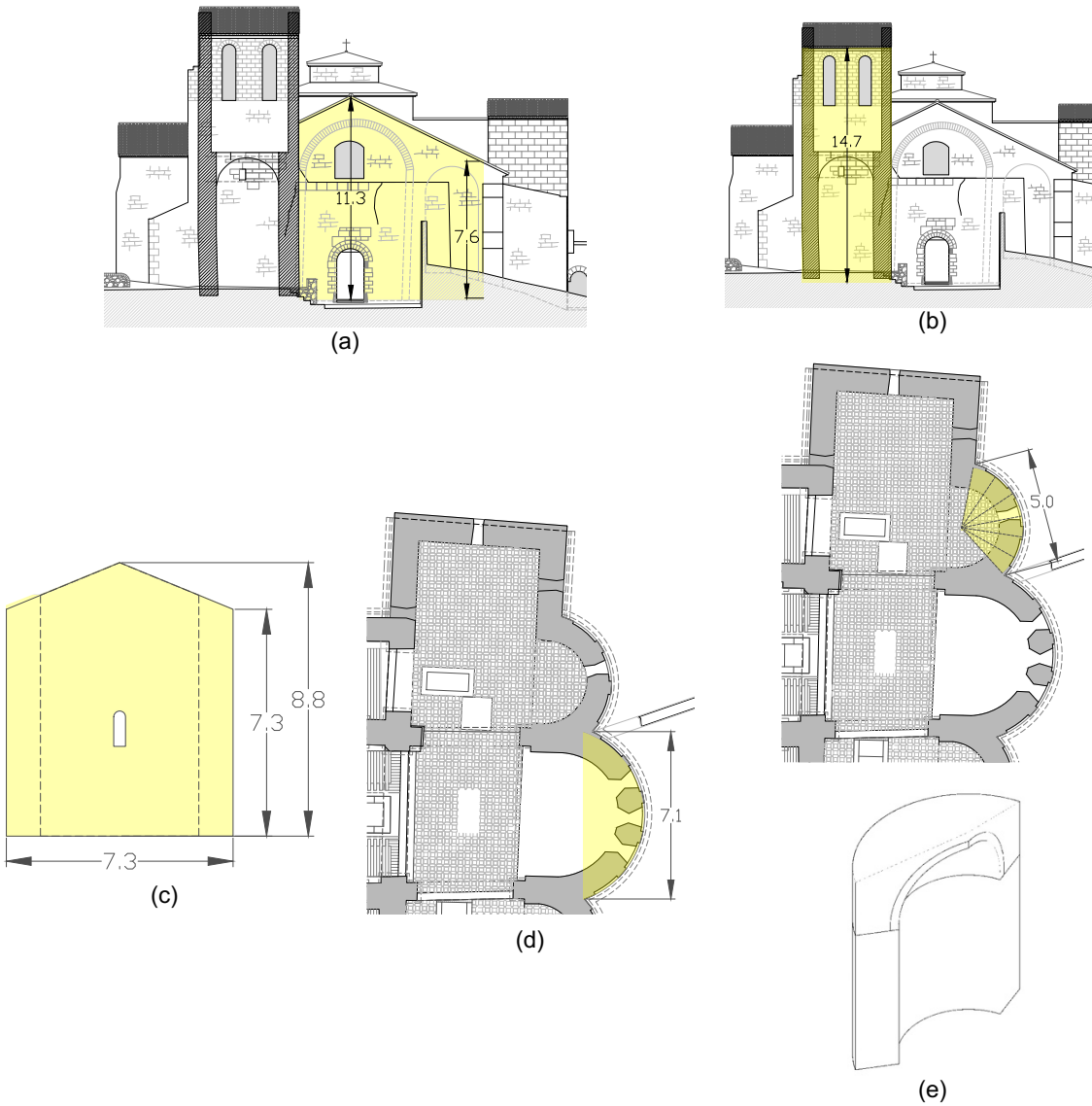

Figure 4.3.3. Overturning macroelements for Sant Miquel de Cruïlles analysis in this section: (a) main facade, case 1: excluding buttressing wall, (b) bell tower, (c) north transept facade including intersection with transept walls, (d) main apse (both cases), (e) lateral apse

In comparing the cases for the overturning of the main facade, case 1 without the buttressing wall has a lower capacity (by 0.005g) and lower ultimate displacement (by 1 cm) compared to case 2 (Figure A.2.9). Therefore, overturning of the main facade without the buttressing wall is the more vulnerable case. The level of damage expected for the facade does not differ significantly based on the code with which it is analyzed. The Spanish seismic code NCSE-02 predicts moderate to extensive damage (level 2 - 3), while EC 8 predicts level 3.

The north transept facade is expected to suffer moderate or extensive damage (level 2 - 3). It is stiffer and has a higher capacity than the main facade (0.083g vs. 0.055g).

The west wall of the bell tower has the lowest activation acceleration mechanism of any element ($a_0 = 0.03g$). Damage is in level 3 for all of the methods. The bell tower as a whole, in contrast, (Figure A.2.15) has a high activation acceleration compared to other mechanisms ($a_0 = 0.27g$).

To be consistent, the main apse of Cruïlles was analyzed with the same approach as the apse of Poblet. The two stress distributions under study are represented below, Figure 4.3.4(a) for the radial arches and Figure 4.3.4(b) for the transverse arches. The result was that the radial arch distribution had very low activation acceleration tending towards instability, just as in Poblet. Considering the transverse distribution instead, with no thrust (Figure 4.3.7), the activation acceleration is $a_0 = 0.15g$ and the performance points are in damage level 1 to 2.

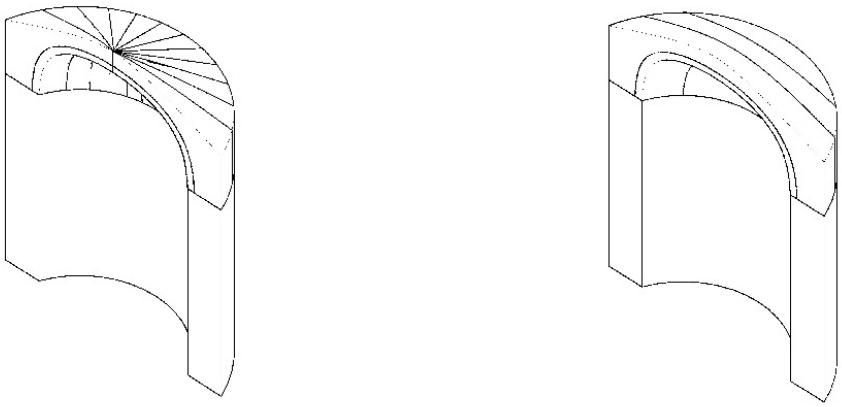

(a) (b)

Figure 4.3.4. Main apse of Sant Miquel de Cruïlles, (a) case 1, radial arch stress distribution and (b) case 2, transverse arch stress distribution

For the lateral apse, a wedge-shaped portion of the apse with a radial stress distribution was studied as seen in Figure 4.3.3(e), primarily because the results were reasonable, unlike for the main apse. The lateral apse is one of the places where damage related to overturning can be seen in the walls presently. From Figure 4.3.9, the results with Method A and B were very close for each respective code and all the performance points are in damage level 2. It is more than twice as stiff as the main apse but has almost the same activation acceleration ($a_0 = 0.16g$).

Since the response spectrum for Cruïlles from Eurocode 8 (Figure 4.1.1) has higher accelerations than for the NCSE-02 spectrum, the EC 8 performance points have higher displacements. The EC 8 reference ground acceleration is 0.113g while the reference acceleration from NCSE-02 is only 0.07g. Based on the activation acceleration alone, it can be concluded that according to EC 8, the mechanism for the main facade and north transept facade would be activated in the reference seismic event while

according to NCSE-02, it would only activate the main facade. Once again, the quite different results from the two codes can be noticed, with the EC 8 spectrum being higher although the NCSE-02 spectrum has been amplified by the applicable importance factor of 1.3 and the EC 8 spectrum has not.

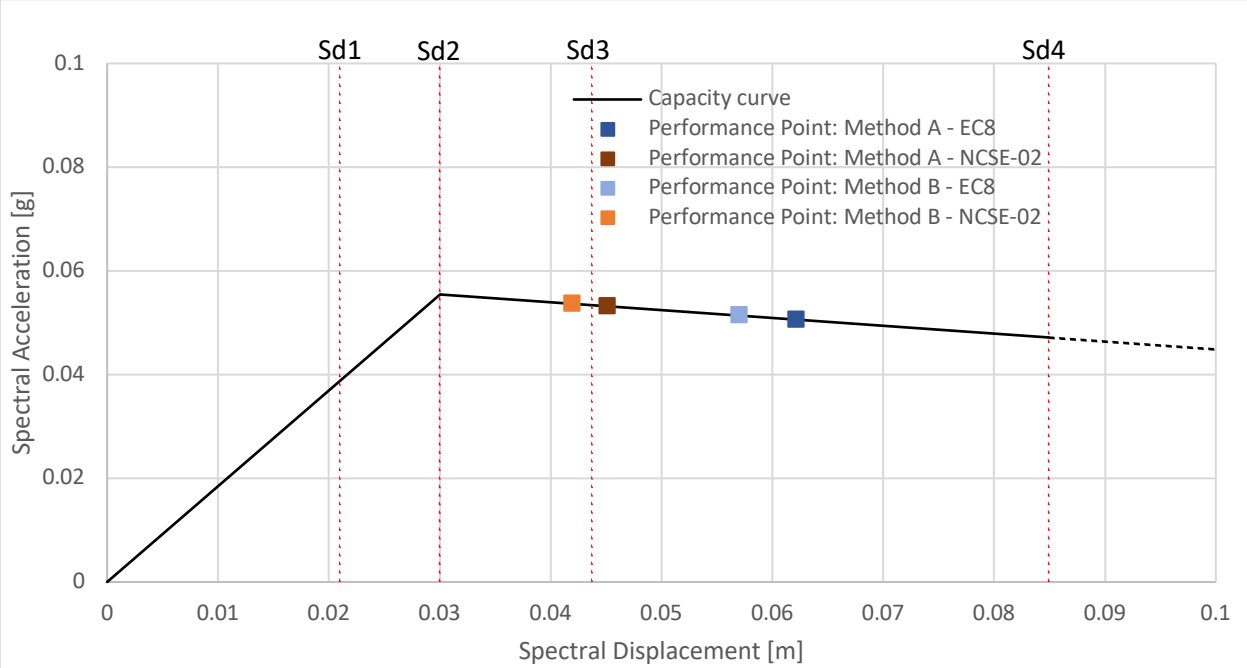

Figure 4.3.5. Cruïlles main facade overturning, excluding buttressing wall (Case 1)

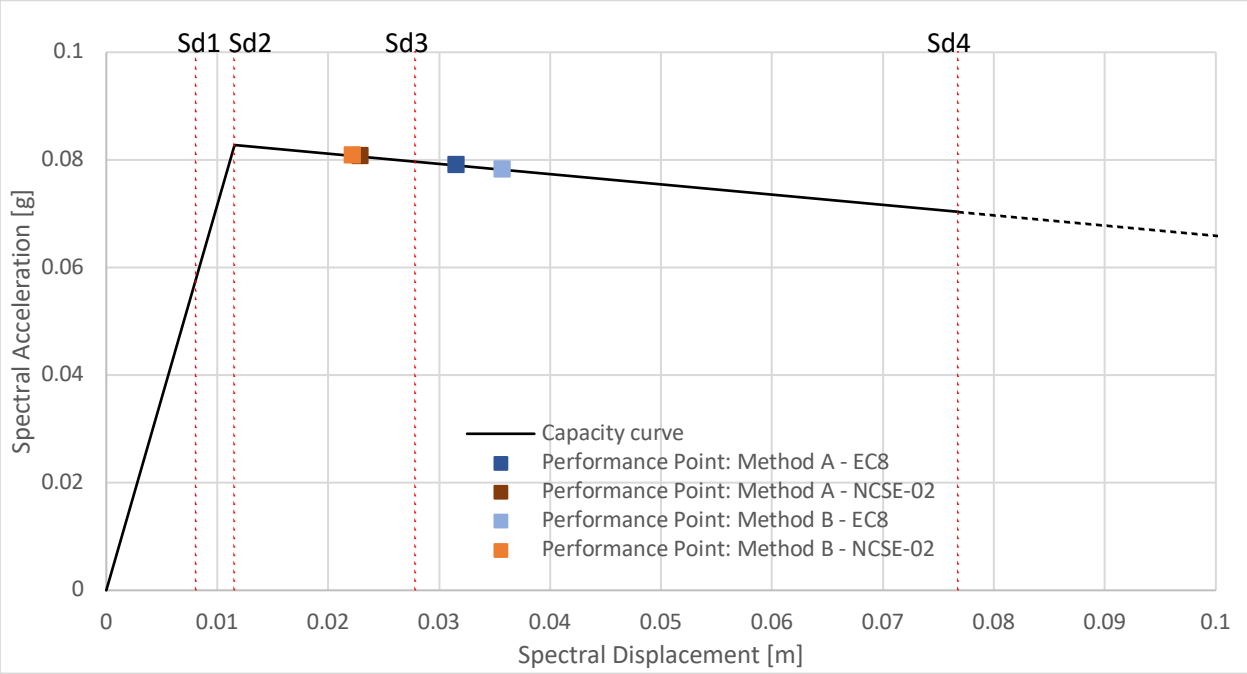

Figure 4.3.6. Cruïlles north transept facade overturning, case 1: including intersection with transept walls

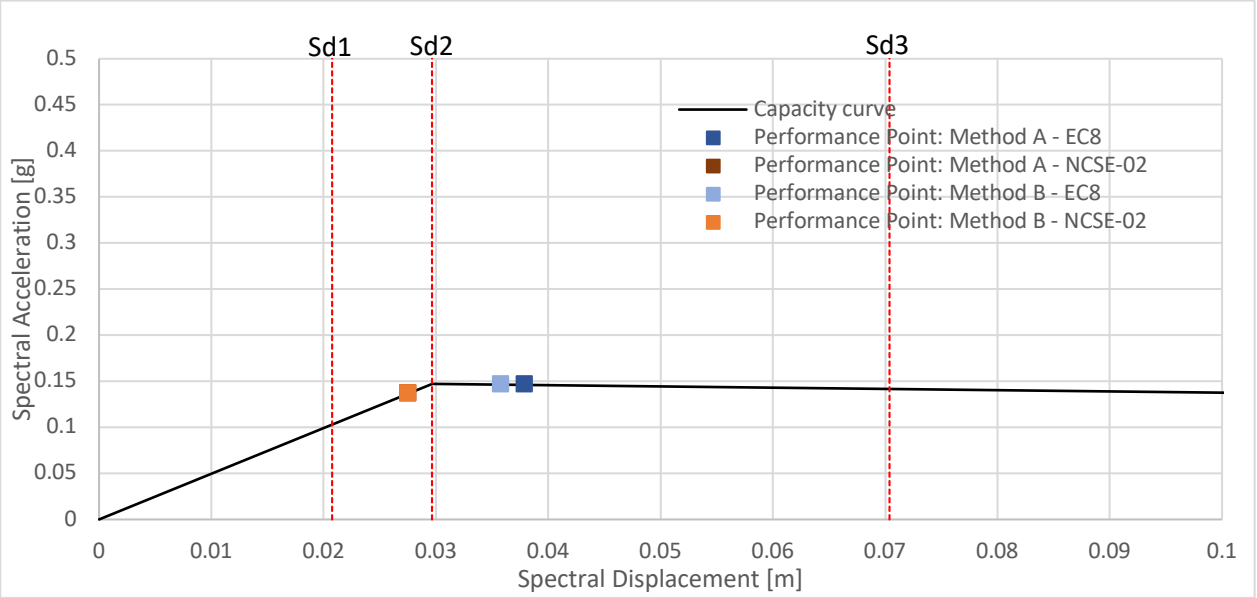

Figure 4.3.7. Sant Miquel de Cruïlles main apse overturning, case 2: transverse arch stress distribution

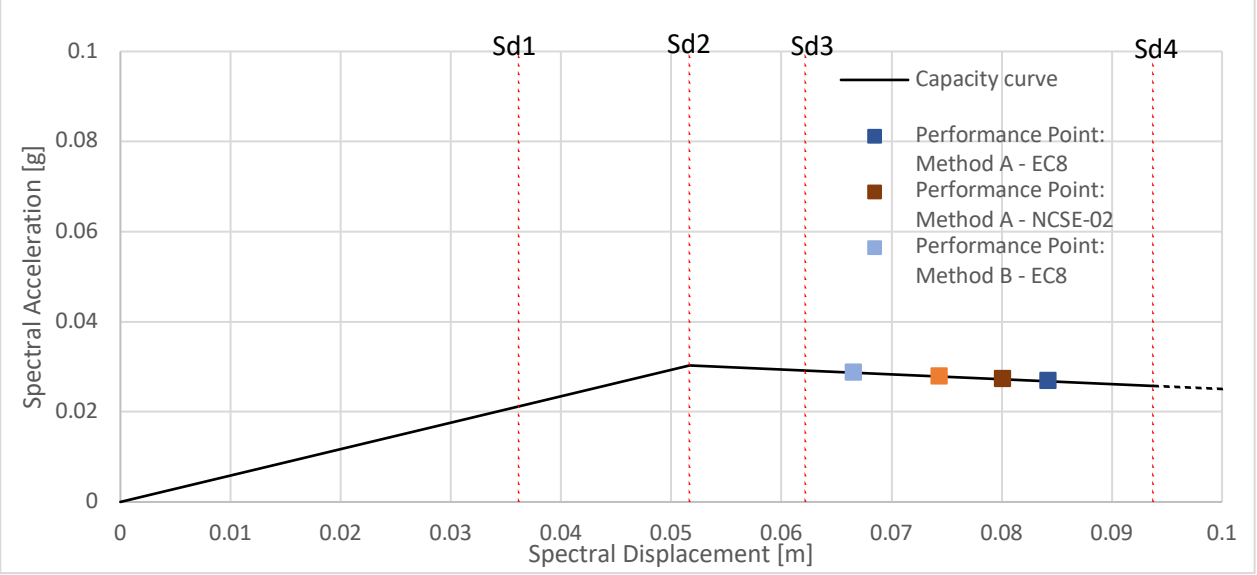

Figure 4.3.8. Sant Miquel de Cruïlles west wall of bell tower overturning

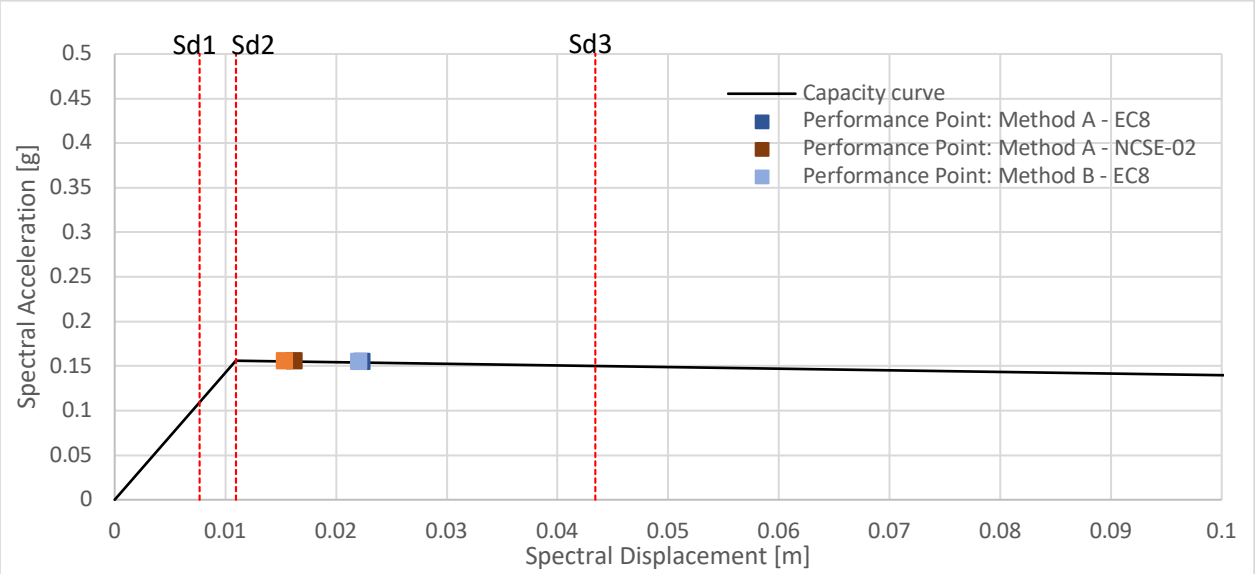

Figure 4.3.9. Cruïlles lateral apse overturning

To draw a few comparisons between all of the analyzed macroelements, even the ones provided in the Appendix, Table 4.3.1 supplies the results of the yield accelerations, or the activation accelerations that would cause each macroelement to overturn. The cases of highest capacity are the gable of the main facade, bell tower, main apse, and lateral apse. The north transept has a capacity between the reference ground accelerations from NCSE-02 and EC 8 (0.07g and 0.113g, respectively) so it is unclear whether it would overturn; the rest of the elements would be activated by even 0.07g.

Finally, it is possible to analyze the differences between the two methods and codes. The percent difference in results is tabulated in Table 4.3.2, sorted by method, by code, and by displacement or acceleration (see Table A.3.1 for more mechanisms). The highlighted color indicates the value that was higher in that case, i.e. for the main facade, in the performance point calculation using Method A, the displacement was 32% higher for the EC 8 calculation compared to the NCSE-02 calculation. It is seen that EC 8 has greater displacements than NCSE-02, for both Methods A and B, for most of the cases. The differences in acceleration are always lower than for displacement because of the shallow slope of the capacity curve. Method A produced greater results than Method B for many of the cases, although most showed no difference between the methods. Again, as in Poblet, we see that the percent difference is generally high between codes, and low when comparing between methods A and B for the same code.

Table 4.3.1. Activation acceleration for all calculated overturning mechanisms for Sant Miquel de Cruïlles

Macroelement	**Overturning activation acceleration a_0**
Main facade, case 1: excluding buttressing wall	0.055
Main facade, case 2: including buttressing wall	0.060
Main facade, case 3: beneath the arch	0.064
Gable of the main facade	0.647
North transept facade, case 1: including intersection with transept walls	0.083
North transept facade, case 2: within transept walls	0.080
South transept facade, case 1: including intersection with transept walls	0.066
South transept facade, case 2: within transept walls	0.065
West wall of bell tower	0.030
Entire bell tower	0.274
Main apse, case 2: transverse arch stress distribution	0.147
Lateral apse	0.156

Table 4.3.2. Percent difference in performance points for the selected cases of kinematic mechanisms of Cruïlles

		Percent difference in results (%)			
		Between EC 8 and NCSE-02		**Between Method A and Method B**	
		Method A	**Method B**	**EC 8**	**NCSE-02**
Main facade	d	32	30	9	7
	a	5	4	2	1
North transept facade, case 1	d	32	47	12	3
	a	2	3	1	0
West wall of bell tower	d	5	11	23	7
	a	2	3	7	2
Main apse, case 2	d	32	26	6	0
	a	7	7	0	0
Lateral apse	d	32	36	1	6
	a	1	1	0	0

4.4. Evaluation of the method and possible improvements

The kinematic limit analysis is not as subjective as the vulnerability analysis method. The method depends on an accurate calculation of the dimensions of the macroelement and its material properties: weight density, compressive strength and elastic modulus. When these aspects of the macroelement are correctly input for the calculations, performing Method A and Method B is not complicated. Difficulties arise, as they do with every type of structural analysis, when the geometry or material properties cannot accurately be ascertained.

The choice of which mechanisms to analyze is where subjectivity factors into this method. Due to time constraints, this study could only address overturning mechanisms, and only for the macroelements recognized as most vulnerable. It is possible that other parts of the church that were not analyzed are very vulnerable to overturning. Other failure mechanisms such as shear may be more likely for certain

elements, but if the calculation is not performed, the true capacity of each element can never be known. In the end, the element may even fail due to a combination of mechanisms that cannot be represented in a simple analysis like this one.

In this analysis, a triangular stress distribution was used when considering the compression strength of the material. However, it is also possible to use a rectangular distribution, which would slightly alter the calculation of α_0.

The selection of the first point for iterations in the capacity spectrum method (Method B) can sometimes be a crucial step. The first assumption for the displacement of the performance point is the elastic displacement demand for the equivalent system. Occasionally, this point falls beyond the ultimate displacement of the capacity curve (if the element has low stiffness or low ductility). In this case, the ultimate displacement should be used as the starting point. The reduced spectrum should intersect the capacity curve and the next iteration should use the displacement of their intersection point. However, for some cases, the iterations diverged, for no clear reason. (ATC, 1996) stated that it is possible to choose as a first assumption "any other point chosen on the basis of engineering judgment," therefore, different values for the displacement were tested until one yielded a reduced spectrum which intersected with the capacity curve within 1 mm of the assumed displacement. It is unfortunate that convergence is not guaranteed when starting with the suggested displacement. This phenomenon happened more often with the NCSE-02 spectrum than the EC 8 spectrum, probably because this spectrum is not as steep as the EC 8 spectrum, therefore, a small reduction in the spectrum can yield a large reduction in the displacement of the demand-capacity intersection. This method must thus be used by a cautious and patient engineer who is willing to experiment with the first value of the displacement when it does not converge.

Of course, one must keep in mind that this method depends on the failure of the element as a rigid body, which can be a gross oversimplification in some cases. Historically, however, it has proved relatively representative in analyses of church macroelements.

In the case of very stiff structures with a small yield displacement, the damage thresholds Sd_1 and Sd_2 are very close together. The difference between them may be fractions of a millimeter, meaning that the structure could theoretically pass from damage level 0 to 2 with just a tiny increase in displacement. This is unlikely in a real structure.

Based on the percent difference in the results it seems that the choice of the code (EC 8 or NCSE-02) can greatly affect the calculation. As expected, the code that has a larger displacement demand for that structure is the one yielding performance points with larger displacements. It is hard to make generalizations about which method or code is systematically more accurate but it seems that the elevated elements (gable of facade, belfry, bell tower on top of transept) and those that were less stiff

(some of the facades) saw higher percent differences than the other elements. It can also be said that in the calculations using one code, the two methods usually yielded results close together.

Based on the analysis performed on these two churches, the method seems to be a useful one for studying local failures. It is more useful than a complex model for determining the capacity of a macroelement with regard to a certain failure mechanism. The overturning mechanisms are the easiest to analyze with this method, which is why many of them have been analyzed in this report, but kinematic limit analysis can also be used for in-plane shear mechanisms and others.

5. POSSIBLE INTERVENTIONS

5.1. Possible interventions in Poblet

Poblet actually has a high vulnerability index, $i_{v,high} = 0.65$, which should be reduced by some interventions. A first recommendation would be to consider interventions that have been performed on other churches after earthquakes; Italy has rebuilt many with strengthening techniques that may be applicable to these cases too.

The gable belfry, which appeared to be the weakest element, actually had a relatively high capacity ($a_y = 0.15g$) and thus would not be damaged in an earthquake of the reference ground acceleration. Yet, as its support may be uneven (partially on the facade and partially on the vault), more detailed analysis may be a good idea to see the issues it may have. An intervention would be complex and would have to avoid adding rigidity to the structure and worsening its behavior (Lagomarsino, 2012).

The weakest macroelement is the transept facade, both the case limited by the walls and vault, and the case inclusive of the connection. A possible intervention that could be made is the improvement of the connections between the transept walls and facade. This could be performed with some ties in the transept anchored on the facade with an appropriate anchor plate. Or, confining rings of steel cables are another option. The roof should be adequately connected so that it can help to relieve some seismic forces in-plane. The insertion of a lightweight tie beam at the top of the building is also an option although it may be a more invasive installation compared to the others (Modena et al., 2011).

5.2. Possible interventions in Sant Miquel de Cruïlles

If a strong earthquake should hit the church of Sant Miquel de Cruïlles, it may sustain considerable damage. Based on the vulnerability index method, the church has a vulnerability of about $i_v = 0.5$ and damage index $i_d = 0.1$. A tripling of the damage index could bring the church to the point of being unusable. By the kinematic limit analysis, the mechanisms with the lowest activation accelerations are the wall of the bell tower and the main facade (all three cases), followed closely by the south transept facade.

The wall of the bell tower, besides being tall and slender, is also worrisome for its many masonry discontinuities due to different construction periods, as well as the concrete floor that was added inside. The north side of the tower has buttresses and the east side is braced by the aisle. Therefore, the out-of-plane mechanism in the west direction is the most likely. The bell tower could possibly benefit from confining with tie-rods or external confining with steel cables; buttresses matching the others around the

church are also a possibility. Due to the rubble masonry, any installation would have to have suitable anchorage for load transfer.

Tie-rods would likely be useful for the main and transept facades, so that they stay attached to the walls and avoid out-of-plane movement. Buttresses are also an option, especially for the transept facades, where the aesthetics of the intervention are less important because they are not very visible from the front of the church.

The apse presents the most notable damage in the church. It must be dealt with carefully since it has important Romanesque paintings both in the vault and the walls. The most common effective way to compensate horizontal forces in a vault is with a tie-rod. This would be especially important if damage should occur in the connection of the apse to the walls, which are currently containing the thrust from the apse; in this case, the tie-rod would hold the vault from spreading.

Due to the weakness of the rubble masonry, if radial cracks in the half dome which are already present should worsen, there is doubt whether the half dome would be able to support itself by acting as a series of stable arches. Thus, a tension ring about the base of the half dome would be an option, to take out-of-plane actions and prevent cracks from spreading or causing collapse.

It is possible that with the history of structural interventions in Cruïlles and the lack of quality ashlar masonry, there may be patches with voids, even in the regions that are hidden by plaster. It would be interesting to conduct sonic tests in order to evaluate the quality of the wall. If there are regions with voids or cracks, they may benefit from grout injections which would help increase the strength and global behavior of the entire structure.

6. CONCLUSION

6.1. Summary of results

This report first presented the vulnerability index analysis of the churches of Sant Miquel de Cruïlles and Santa Maria de Poblet. For Cruïlles, the damage index was higher but the vulnerability index lower in comparison to Poblet. The acceleration required to reach the limit states was also higher for Cruïlles. The vulnerability indices both fell into the range found in (De Matteis, Brando, Corlito, et al., 2019), so the churches can be considered to be of comparable vulnerability to most Italian churches. Both Poblet and Cruïlles are expected to reach the damage limit states for the code-specified reference ground accelerations. For an earthquake of 475-year return period, Poblet would be expected to reach damage level $\mu_D = 1.9$ and Cruïlles would reach level $\mu_D = 2.4$.

The kinematic limit analysis method was carried out next. It found that damage will be experienced, of level "moderate" to "extensive," in almost all elements for both churches. For Poblet, the elements with highest capacity with respect to overturning are the gables of the facades and the apse case 4 (no infill and a transverse arch stress distribution). The weakest element is the transept facade (both cases 1 and 2), followed by the main facade and bell tower. Most of the elements have an activation acceleration higher than the reference ground acceleration. For Cruïlles, the elements with highest capacity are the gable of the main facade, bell tower, main apse, and lateral apse. The rest of the elements may be vulnerable to overturning given the reference ground acceleration. So, for local failures assessed by the kinematic limit analysis method, Cruïlles seems to be more at-risk than Poblet, since most of its elements have capacities below the reference ground acceleration.

6.2. Vulnerability of Romanesque churches in Catalonia

This thesis presents two quite unique churches. Although they hail from roughly the same time period, they are different in size, masonry type, regional seismicity, and vulnerability. Nevertheless, this report will try to draw conclusions between them and to Catalonian Romanesque churches as a whole.

Vulnerabilities often present in Romanesque churches include openings in the masonry and vaults. They may have large rose windows or doors but on the whole Romanesque windows are smaller than, for example, Gothic ones. In these case studies, Poblet had large openings while Cruïlles had small ones. Also present in Romanesque churches are large heavy vaults. They may be much thicker than Gothic vaults, and their thrust may cause structural problems over time if not adequately balanced, such as the spreading of piers, rotating of clerestory walls or bases of piers.

Anti-seismic measures may include buttresses, which are present systematically throughout Cruïlles and in some bays in Poblet. Cruïlles also contained tie-rods, the only other measure seen in either

church that specifically improves seismic functioning. Generally, not many anti-seismic measures are present in Romanesque churches, making them vulnerable. In Cruïlles, only 5 out of the 20 mechanisms applicable to the church had a non-zero anti-seismic score, and in Poblet, just 1 of the 22.

Conclusions drawn from this study can be applied to similar churches. Thin slender elements are vulnerable, as has been shown in other studies. The walls of Sant Miquel de Cruïlles are quite thin, usually less than one meter, which makes the facades vulnerable to overturning. It is important to remember that failure planes may occur along boundaries of different masonry types, so multiple failure cases should be studied to see the most vulnerable ones. In churches that have undergone many structural interventions throughout their lifetimes, this can be a significant concern. The existing cracks of the structure should always be taken into account as hints of the most vulnerable mechanisms.

6.3. Comparison of analysis methods

From the studies presented herein, a few observations can be made. First, the vulnerability level may be influenced by elements that appear to be very vulnerable (e.g. gable belfry of Poblet). When the kinematic limit analysis is conducted, the macroelements may not prove to be as weak as expected. The vulnerability method is a more judgment-based qualitative approach, sensitive to the opinion of the analyst, whereas the kinematic limit analysis takes in the geometry to quantitatively assess the capacity of the structure. If a reliable geometrical survey cannot be obtained, this analysis could be problematic.

For Cruïlles, the damage index was higher but the vulnerability index lower in comparison to Poblet. The acceleration required to reach the limit states was also higher for Cruïlles. This is surprising considering the current damage state of the apse; it seems intuitive that a very small acceleration would be required to cause further damage. However, the vulnerability index method does not adequately describe local behavior like the kinematic limit analysis does. Plus, neither of the methods offers a way to reduce capacity due to existing damage because that would be too complex to quantify.

The kinematic limit analysis method rated the level of damage expected in each element of the church rather than in the church as a whole, like the vulnerability index method. With only results from the vulnerability index method, an engineer might add some anti-seismic measures to the main nave for global stability and neglect a transept facade that is very weak. The kinematic limit analysis method gives a better understanding of where interventions may be necessary to improve the local and then global behavior.

The vulnerability index method is certainly much faster than the kinematic limit analysis and has proven to be useful throughout years of Italian earthquake surveys. It has a set procedure and is performed the same way with every church. The kinematic method is more variable, tailored to each church's geometry

and architectonic configuration. There is no clear end to the process; at some point, the mechanisms become significantly unfeasible and the engineer must assume that she has likely addressed the most dangerous failure mechanisms of the structure.

6.4. Future work

The vulnerability index method is derived from seismic surveys designed to analyze churches on a statistical basis rather than an individual one, although it can offer information about individual churches too. It would be interesting to implement the method on more Romanesque churches in Catalonia, to see if patterns can be drawn between typologies or similarities can be found in the macroelements and their behavior.

As mentioned early in this work, not many studies combine and compare the vulnerability index method with kinematic limit analysis. It would be interesting to perform kinematic limit analysis on churches that have already been studied in post-earthquake surveys with the vulnerability index method. It would be possible to see if the failure mechanisms indeed were activated during the earthquake at the expected acceleration, and whether the damage matched that expected by the two analysis methods.

The recently-proposed method by (Lagomarsino et al., 2019) will presumably be tested in the next few earthquakes, and it will be interesting to see how it fares. Hopefully its results will continue to prove more accurate than the current method and representative of a wider array of churches. It should soon be applied to the vulnerability index calculation as well, and it will be interesting to note whether it makes different predictions about the vulnerability of each church.

It is clear that the field of seismic analysis is perpetually evolving; and improving simplified methods for expedited analysis in order to safeguard as many valuable heritage structures as possible should continue to be a priority in this field.

This page is left blank on purpose.

7. REFERENCES

Álvarez-Cascos Fernández, F. (Ministro de F. (2002). Norma de Construcción Sismorresistente NCSE-02.

Anejo Nacional AN/UNE-EN 1998-1. (1998).

Angeletti P, Ferrini M, Lagomarsino S (1997) Rilievo e valutazione della vulnerabilità sismica delle chiese: un esempio in Lunigiana e Garfagnana. In: Proceedings of VIII ANIDIS conference, Taormina, vol 2, 22–24 Sept 1997 (in Italian)

ATC. (1996). Seismic evaluation and retrofit of concrete buildings. Redwood City, California: Applied Technology Council. Retrieved from http://digitalcommons.calpoly.edu/cgi/viewcontent.cgi?article=1052&context=cenv_fac

Baldiri, B. (2019). Monesterios de Cataluña. Retrieved from https://www.monestirs.cat

BBC. (2018). Catalonia region profile. Retrieved from https://www.bbc.com/news/world-europe-20345071

Benincà, I. G., Barbetta, I. E., Munari, I. M., Modena, C., Valluzzi, M. R., & Zenere, M. (2009). *Manuale d'uso del Programma c-Sisma 3.0 PRO*. Padova.

Brando, G., De Matteis, G., & Spacone, E. (2017). Predictive model for the seismic vulnerability assessment of small historic centres: Application to the inner Abruzzi Region in Italy. *Engineering Structures*, *153*(September), 81–96. https://doi.org/10.1016/j.engstruct.2017.10.013

Cattaneo, S. (2014). Vulnerabilità sismica delle chiese in muratura: il meccanismo di collasso per risposta trasversale dell'aula.

Cecchi, R., & Calvi, M. (2006). Italian Guidelines for evaluation and mitigation of seismic risk to cultural heritage.

CEN. (1998). *Eurocode 8 (2004): EN 1998-1: Eurocode 8 - Design of structures for earthquake resistance*. Brussels, Belgium: European Committee for Standardization.

Cobreras, J. (2003). *Guia Total - Las Rutas del Romanico en España*. (A. Touring, Ed.). Madrid.

De Matteis, G., Brando, G., & Corlito, V. (2019). Simplified Assessment of the Seismic Vulnerability of

Churches After the 2009 L'Aquila Earthquake. In *Structural Analysis of Historical Constructions* (Vol. 18, pp. 1280–1289). RILEM. https://doi.org/10.1007/978-3-319-99441-3

De Matteis, G., Brando, G., Corlito, V., Criber, E., & Guadagnuolo, M. (2019). Seismic vulnerability assessment of churches at regional scale after the 2009 L'Aquila earthquake. *International Journal of Masonry Research and Innovation*, *4*(1/2), 174–196. https://doi.org/10.1504/ijmri.2019.096824

De Matteis, G., Criber, E., & Brando, G. (2016). Damage Probability Matrices for Three-Nave Masonry Churches in Abruzzi after the 2009 LAquila Earthquake. *International Journal of Architectural Heritage*, *10*(2–3), 120–145. https://doi.org/10.1080/15583058.2015.1113340

Doglioni, F., Moretti, A., Petrini, V., & Angeletti, P. (1994). *Le Chiese e il Terremoti: Dalla Vulnerabilità Constatata nel Terremoto del Friuli al Miglioramento Antisismico nel Restauro, Verso una Politica di Prevenzi*. (L. E. Associati, Ed.). Trieste, Italy: Edizioni Lint.

Dominguez, A. C., 2012. Applicacion de la estatica grafica a la iglesia del monesterio de Poblet. Master Thesis. School of Architecture of Barcelona, Technical University of Catalonia.

Fajfar, P. (2000). A Nonlinear Analysis Method for Performance-Based Seismic Design. *Earthquake Spectra*, *16*(3), 573–592. https://doi.org/10.1193/1.1586128

FEMA. (1997). NEHRP Guidelines for the seismic rehabilitation of buildings (FEMA Publication 273). Washington, D.C.: Federal Emergency Management Agency.

Ferreira, T. M., Vicente, R., Mendes da Silva, J. A. R., Varum, H., & Costa, A. (2013). Seismic vulnerability assessment of historical urban centres: case study of the old city centre in Seixal, Portugal. *Bulletin of Earthquake Engineering*, *11*, 1753–1773.

Generalitat de Catalunya. (n.d.-a). ESGLÉSIA DE SANT MIQUEL DE CRUÏLLES. Retrieved May 14, 2019, from http://invarquit.cultura.gencat.cat/Cerca/Fitxa?index=0&consulta=&codi=115

Generalitat de Catalunya. (n.d.-b). Monestir de Santa Maria de Poblet. Retrieved June 25, 2019, from http://invarque.cultura.gencat.cat/FitxaGeneral?index=0&consulta=MSUxK3NhbnRhIG1hcmlhIGRlIHBvYmxldCBtb25lc3RpciUyKy0xJQ%3D%3D&codi=1413

Generalitat de Catalunya. (2014). Pla especial d'emergències sísmiques a catalunya. SISMICAT. Retrieved from http://interior.gencat.cat/web/.content/home/030_arees_dactuacio/proteccio_civil/plans_de_proteccio_civil/plans_de_proteccio_civil_a_catalunya/documents/pla_sismicat_document.pdf

Generalitat de Catalunya. (2018). Mapa de mesozonació sísmica de Catalunya a escala 1:250.000. Institut Cartogràfic i Geològic de Catalunya. Retrieved from http://www.icgc.cat/es/Administracion-y-empresa/Descargas/Cartografia-geologica-y-geotematica/Mapas-geofisicos-y-sismicos/Mapa-de-mesozonacion-sismica-de-Cataluna-1-250.000

Godes, J. M. i, & Adell, J.-A. (2001). *La Catalunya Nova - Viatge al romànic català* (1st ed.). Barcelona: RACC-62.

Google Maps. (2019). Retrieved from maps.google.com

Grünthal, G. (1998). *Escala Macro Sísmica Europea EMS - 98* (Vol. 15). Retrieved from http://lib.riskreductionafrica.org/bitstream/handle/123456789/1193/1281.European Macroseismic Scale 1998.pdf?sequence=1

G. U. no. 47, Recommendations P.C.M. (2011). *Assessment and mitigation of seismic risk of cultural herit- age with reference to the Technical Code for the design of constructions, issued by D.M. 14/1/2008. Directive of the Prime Minister, 9/02/2011 (suppl. ord. no. 54)*. (In Italian)

Huerta, S. (2001). Mechanics of masonry vaults: the equilibrium approach. *Proc. of the 1st International Congress on Structural Analysis of Historical Constructions, Guimaraes*, (January), 47–70.

Kazantzidou-Firtinidou, D., Lestuzzi, P., Podestà, S., Luchini, C., & Bozzano, C. (2016). Improvement of Risk-UE LM2 capacity curves for reliable seismic vulnerability assessment at urban scale in Switzerland. *1st International Conference on Natural Hazards & Infrastructure*.

Lagomarsino, S. (2012). Damage assessment of churches after L'Aquila earthquake (2009). *Bulletin of Earthquake Engineering*, *10*(1), 73–92. https://doi.org/10.1007/s10518-011-9307-x

Lagomarsino, S., Cattari, S., Ottonelli, D., & Giovinazzi, S. (2019). *Earthquake damage assessment of masonry churches: proposal for rapid and detailed forms and derivation of empirical vulnerability curves*. *Bulletin of Earthquake Engineering*. Springer Netherlands. https://doi.org/10.1007/s10518-018-00542-8

Lagomarsino, S., & Podestà, S. (2004a). Seismic vulnerability of ancient churches: I. Damage assessment and emergency planning. *Earthquake Spectra*, *20*(2), 377–394. https://doi.org/10.1193/1.1737735

Lagomarsino, S., & Podestà, S. (2004b). Seismic vulnerability of ancient churches: II. Statistical Analysis of Surveyed Data and Methods for Risk Analysis. *Earthquake Spectra*, *20*(2), 395–412.

https://doi.org/10.1193/1.1737736

Leite, J., Lourenco, P. B., & Ingham, J. M. (2013). Statistical assessment of damage to churches affected by the 2010-2011 canterbury (New Zealand) earthquake sequence. *Journal of Earthquake Engineering*, *17*(1), 73–97. https://doi.org/10.1080/13632469.2012.713562

Milutinovic, Z. V., & Trendafilosk, G. S. (2004). *WP4 Vulnerability of current buildings*. https://doi.org/10.1007/978-1-4020-3608-8_23

Modena, C., Valluzzi, M. R., da Porto, F., & Casarin, F. (2011). Structural Aspects of The Conservation of Historic Masonry Constructions in Seismic Areas: Remedial Measures and Emergency Actions. *International Journal of Architectural Heritage: Conservation, Analysis, and Restoration*, *5:4-5*, 539–558. https://doi.org/10.1080/15583058.2011.569632

Montaner, L. D. y. (1925). *Historia y Arquitectura del Monestir de Poblet*. Barcelona: Montaner y Simón.

NTC. (2018). Aggiornamento delle “Norme tecniche per le costruzioni.” *Gazzetta Ufficiale Della Repubblica Italiana*, 1–198.

NTC. (2019). Istruzioni per l’applicazione dell’«Aggiornamento delle “Norme tecniche per le costruzioni”» di cui al decreto ministeriale 17 gennaio 2018. *Gazzetta Ufficiale Della Repubblica Italiana*.

Oliver, B. R., & Gresko, F. G. (n.d.). A Brief History of the Benedictine Order. Retrieved July 1, 2019, from osb.org

Penna, A., Calderini, C., Sorrentino, L., Carocci, C. F., Cescatti, E., Sisti, R., … Prota, A. (2019). Damage to churches in the 2016 central Italy earthquakes. *Bulletin of Earthquake Engineering*. https://doi.org/10.1007/s10518-019-00594-4

Pladevall i Font, A., & Gurri i Serra, F. (2014). Romanesque Art Routes. Generalitat de Catalunya.

Rotger, A. (2011, April). La revolta dels remences: la transcripció d’un document inèdit. *Sàpiens*. Retrieved from https://www.sapiens.cat/temes/catalunya/la-revolta-dels-remences_11015_102.html

Saloustros, S. (2013). *Structural Analysis of the Church of the Poblet Monastery*. Polytechnic University of Catalonia.

Saloustros, S., Pelà, L., Roca, P., & Portal, J. (2014). Assessment of structural damage in historical constructions using numerical models: the case of the church of the Poblet Monastery. *Engineering Failure Analysis*, *48*, 41–61. https://doi.org/10.1016/j.engfailanal.2014.10.015

Saloustros, S., Pelà, L., Roca, P., & Portal, J. (2015). Numerical analysis of structural damage in the church of the Poblet Monastery. *Engineering Failure Analysis*, *48*, 41–61. https://doi.org/10.1016/j.engfailanal.2014.10.015

Sorrentino, L., Liberatore, L., Decanini, L. D., & Liberatore, D. (2014). The performance of churches in the 2012 Emilia earthquakes. *Bulletin of Earthquake Engineering*, *12*(5), 2299–2331. Retrieved from https://doi.org/10.1007/s10518-013-9519-3

Susagna i Vidal, M. T., & Goula i Suriñach, X. (1999). *Atles sísmic de Catalunya* (Vol. 1. Catàleg).

The Cistercian Route. (2019). Retrieved June 10, 2019, from http://www.catvisit.com/en/the-cistercian-route/

Valente, M., Barbieri, G., & Biolzi, L. (2017). Damage assessment of three medieval churches after the 2012 Emilia earthquake. *Bulletin of Earthquake Engineering*, *15*(7), 2939–2980. https://doi.org/10.1007/s10518-016-0073-7

Vigué, J. (1989). *Catalunya Romànica VIII L'Empordà I*. Barcelona: Fundació Enciclopèdia Catalana.

Vigué, J. (1995). *Catalunya Romànica XXI El Tarragonès, El Baix Camp, L'Alt Camp, El Priorat, La Conca de Barberà*. Barcelona: Fundació Enciclopèdia Catalana.

This page is left blank on purpose.

A. APPENDIX

A.1. Mechanisms

1 - Overturning of the Facade Detachment of the facade from the walls or evident out of plumb Anti-seismic Measures • presence of longitudinal tie-rods • presence of effective elements of contrast (buttresses, leaning buildings) • good quality clamping between the facade and side walls of the nave Vulnerability Indicators • presence of thrusting elements (roof rafters, vaults, arches) • presence of large openings in side walls near corners	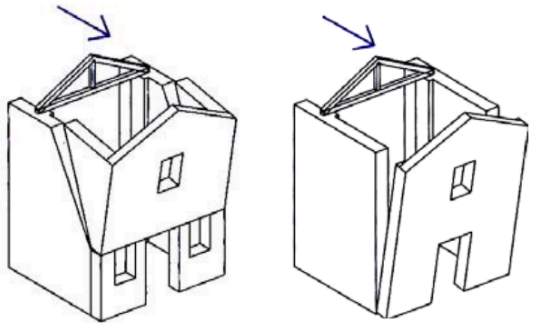
2 - Damage at the top of the facade Overturning of the gable, with horizontal or v-shaped cracking - Disaggregation of masonry or shifting of tie-beams - Rotation of the trusses Anti-seismic Measures • presence of local connections to roof elements • presence of roof braces • presence of lightweight tie-beams (steel, reinforced masonry or other) Vulnerability Indicators • presence of large openings (rose windows) • presence of large and heavy towering gable • rigid tie-beams, ridge beams in reinforced concrete, heavy roof coverings in reinforced concrete	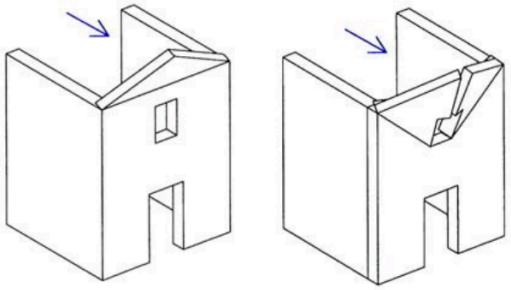
3 - Shear mechanisms in the facade Diagonal cracking (shear) - Vertical or arched cracking (rotation) - Other cracking or bulging Aseismic Measures • presence of tie-rods placed at the rear of the facade • lateral contrast supplied by leaning building; churches in an aggregate Vulnerability Indicators • presence of large or numerous openings (even if in-filled) • thin vertical elements (ratio between height and width)	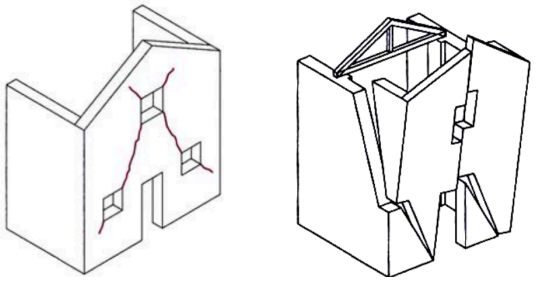

4 - Narthex Cracking in the arches or in the trabeation due to column rotation - Detachment of the facade - Pounding Aseismic Measures • presence of tie-rods • presence of adequately sized columns/pillars Vulnerability Indicators • presence of thrusting (arches, vaults)	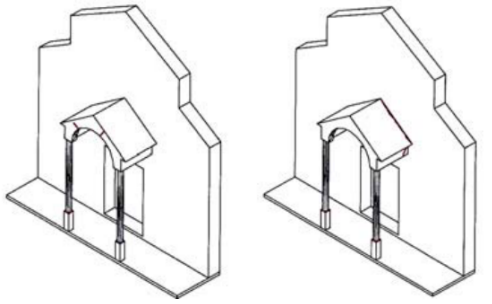
5 - Transversal vibration of the nave Cracking in transversal arches (that might extend in the vaults) - Rotation in side walls - shear cracking in vaults - Out of plumb and crushing of columns Aseismic Measures • presence of pilasters or external buttresses • presence of adjacent leaning buildings • presence of transverse tie-rods Vulnerability Indicators • presence of very thin walls • presence of vaults and arches	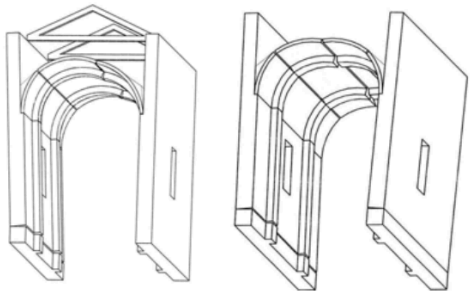
6 - Shear mechanisms in the side walls Diagonal cracking (single or crossed) - Cracking next to wall discontinuity Aseismic Measures • good quality masonry (without different construction phases) • presence of good architraves over the openings • presence of lightweight tie-beams (steel, reinforced masonry or others) Vulnerability Indicators • presence of large openings or wide zones with limited masonry thickness • very rigid tie-beams, heavy reinforced concrete roof covering	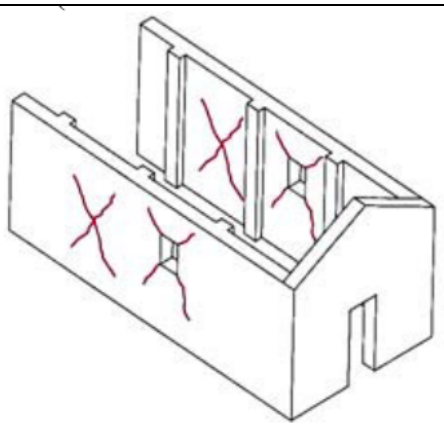
7 - Longitudinal response of the colonnade Cracking in the arches or in longitudinal architraves - Crushing and/or cracking at the base of the pillars - Shear cracking in vaults or lateral naves Aseismic Measures • presence of longitudinal tie-rods • presence of buttresses in the facade Vulnerability Indicators • presence of heavy vaults in the central nave • heavy reinforced concrete roof coverings, very thick reinforced concrete capping in the vaults	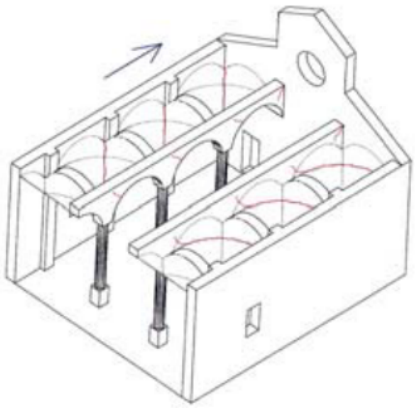

8 - Vaults of the nave Cracking in the vault of the central nave - Detachment of the vaults from the arches Aseismic Measures • presence of effectively placed tie-rods • presence of external or internal buttresses Vulnerability Indicators • presence of concentrated loads from the roof structure • thin vaults, especially if on a wide span • presence of lunettes or interruptions and irregularities to the sides of the vaults	Barrel vault with lunettes 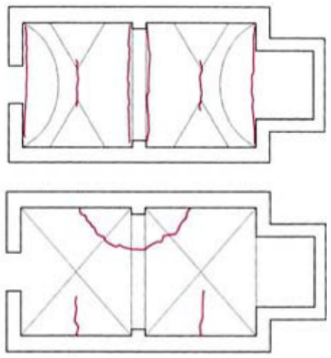 Cross vault
9 - Vaults of the aisles Cracking in vaults or detachment from the arches or the side walls Aseismic Measures • presence of effectively placed tie-rods • presence of external or internal buttresses Vulnerability Indicators • presence of concentrated loads from the roof structure • thin vaults, especially if on a wide span • presence of lunettes or interruptions and irregularities to the sides of the vaults	Pavilion vault 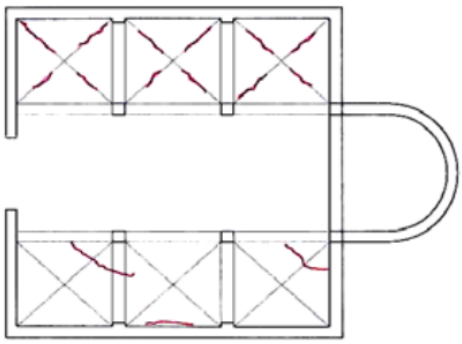 Cross vault
10 - Overturning of the transept facade Detachment of the end wall from the side walls - Overturning or displacement of the gable Aseismic Measures • presence of tie-rods • presence of effective propping elements (buttresses, leaning buildings) • good connection with roof covering (tie-beams, braces) • good quality side walls to facade clamping • presence of lightweight tie-beams (steel, reinforced masonry or others) Vulnerability Indicators • presence of rigid tie-beams, top beams in reinforced concrete, heavy roof coverings • presence of large openings in the facade (rose windows) and/or in side walls • presence of large and heavy towering gable	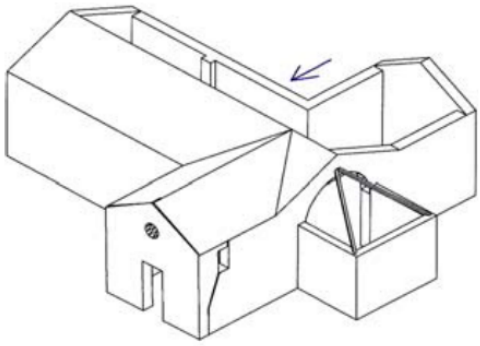

11 - Shear mechanisms in the transept walls Diagonal cracking (single or crossed) - Cracking next to wall discontinuities Aseismic Measures • good quality masonry (without different construction phases) • presence of good architraves over the openings • presence of lightweight tie-beams (steel, reinforced masonry or others) Vulnerability Indicators • presence of large openings or wide zones with limited masonry thickness • presence of stiff tie-beam, heavy roof coverings	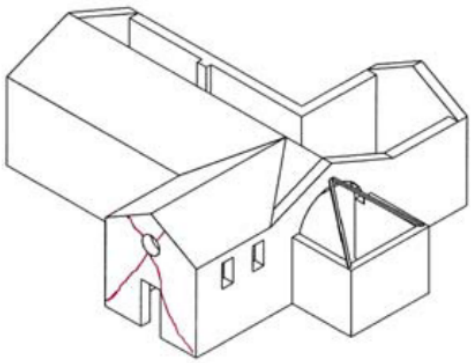
12 - Vaults of the transept Cracking in the vaults or detachment from the arches and/or the side walls Aseismic Measures • presence of effectively placed tie-rods • presence of external or internal buttresses Vulnerability Indicators • presence of concentrated loads from the roof structure • thin vaults, especially if on a wide span • presence of lunettes or interruptions and irregularities to the sides of the vaults	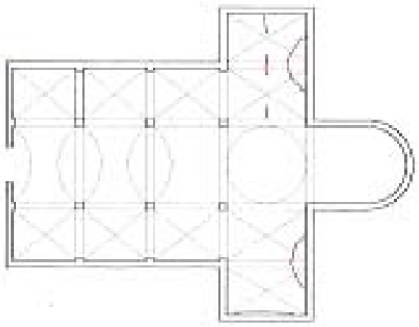
13 - Triumphal arches Cracking in the arch - Sliding of the ashlars - Crushing or horizontal cracking at the base of the piers Aseismic Measures • stiff lateral walls (low ratio arch span/width of the nave, transept and other macroelements) • presence of effectively placed tie-rods • well-hewn key stones and/or adequate arch thickness Vulnerability Indicators • presence of heavy reinforced concrete roof covering • presence of dome, drum or tiburio	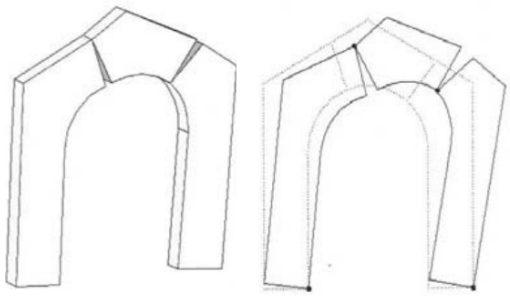
14 - Dome, drum and tiburio Cracking in the dome (curved) with eventual continuation to the drum Aseismic Measures • presence of external rings, at differing heights • presence of external buttresses or pilasters in the drum • dome placed directly on triumphal arches (absence of drum) Vulnerability Indicators • presence of large openings in the drum • presence of concentrated loads from the roof covering	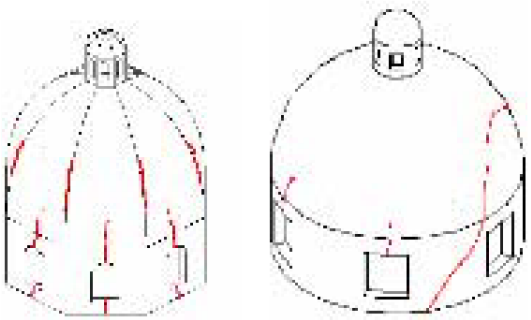

15 - Lantern Cracking of the smaller dome in the lantern - Rotation or displacement of the piers Aseismic Measures • presence of tie-rods or external reinforcing rings • presence of pilasters or buttresses • small size compared to the dome Vulnerability Indicators • very thin lanterns, with large openings and slender pillars	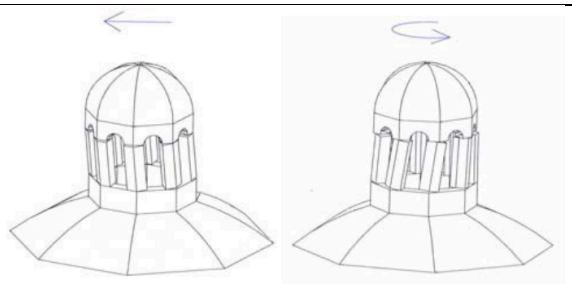
16 - Overturning of the apse Vertical or curved cracking in the walls of the apse - Vertical cracking in polygonal apses - U-shaped cracking in semi-circular apses Aseismic Measures • presence of reinforcement rings (semi-circular or polygonal apses) or tie-rods (rectangular apses) • presence of effective propping elements (buttresses, outlying buildings) • presence of non-thrusting, braced roof Vulnerability Indicators • presence of weakness due to openings (even in-filled) in the walls • presence of thrusting vaults • stiff tie-beams, heavy roof coverings, reinforced concrete roof rafters	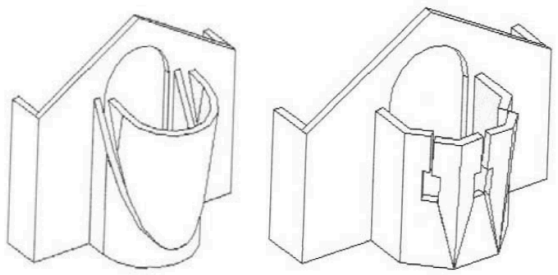
17 - Shear mechanisms in the presbytery and the apse Diagonal cracking (single or crossed) - Cracking next to masonry discontinuity Aseismic Measures • good quality masonry (without different construction phases) • presence of good architraves over the openings • presence of lightweight tie-beams (steel, reinforced masonry or others) Vulnerability Indicators • presence of large openings or areas with limited wall thickness • presence of rigid tie-beams, heavy roof coverings	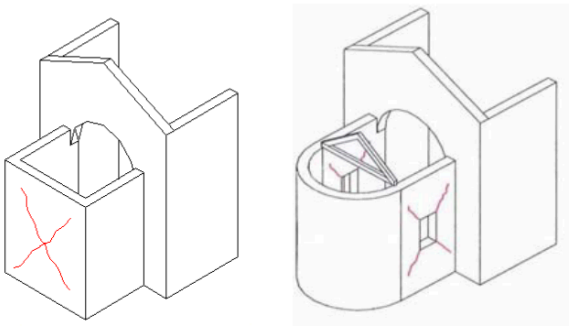
18 - Vaults in the presbytery and the apse Cracking in vaults or detachment from arches or side walls Aseismic Measures • presence of effectively placed tie-rods • presence of internal or external buttresses Vulnerability Indicators • presence of concentrated loads from the roof structure • thin vaults, especially if on a wide span • presence of lunettes or interruptions and irregularities to the sides of the vaults	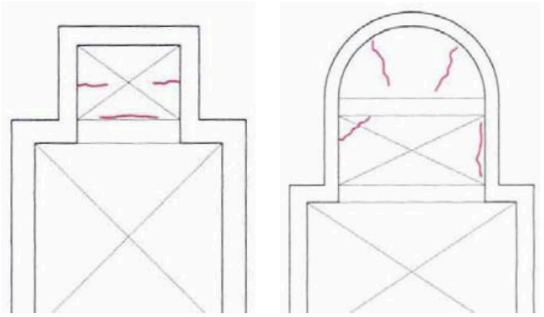

19 - Roof mechanisms: side walls of nave and aisles
Cracking near the head of wooden beams; sliding of the beams - Detachment between tie-beams and masonry - Significant displacement of the covering carpet
Aseismic Measures
- presence of lightweight tie-beams (steel, reinforced masonry, or others)
- presence of good wall to beam connections
- presence of roof braces (crossed planks or steel tie-rods)
- presence of good connections between roof elements

Vulnerability Indicators
- presence of static thrusts in the roof
- presence of rigid tie-beams, heavy roof coverings

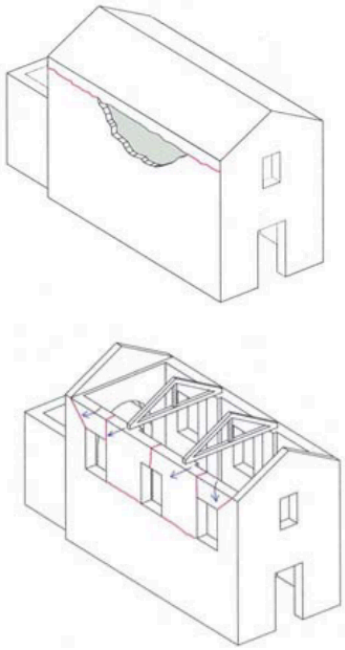

20 - Roof mechanisms: transept
Cracking near the head of wooden beams; sliding of the beams - Detachment between tie-beams and masonry - Significant displacement of the covering carpet
Aseismic Measures
- presence of lightweight tie-beams (steel, reinforced masonry, or others)
- presence of good wall to beam connections
- presence of roof braces (crossed planks or steel tie-rods)
- presence of good connections between roof elements

Vulnerability Indicators
- presence of static thrusts in the roof
- presence of rigid tie-beams, heavy roof coverings

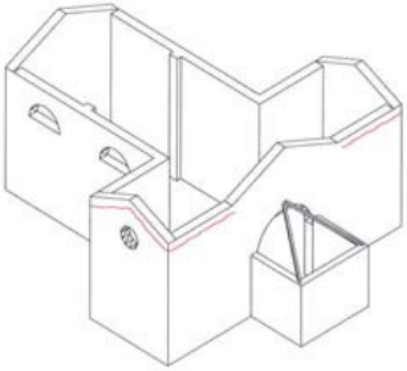

21 - Roof mechanisms: apse and presbytery
Cracking near the head of wooden beams; sliding of the beams - Detachment between tie-beams and masonry - Significant displacement of the covering carpet
Aseismic Measures
- presence of lightweight tie-beams (steel, reinforced masonry, or others)
- presence of good wall to beam connections
- presence of roof braces (crossed planks or steel tie-rods)
- presence of good connections between roof elements

Vulnerability Indicators
- presence of static thrusts in the roof
- presence of rigid tie-beams, heavy roof coverings

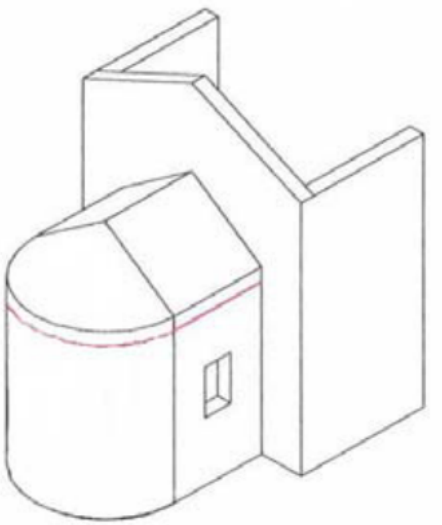

22 - Overturning of the chapels Detachment of the end walls from the side walls Aseismic Measures • presence of effective propping elements (buttresses, leaning buildings) • presence of reinforcement rings or tie-rods • good quality end wall to side wall clamping Vulnerability Indicators • presence of great weaknesses due to wall openings	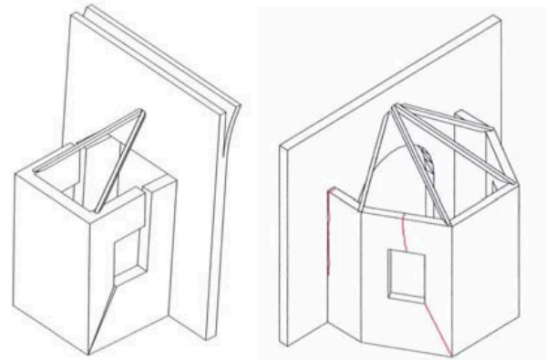
23 - Shear mechanisms in the chapel walls Diagonal cracking (single or crossed) - Cracking next to masonry discontinuities Aseismic Measures • good quality masonry (without different construction phases) • presence of good architraves over the openings • presence of lightweight tie-beams (steel, reinforced masonry or others) Vulnerability Indicators • presence of large openings (even in-filled), or limited masonry thickness • presence of rigid tie-beams, heavy roof coverings	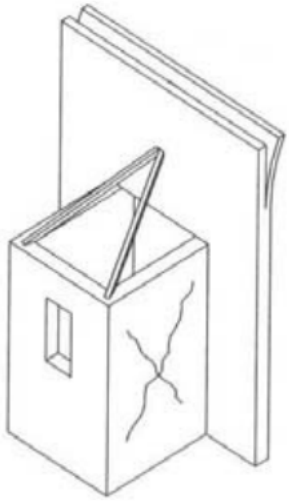
24 - Vaults of chapels Cracking in the vaults or detachment from the walls Aseismic Measures • presence of effectively placed tie-rods • presence of internal or external buttresses Vulnerability Indicators • presence of concentrated loads from the roof covering • thin vaults, especially if on a wide span • presence of lunettes or interruptions and irregularities to the sides of the vaults	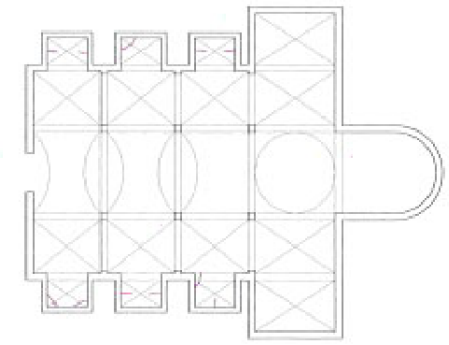
25 - Interactions with adjacent buildings Displacement in correspondence with constructive discontinuity - Cracking in masonry due to pounding Aseismic Measures • presence of adequate connections between the different phases of masonry construction • presence of connecting tie-rods Vulnerability Indicators • presence of a great difference in the stiffness between the two buildings • possibility of concentration of seismic actions in connecting elements	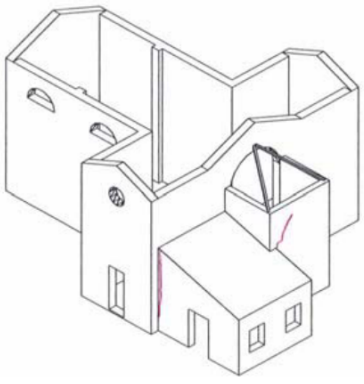

26 - Projections (gable belfry, spires, pinnacles, statues)

Permanent rotation or displacement - Cracking

Aseismic Measures

- presence of connecting pins between the projection and the wall
- elements of small dimensions
- monolithic masonry (squared ashlars)

Vulnerability Indicators

- very thin elements
- overhang support of the element on the underlying wall
- asymmetrical position of the element with respect to the underlying structures

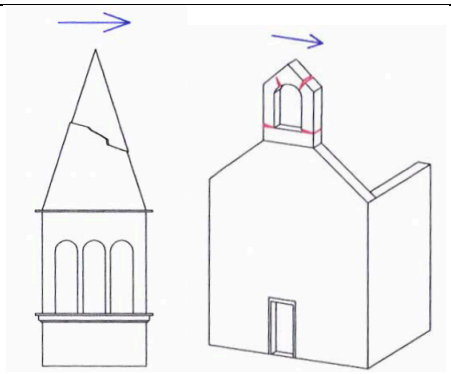

27 - Bell tower

Cracking next to the connection between the bell tower and the church - Shear cracking or sliding - Vertical or curved cracking (bulging of one or more corners)

Aseismic Measures

- good quality uniform masonry (without different construction phases)
- presence of tie-rods at different heights
- presence of an adequate joint between the church walls (if adjacent)
- presence of good wall to wall connections in the church (if incorporated)

Vulnerability Indicators

- presence of large openings at different heights
- asymmetrical support on the church wall at its base (incorporated towers)
- irregular support elements at ground level of towers (presence of arches on some sides, overhung walls)

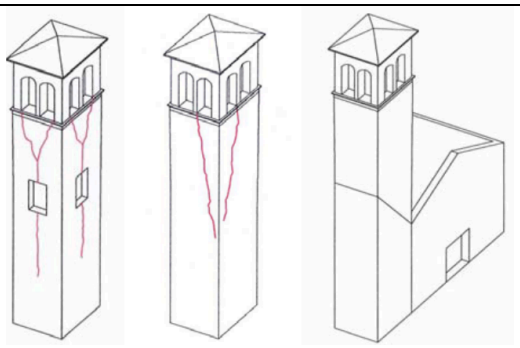

28 - Belfry

Cracking in arches - Rotation and sliding of piers

Aseismic Measures

- presence of squat piers and/or arches with small openings
- presence of tie-rods or reinforcement rings

Vulnerability Indicators

- presence of heavy roof coverings or other significant weights
- presence of thrust from the roof covering

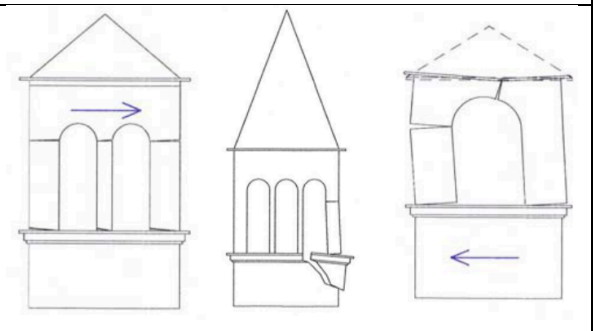

A.2. Kinematic limit analysis results for macroelement overturning

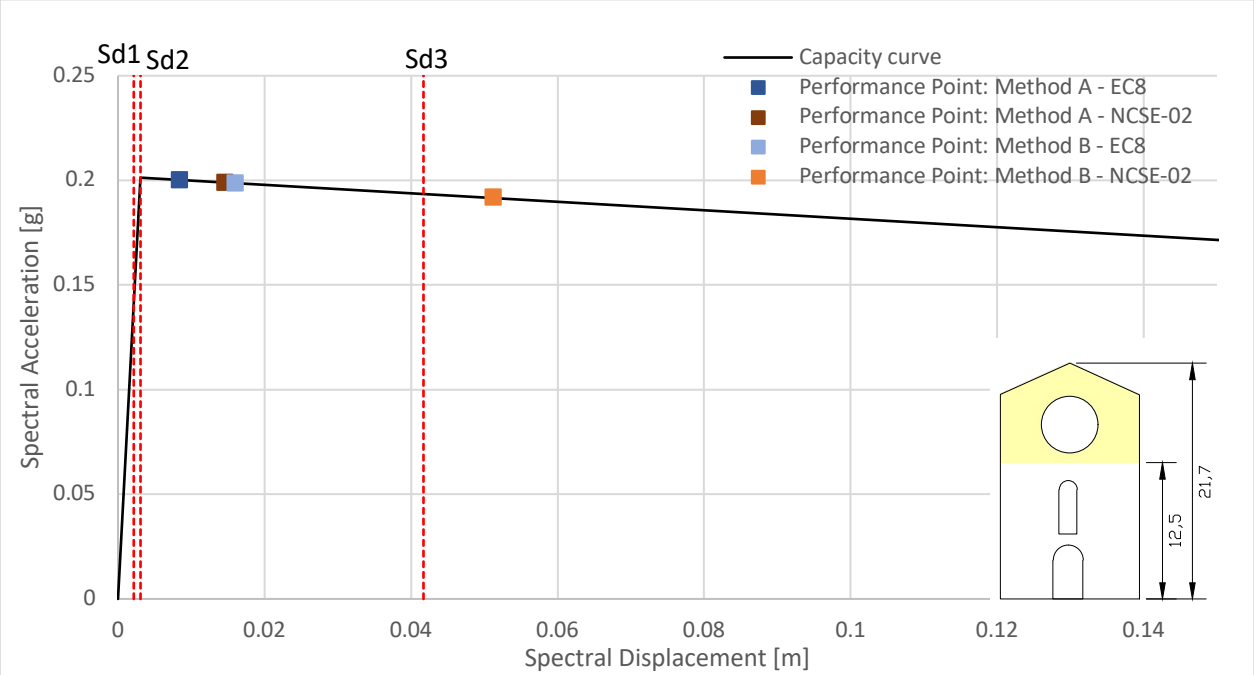

Figure A.2.1. Overturning of Poblet main facade above galilee ($R = 2.10$)

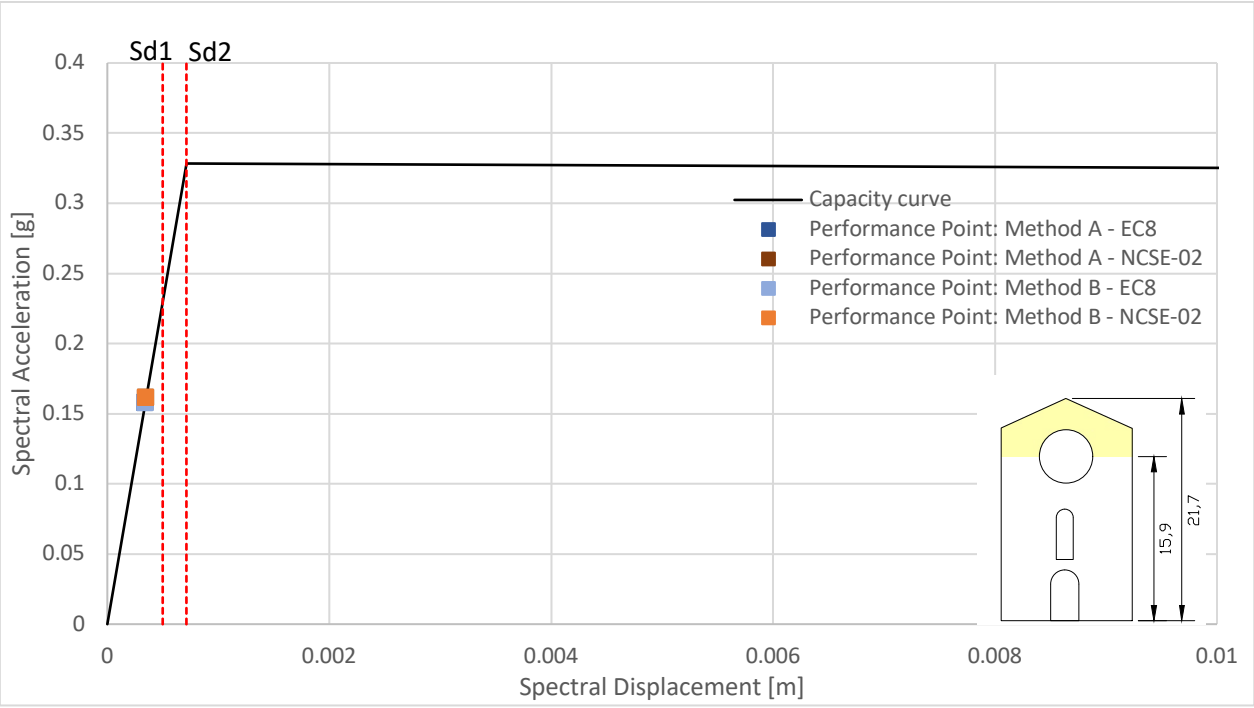

Figure A.2.2. Overturning of Poblet main facade above the center of the rose window ($R = 1.13$)

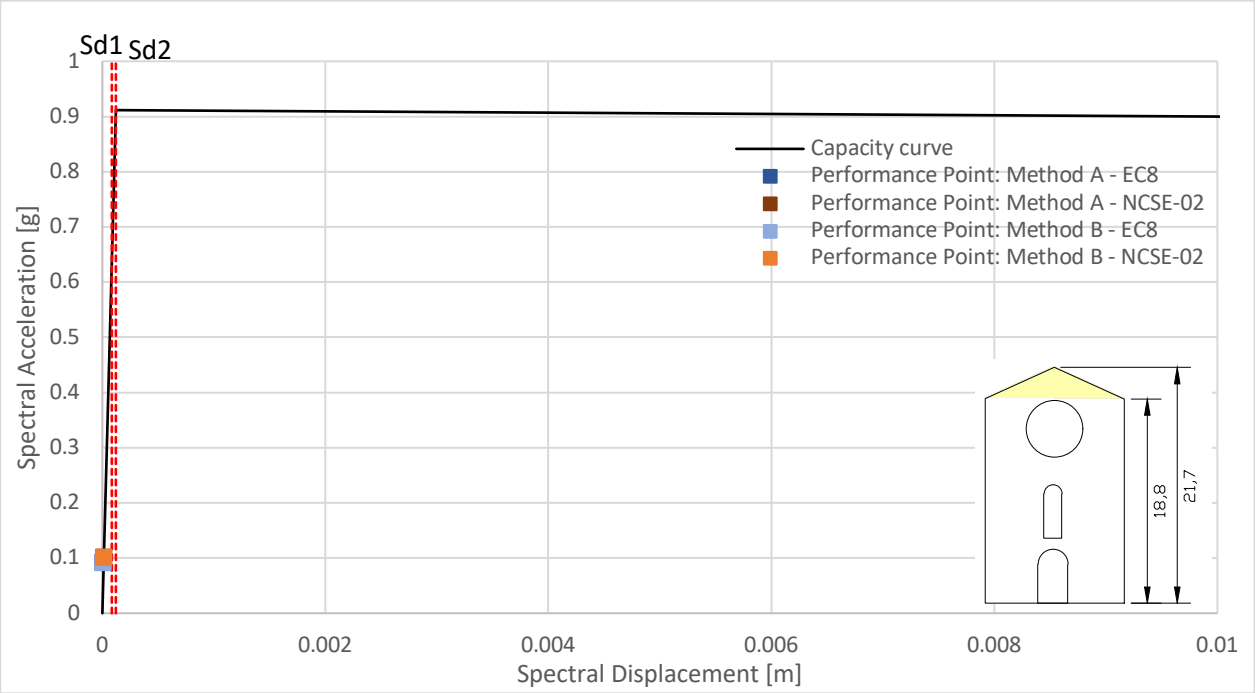

Figure A.2.3. Poblet main facade gable overturning ($R = 1.02$)

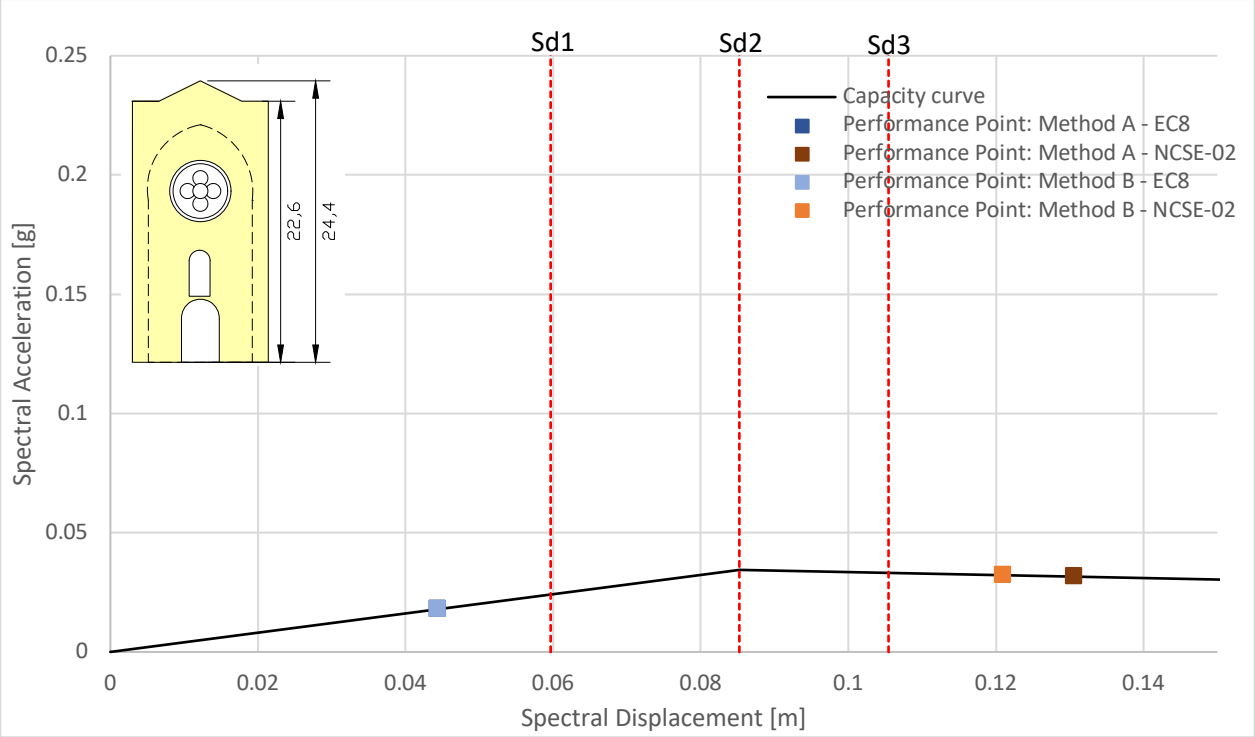

Figure A.2.4. Poblet transept facade overturning, case 2: including the intersection with transept walls and vault

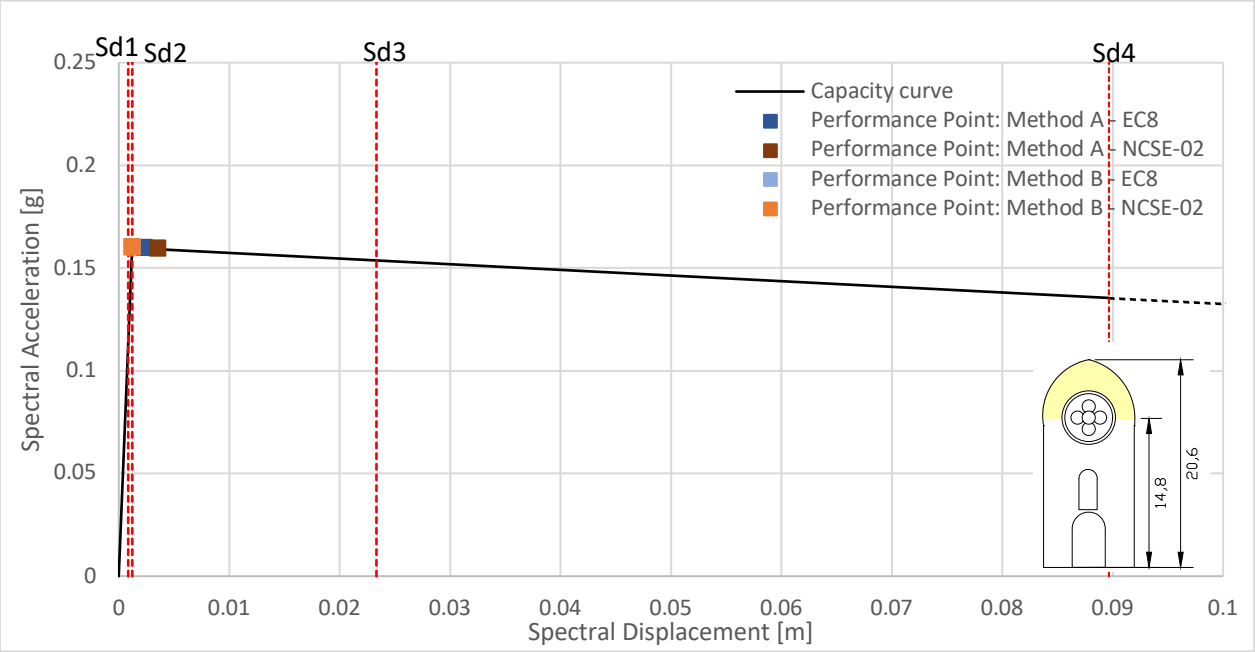

Figure A.2.5. Overturning of Poblet transept facade limited by the vault and walls, above the middle of the rose window ($R = 1.18$)

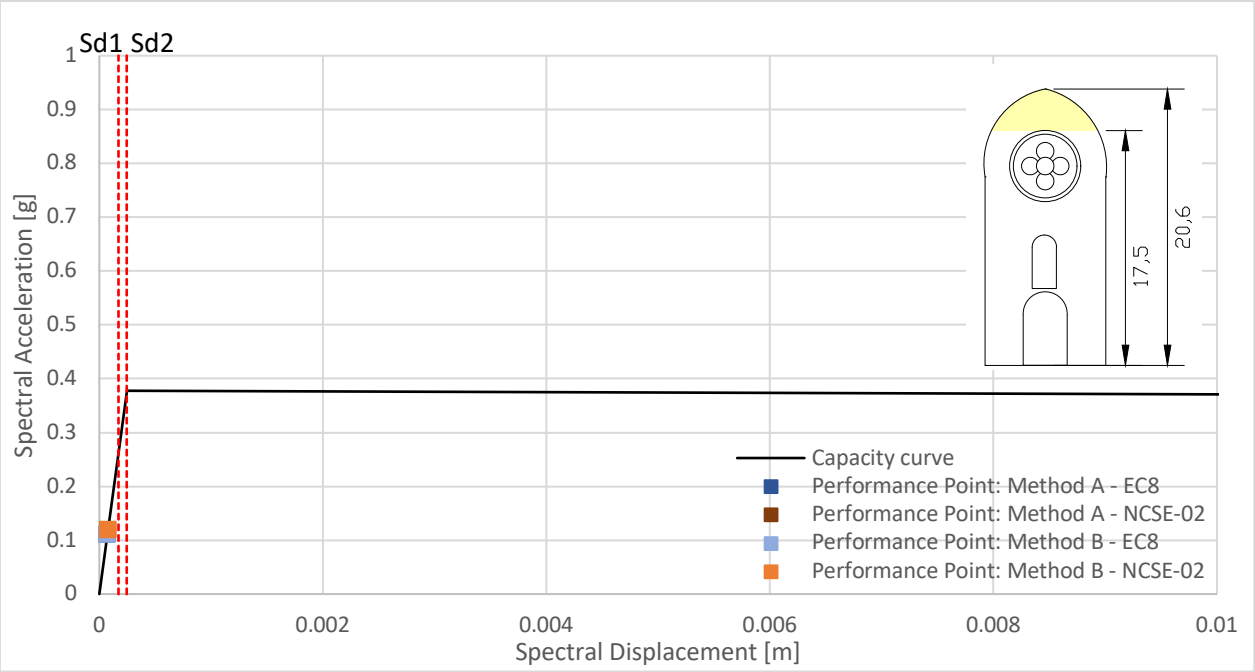

Figure A.2.6. Overturning of gable of Poblet transept facade limited by the vault and walls ($R = 1.03$)

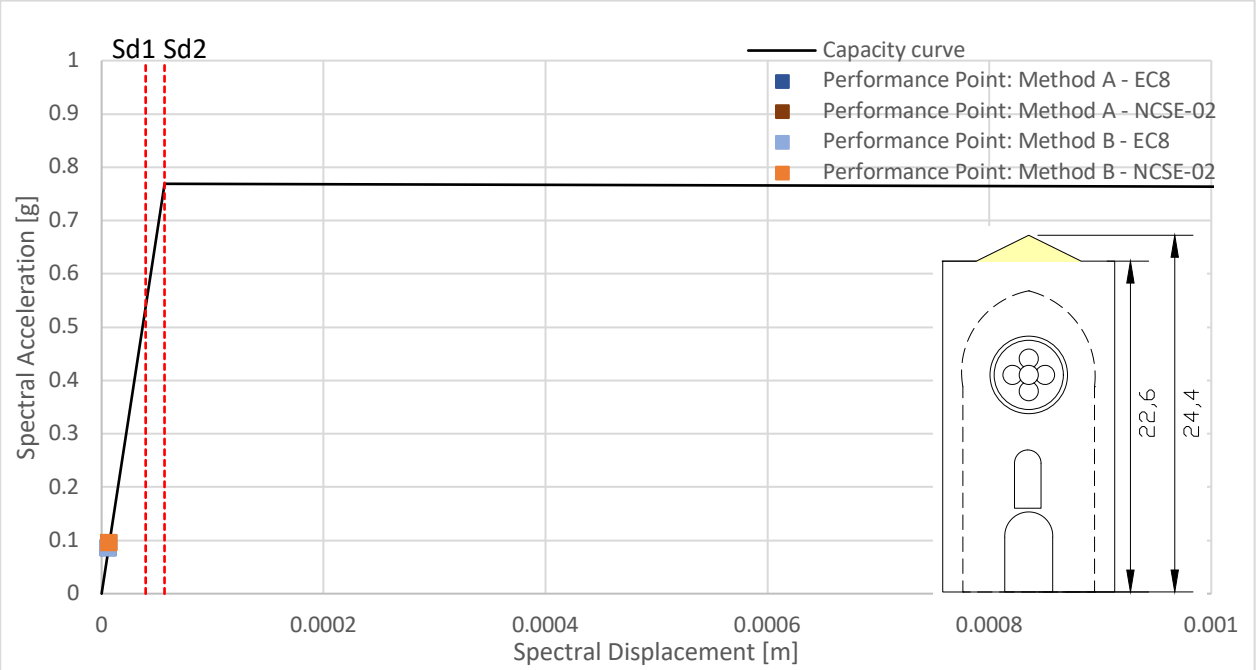

Figure A.2.7. Exterior gable of Poblet transept facade overturning ($R = 1.01$)

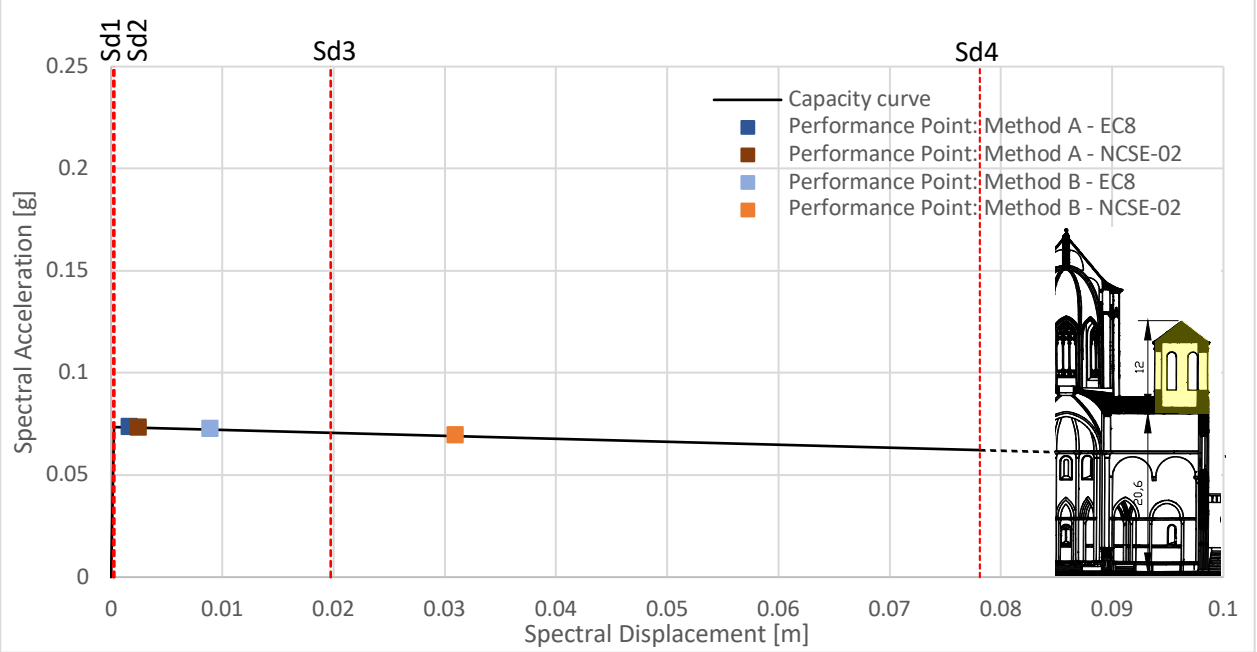

Figure A.2.8. Poblet bell tower overturning ($R = 1.06$)

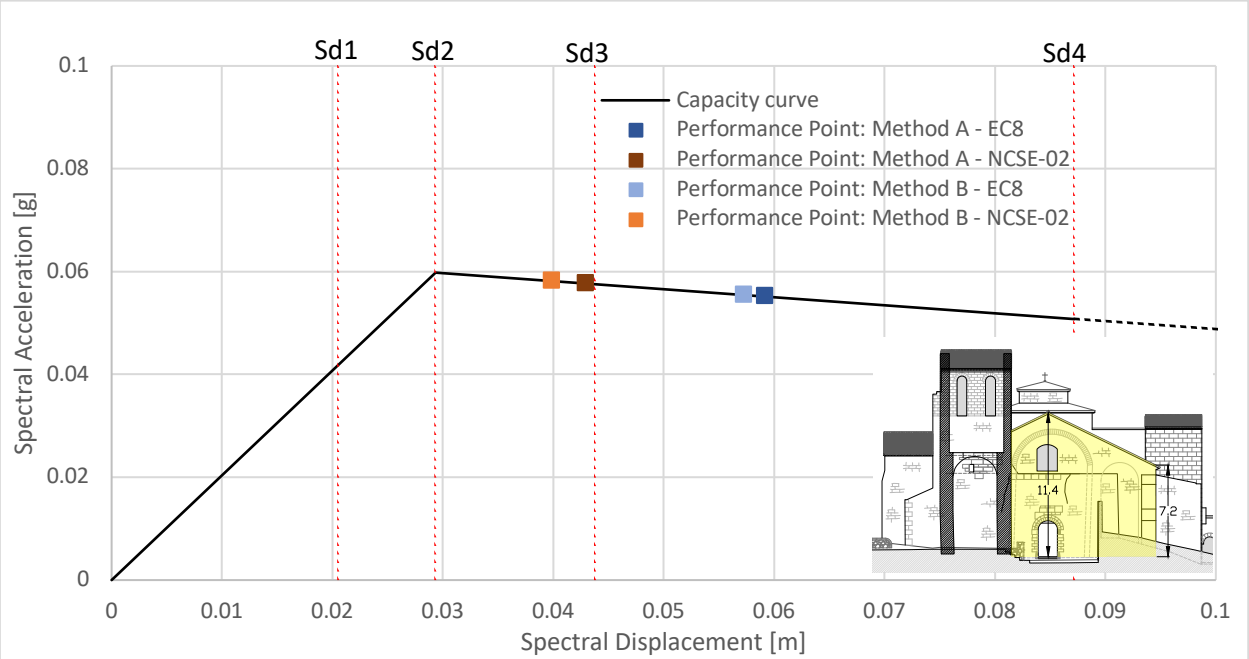

Figure A.2.9. Sant Miquel de Cruïlles main facade overturning, case 2: including buttressing wall

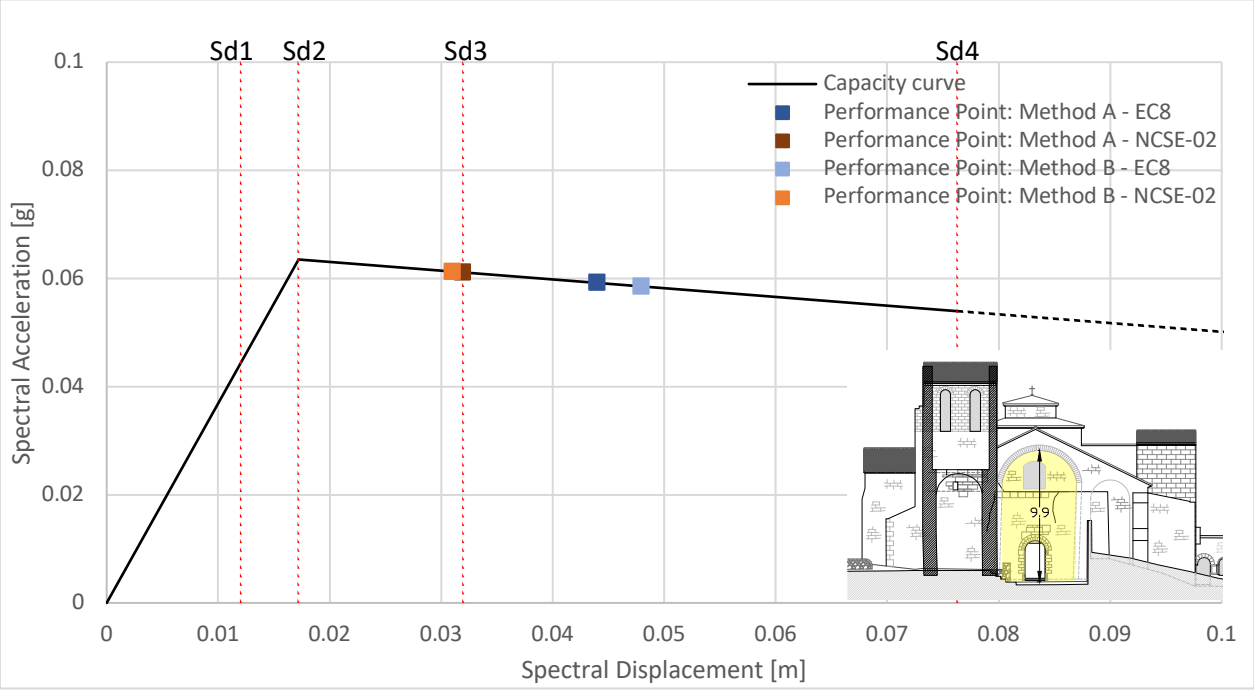

Figure A.2.10. Sant Miquel de Cruïlles main facade overturning, case 3: beneath the arch

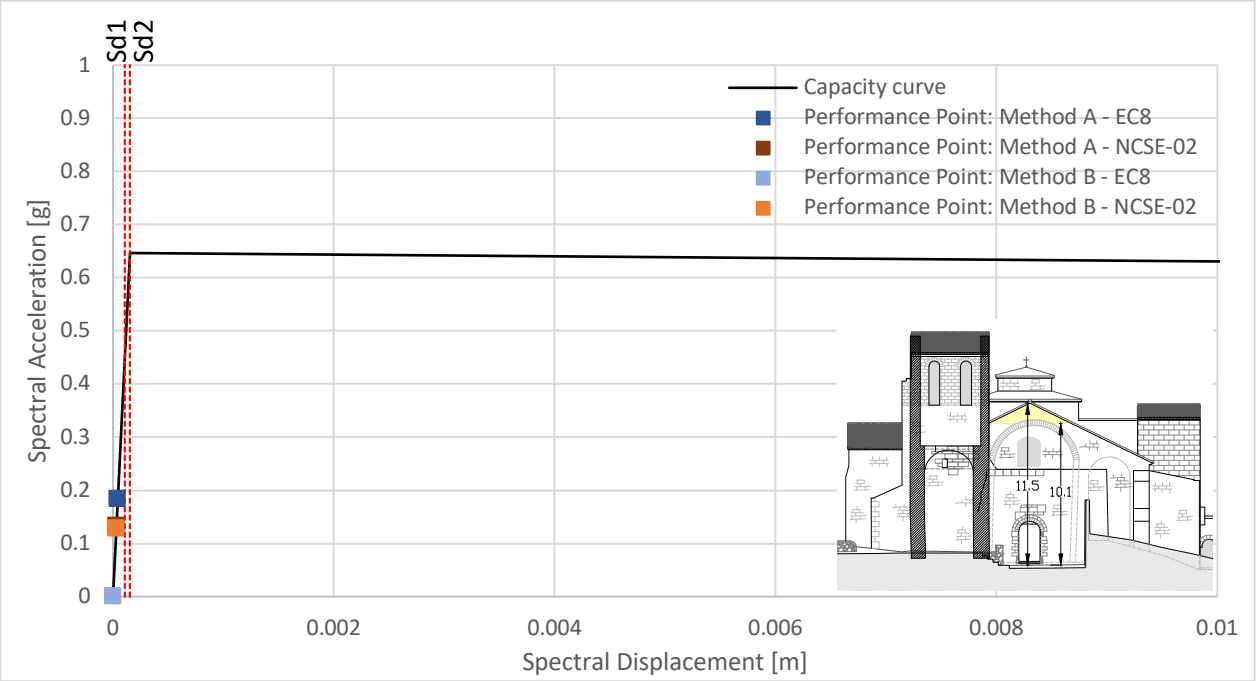

Figure A.2.11. Sant Miquel de Cruïlles gable of main facade overturning ($R = 1.03$)

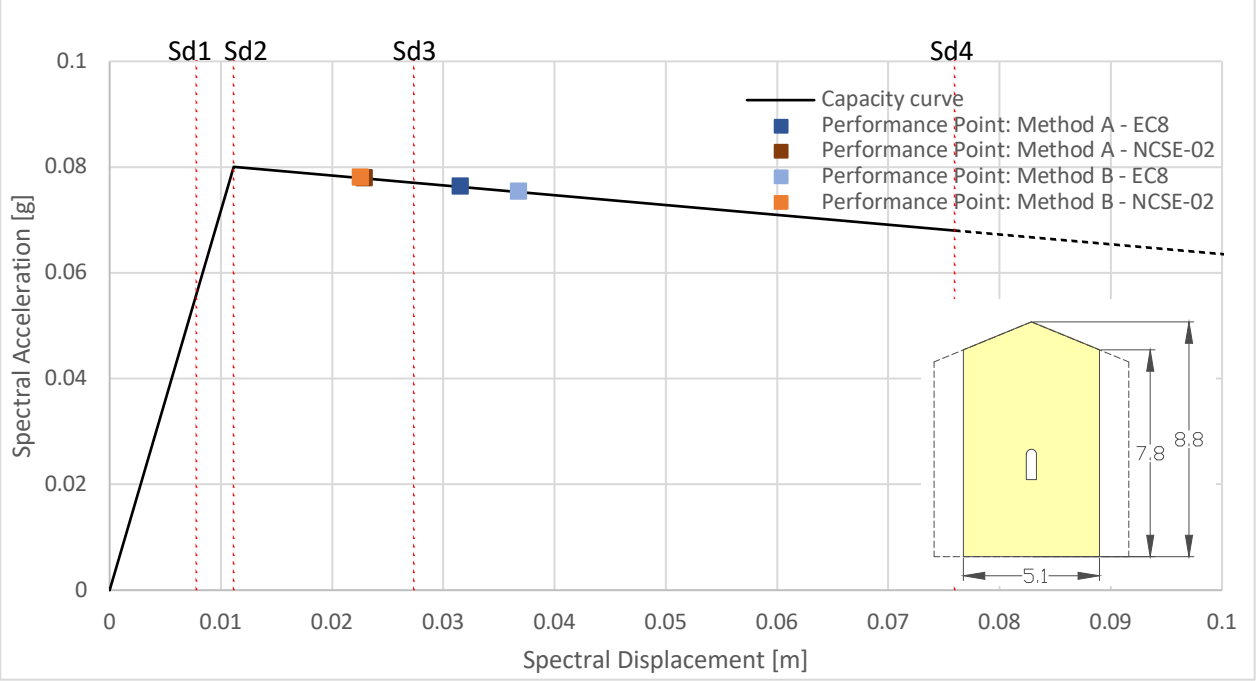

Figure A.2.12. Sant Miquel de Cruïlles north transept overturning, case 2: limited by the transept walls

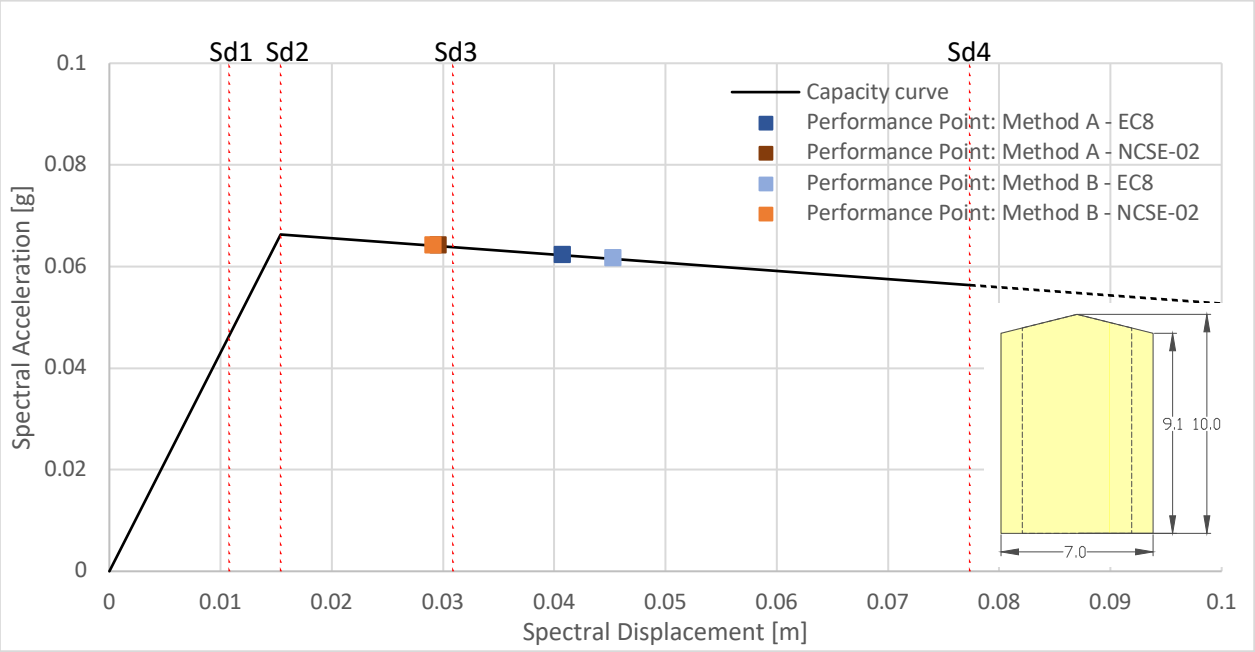

Figure A.2.13. Sant Miquel de Cruïlles south transept overturning, case 1: including intersection with transept walls

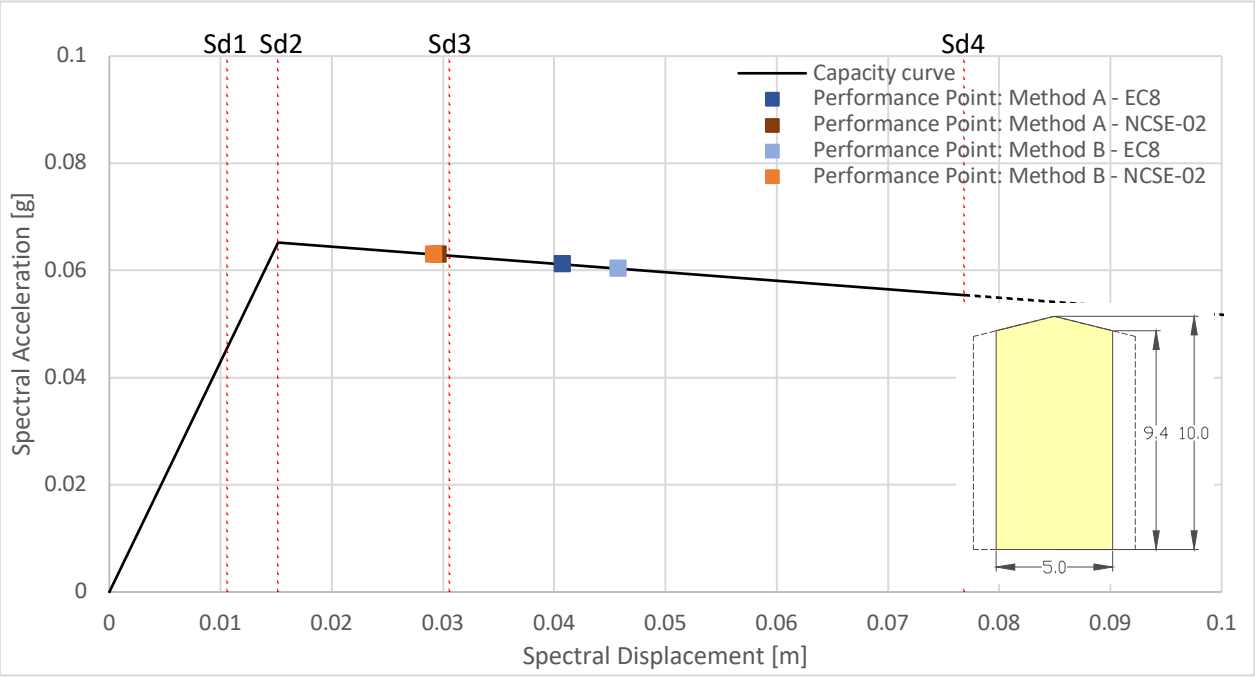

Figure A.2.14. Sant Miquel de Cruïlles south transept overturning, case 2: limited by transept walls

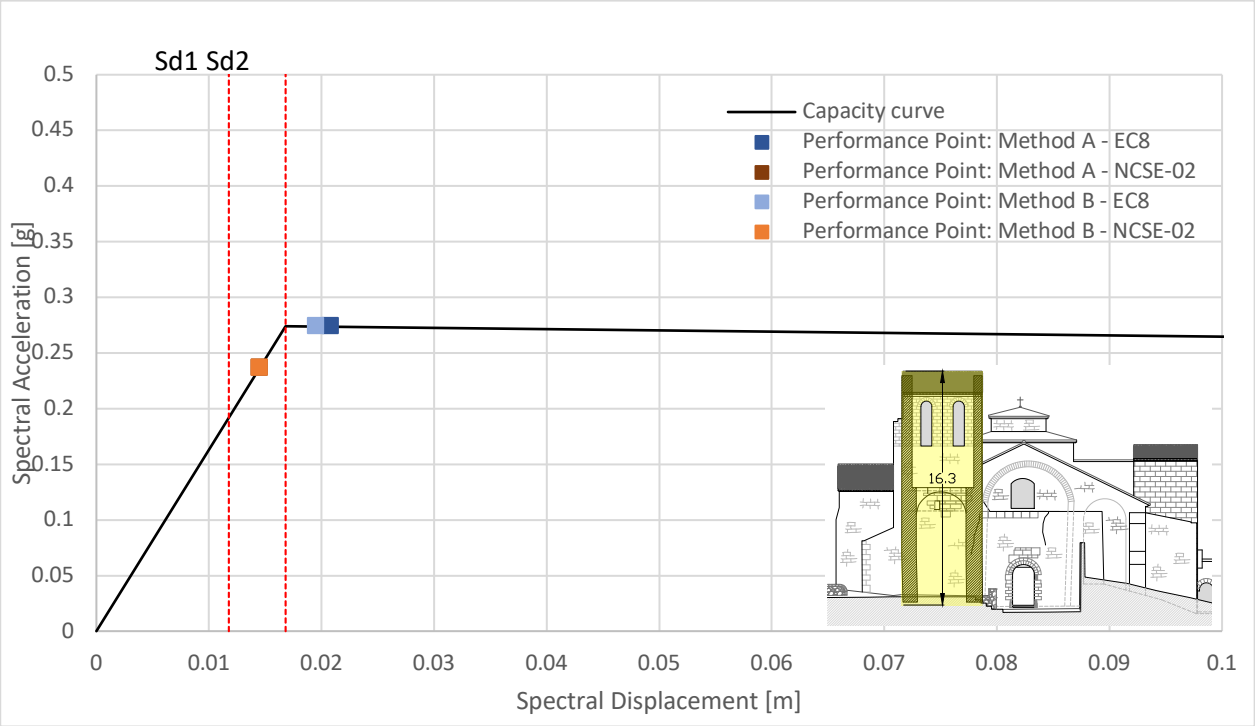

Figure A.2.15. Cruïlles bell tower overturning

A.3. Table of percent difference in results for kinematic limit analysis

Table A.3.1. Percent difference in results for all cases of kinematic mechanisms of Poblet and Cruïlles

		Percent difference in results (%)			
		Between EC 8 and NCSE-02		Between Method A and Method B	
		Method A	Method B	EC 8	NCSE-02
Santa Maria de Poblet					
Main facade 1	d	60	55	0	6
	a	12	13	0	0
Main facade 2	d	54	105	62	111
	a	1	4	1	4
Main facade 3	d	2	2	0	0
	a	2	2	0	0
Main facade 4	d	10	10	0	0
	a	10	10	0	0
Transept facade 1	d	71	65	0	6
	a	14	15	0	1
Transept facade 1*	d	99	93	0	8
	a	55	57	0	2
Transept facade 2	d	42	0	62	98
	a	0	0	0	0
Transept facade 3	d	49	6	221	213
	a	49	6	221	213
Transept facade 4	d	12	12	0	0
	a	12	12	0	0
Apse	d	16	16	0	0
	a	16	16	0	0
Gable belfry	d	53	86	3	35
	a	2	5	0	2
Bell tower	d	40	110	137	170
	a	0	4	1	6
Sant Miquel de Cruïlles					
Main facade 1	d	32	30	9	7
	a	5	4	2	1
Main facade 2	d	32	36	3	7
	a	4	5	1	1
Main facade 3	d	32	200	200	3
	a	32	200	200	3
Main facade 4	d	32	43	9	3
	a	3	5	1	0
North transept facade, case 1	d	32	47	12	3
	a	2	3	1	0
North transept facade, case 2	d	32	48	15	1
	a	2	3	1	0
South transept facade, case 1	d	32	44	11	2
	a	3	4	1	0
South transept facade, case 2	d	32	44	12	1
	a	3	4	1	0

West wall of bell tower	d	5	11	23	7
	a	2	3	7	2
Bell tower	d	36	29	7	0
	a	14	15	0	0
Main apse, case 2	d	32	26	6	0
	a	7	7	0	0
Lateral apse	d	32	36	1	6
	a	1	1	0	0